## Test (4): MassBay: ASCOT–01

### Purpose

To demonstrate the consistency between the rigid–lid streamfunction, rigid–lid surface pressure and free surface (surface pressure) formulations in a shallow coastal domain. Test the various options for creating surface pressure initializations. Make use of verification data

### Status

A nestable, rotated spherical domain is defined as

$$\begin{aligned} n_x,\ n_y &= 53,\ 90 \\ dx,\ dy &= 0.015°,\ 0.015° \\ &\sim 1.668\text{km},\ 1.668\text{km} \\ lat_c,\ lon_c &\sim 42.31\text{N},\ 70.48\text{W} \\ rotation &= 25.5° \end{aligned}$$

16 model levels are spread throughout the water column in a double $\sigma$–system (illustrated in figure 2).

The initial field are created from an objective analysis of CTD data obtained June 6–10, 2001 during ASCOT–01 (figure 1, at right). These data are augmented with a $\frac{1}{8}°$ climatology constructed from June NODC, NMFS & MWRA data in and around Massachusetts Bay using the *HydroBase* software. These two data sets are combined in a 2 scale objective analysis, centered on 8 June 2001, with the correlation scales shown at right. A dynamic height is computed from the mapped temperature and salinity field with a reference level of 35m. The dynamic height is "adjusted" to topography by smooth extensions of the density field under topography. The dynamic height is also "adjusted" to coasts by constructing a vorticity field which is then inverted in a Poisson equation which enforces constant dynamic height along the coasts. Finally the Dirichlet boundary conditions used to construct the transport streamfunction are obtained by interpolation from a Gulf of Maine initialization made from the same data. These fields are illustrated in figure 3.

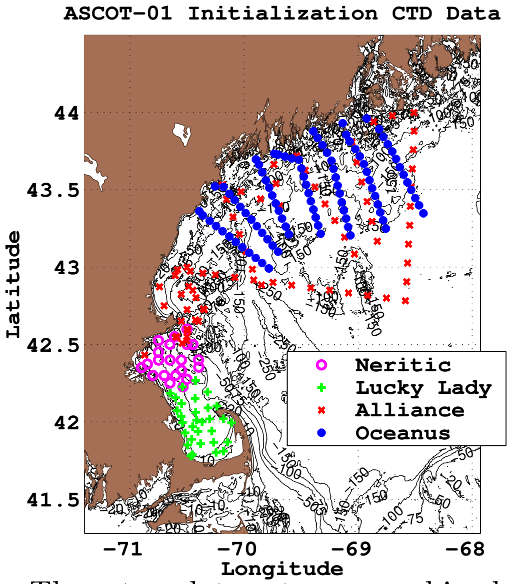


**OA Scales**

| | Synoptic | Mean |
|---|---|---|
| **Decay (km)** | 20 | 224 |
| **Zero-Cross (km)** | 50 | 540 |
| **Time-Decay (day)** | 100 | 10000 |

*(A) Streamfunction formulation*

The streamfunction formulation simulations form the baseline for comparing the surface pressure formulation simulations. Various CPP options are then turned on to include the various supporting changes for the surface pressure formulation

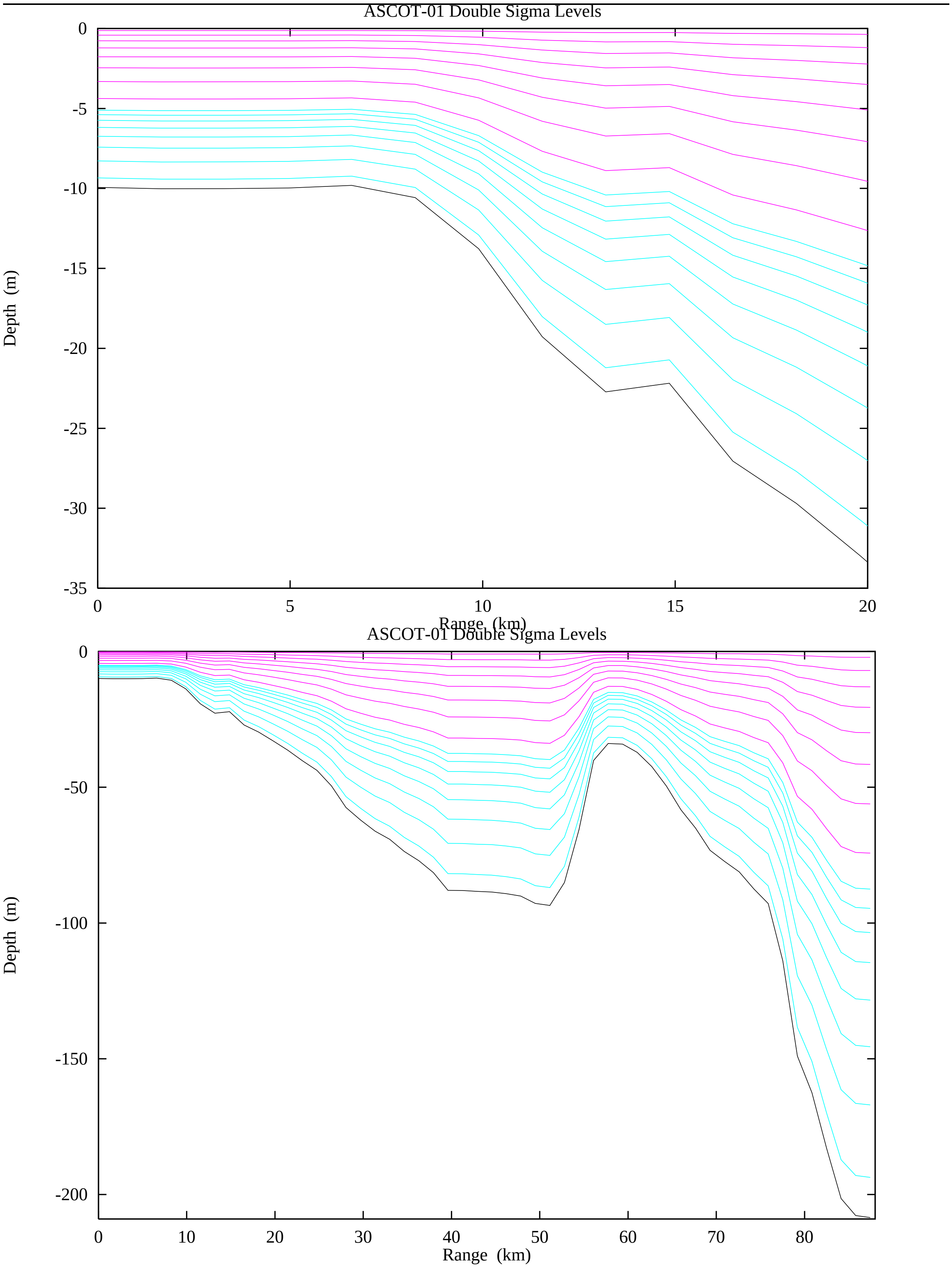


Figure 2 : Double $\sigma$–system used in Massachusetts Bay simulations.

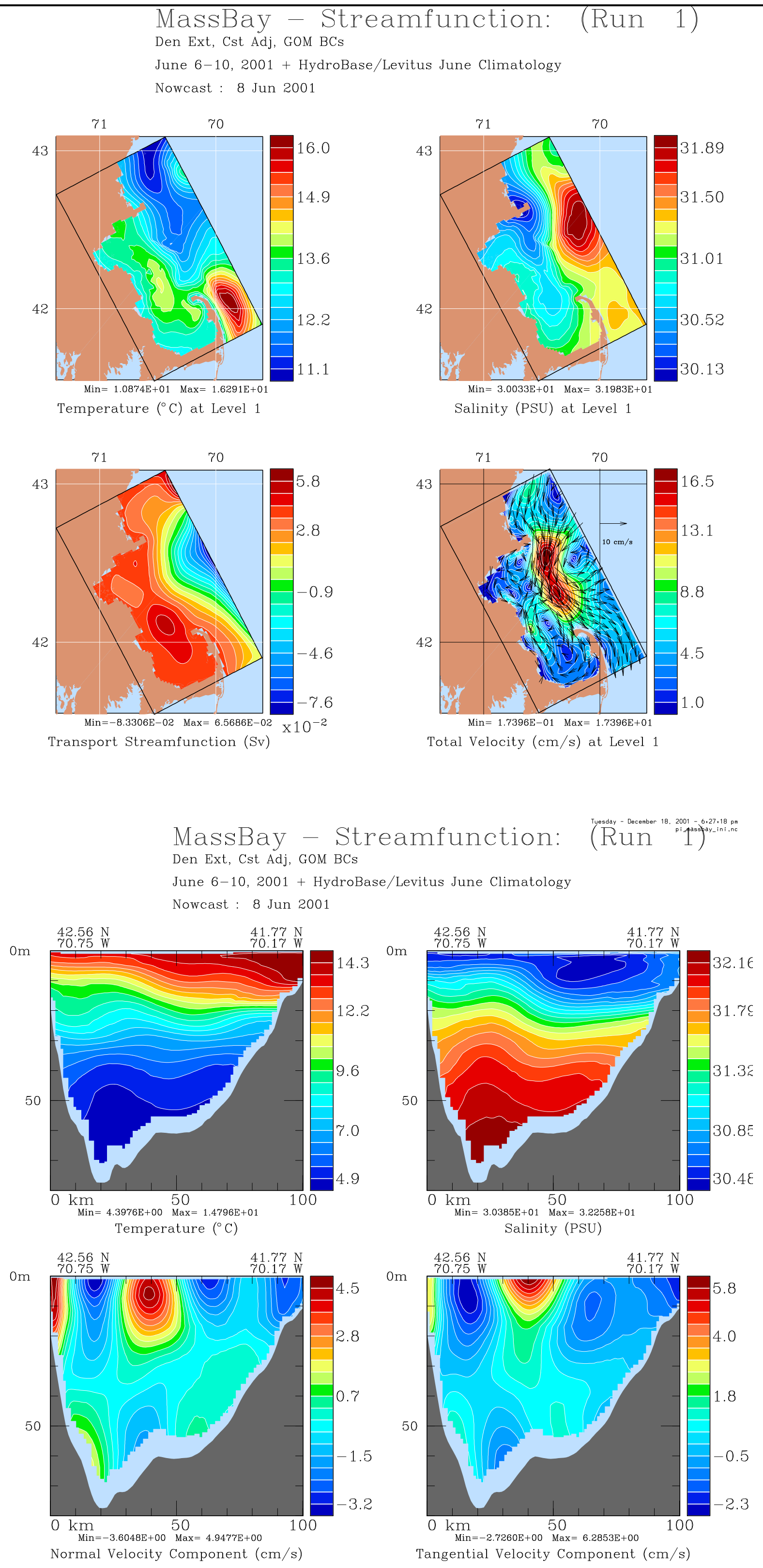


Figure 3 : Massachusetts Bay initialization. Surface fields and a vertical section running North–South through the middle of Massachusetts Bay.

(*i*) Baseline simulation

The baseline simulation is briefly presented in figures 4–7.

This simulation has a couple of nice features. The kinetic energy is bounded (as shown in figure 4) without signs of potential explosive growth. Interior to Massachusetts Bay, typical circulations are developed. The structures here are two main eddies, one large one near Cape Cod Bay, the other just south of Cape Ann.

There are a couple of problems too. The biggest is the southern boundary, which fails to allow enough exiting. Fairly early on, the flow is turned back northward along the eastern boundary. This is clearly visible on day seven. This return flow, however, both weakens as the simulation progresses and remains confined to the outer "buffer" area of the domain.

Overall, the simulation is judged "good enough" for testing purposes.

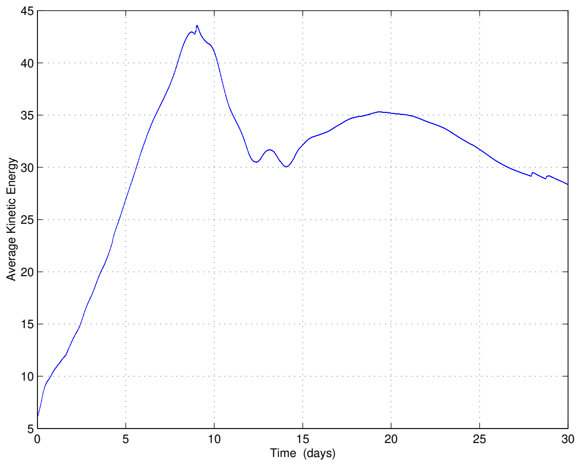


Figure 4 : Kinetic Energy for baseline simulation.

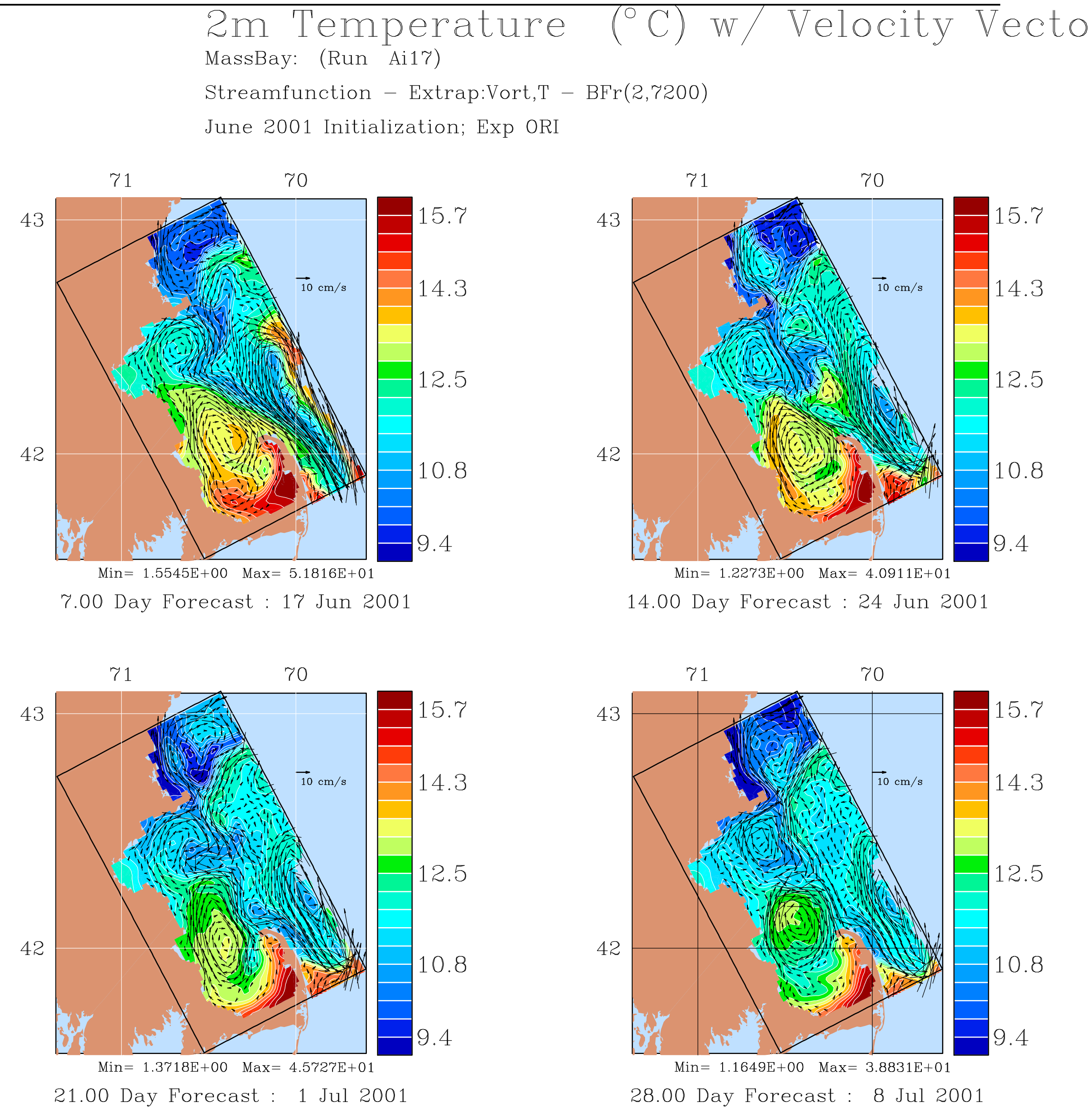


Figure 5 : Baseline streamfunction formulation. Near surface temperature with total velocity vectors.

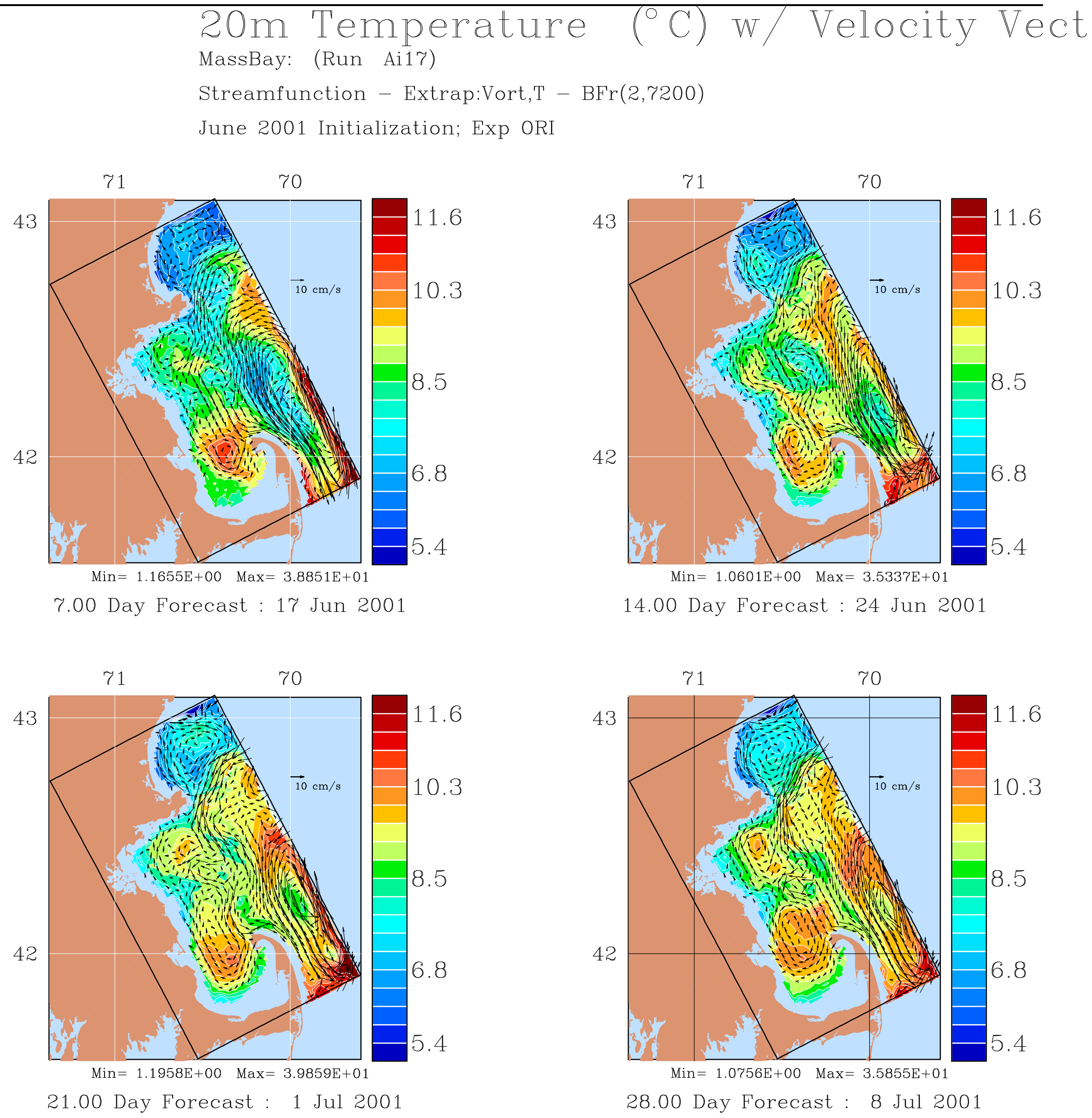


Figure 6 : Baseline streamfunction formulation. Mid–level temperature with total velocity vectors.

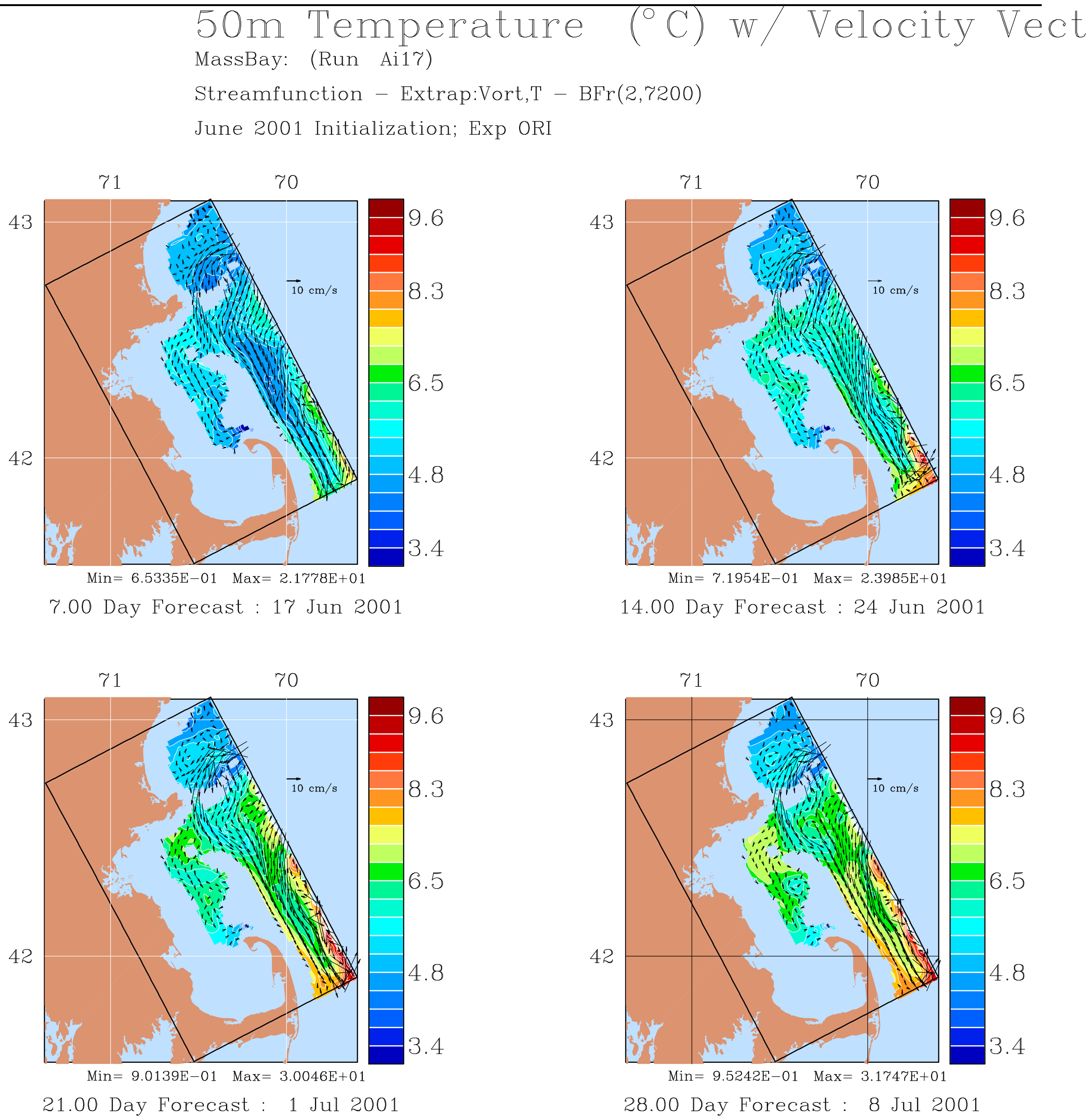


Figure 7 : Baseline streamfunction formulation. Deep temperature with total velocity vectors.

*(ii)* Pressure formulation momentum fluxes. (CPP option `mfluxavg`)

In order to maintain the vertically integrated conservation of mass, the pressure formulation requires a modified discretization (6 point) of the momentum fluxes. For compatibility, Lozano & Lanerolle provided the option of using this discretization in the streamfunction formulation.

This simulation and its comparisons to the baseline simulation are presented in figures 8–15. The kinetic energy shows reasonable agreement to the baseline. The RMS and PCC statistics show much larger deviations than were present in either the periodic jet or $P^2S^3$ tests at this stage.

The surface flows are reasonably similar, the main differences are that the Maine Coastal Current doesn't penetrate as deeply into Massachusetts Bay and the southward flow past Cape Cod get deflected eastward at a more northerly position. The temperature differences are largest outside of Mass. Bay, over Stellwagen Bank and off Race Point. The mid–level flows are somewhat more similar, the biggest difference is that the spurious eastern boundary northern flow is reduced in this simulation. The holds for the deep comparison. The temperature differences in these levels show similar trends to the surface differences.

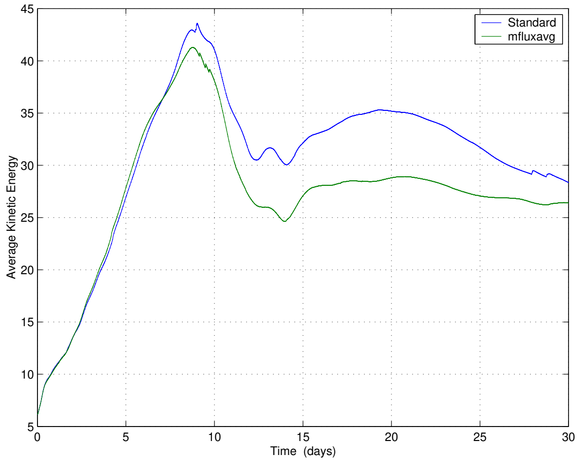


Figure 8 : Kinetic Energy comparison between baseline simulation *(Ai)* and simulation with CPP option `mfluxavg` *(Aii)*.

**RMS Error** **Pattern Correlation Coefficient**

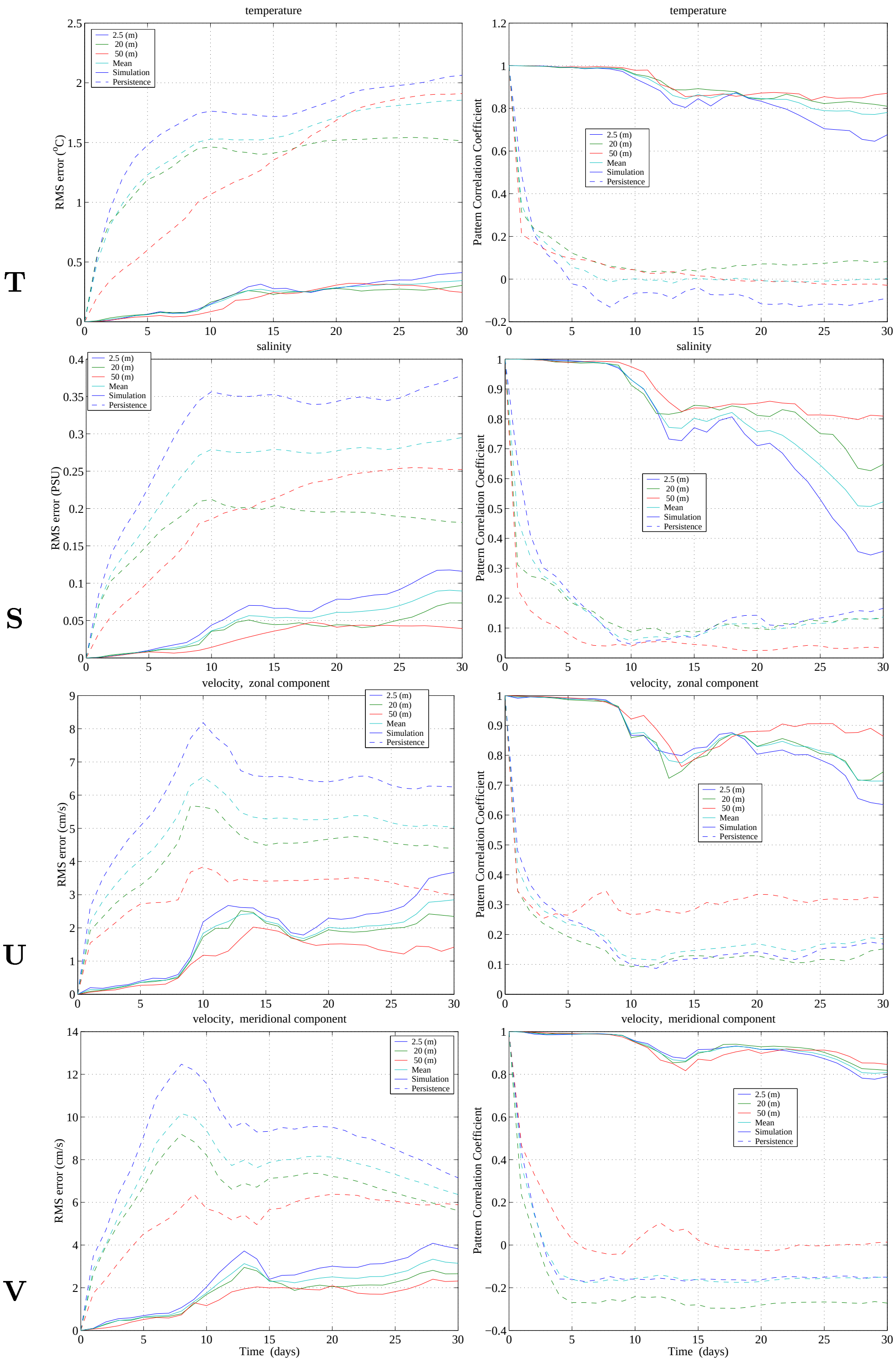


Figure 9: Comparison of baseline run *(i)* versus 6 point flux algorithm *(ii)*

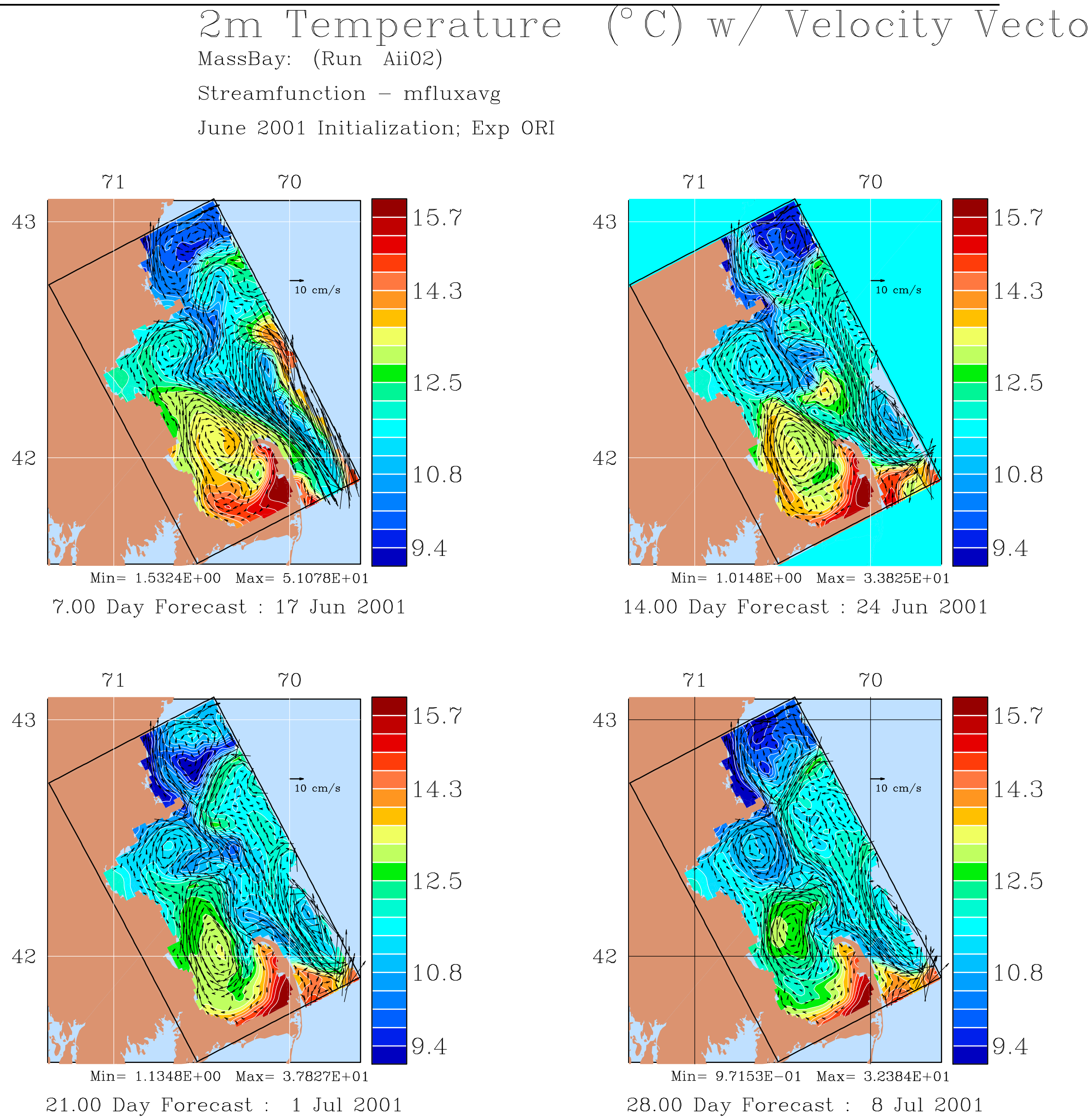


Figure 10 : Pressure formulation momentum fluxes added (CPP option **mfluxavg**). Near surface temperature with total velocity vectors.

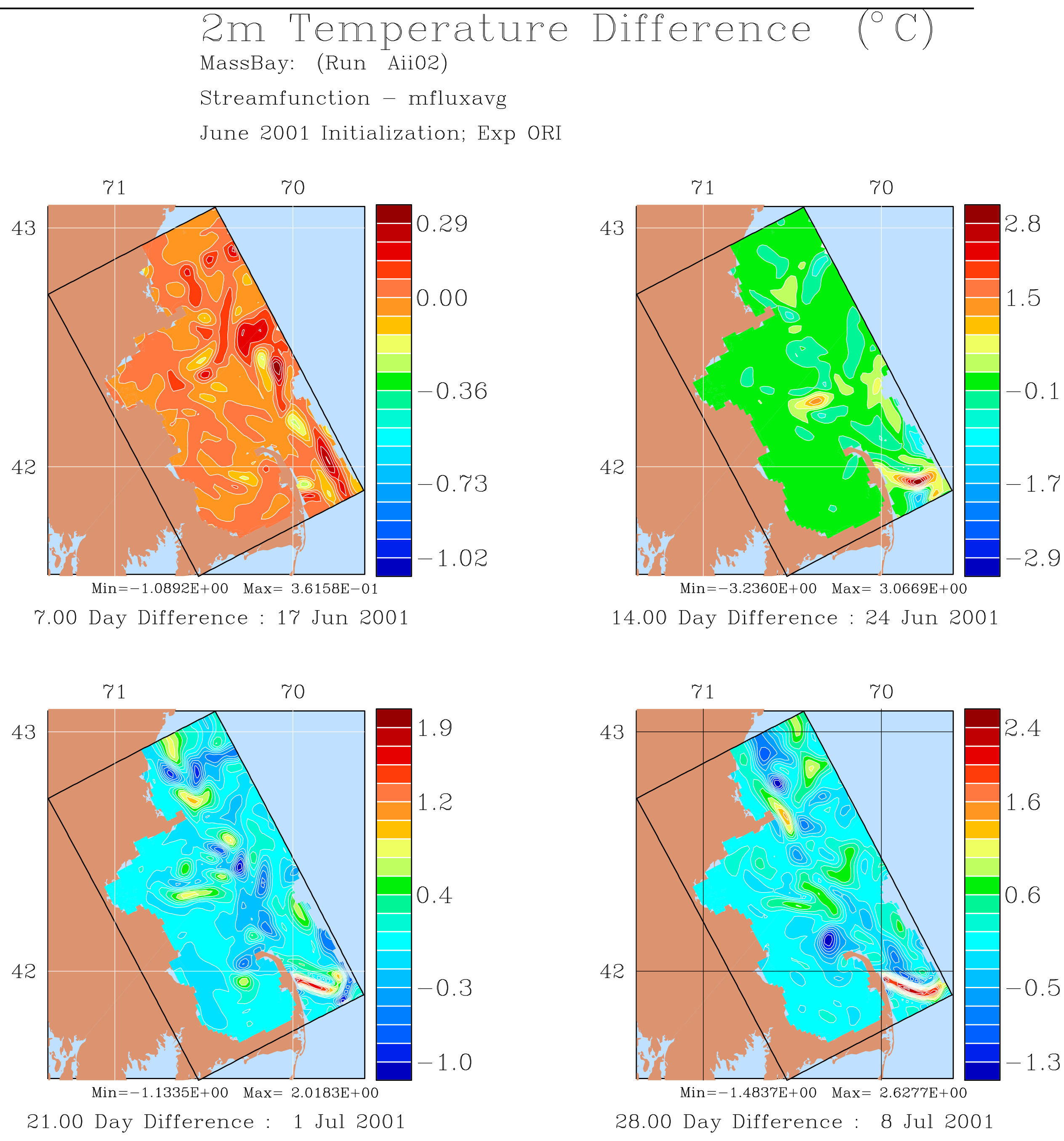


Figure 11 : Near Surface comparison of baseline simulation to simulation with pressure formulation momentum fluxes added (CPP option `mfluxavg`).

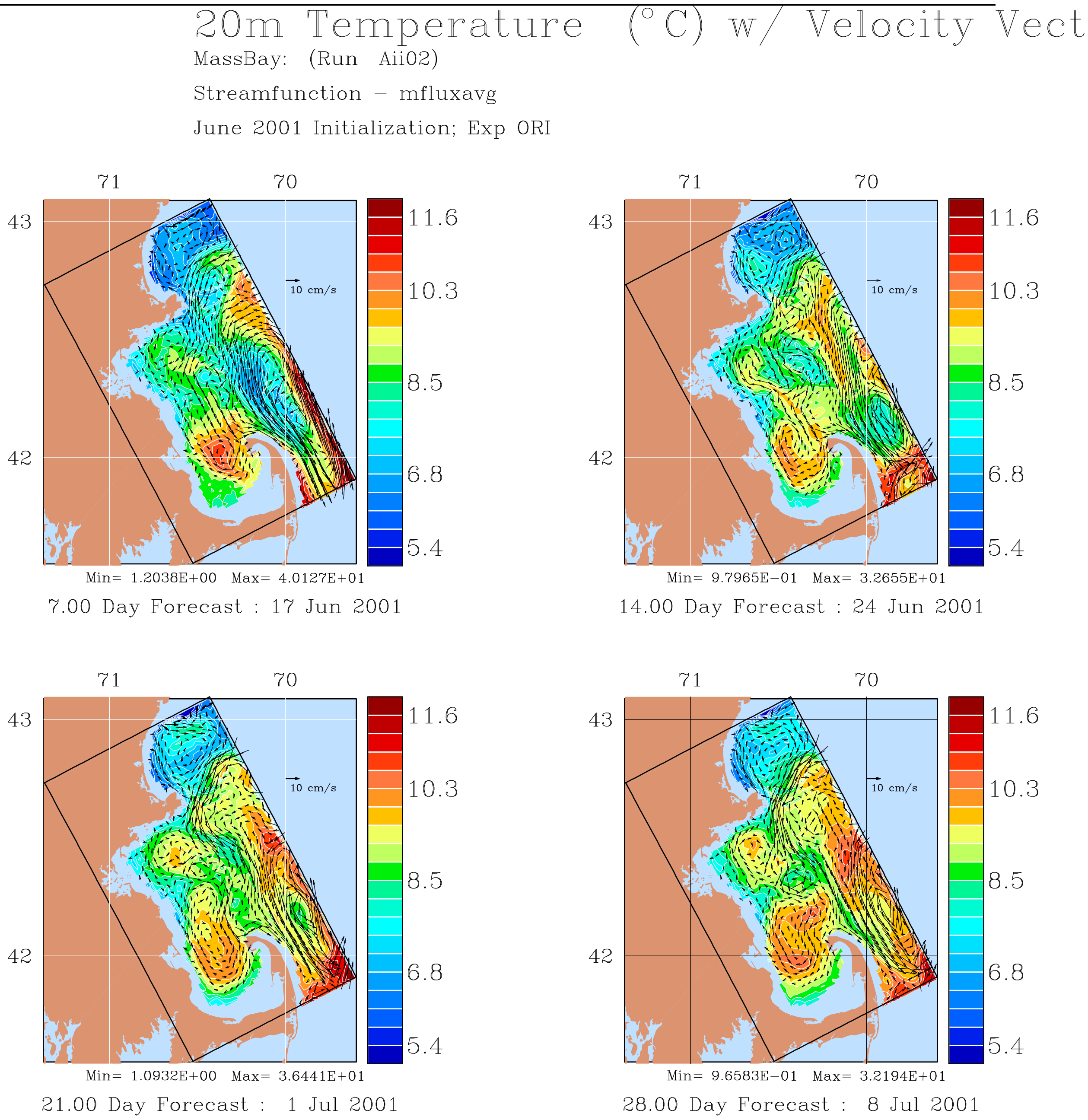


Figure 12 : Pressure formulation momentum fluxes added (CPP option `mfluxavg`). Mid–level temperature with total velocity vectors.

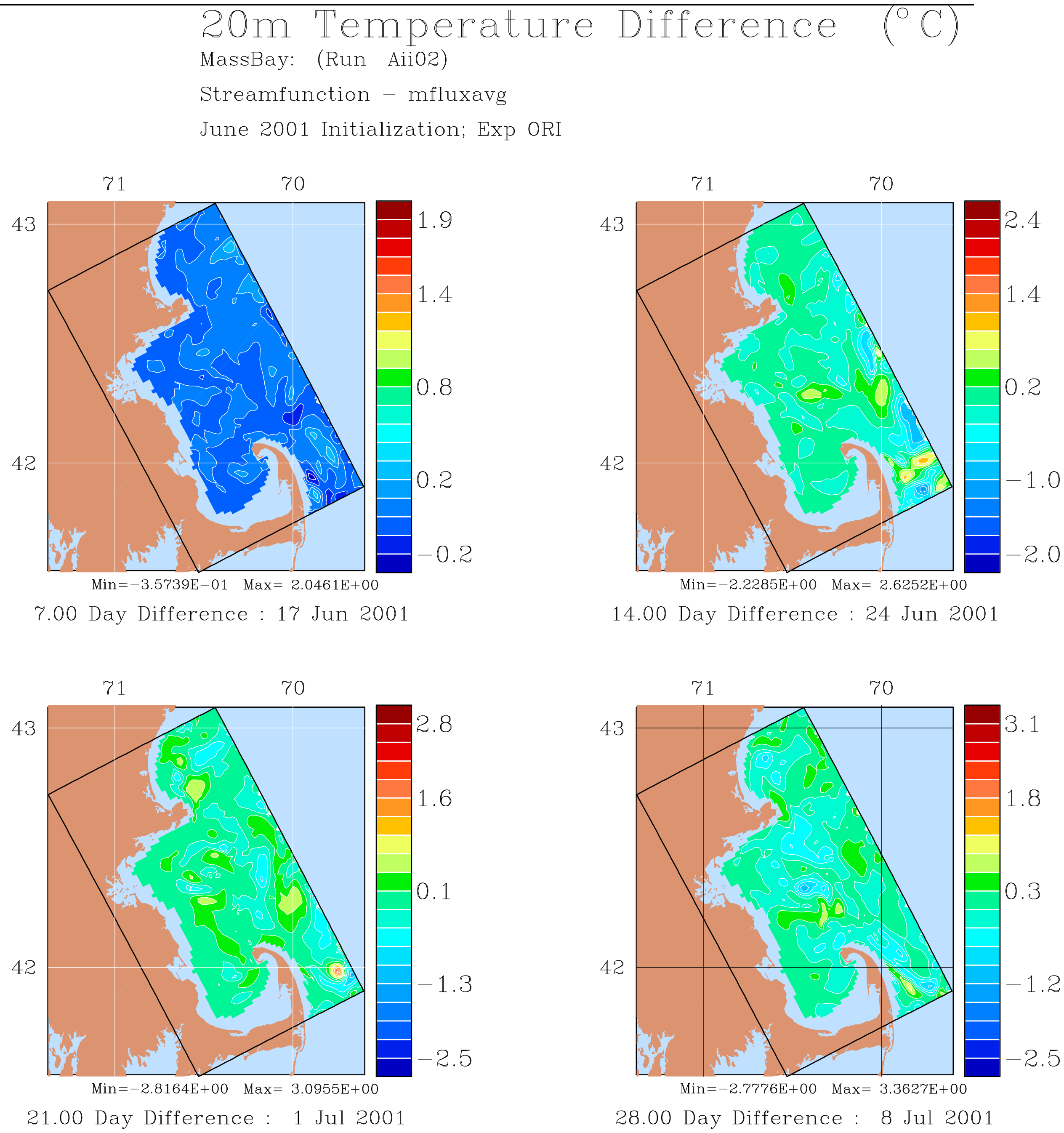


Figure 13 : Mid–level comparison of baseline simulation to simulation with pressure formulation momentum fluxes added (CPP option `mfluxavg`).

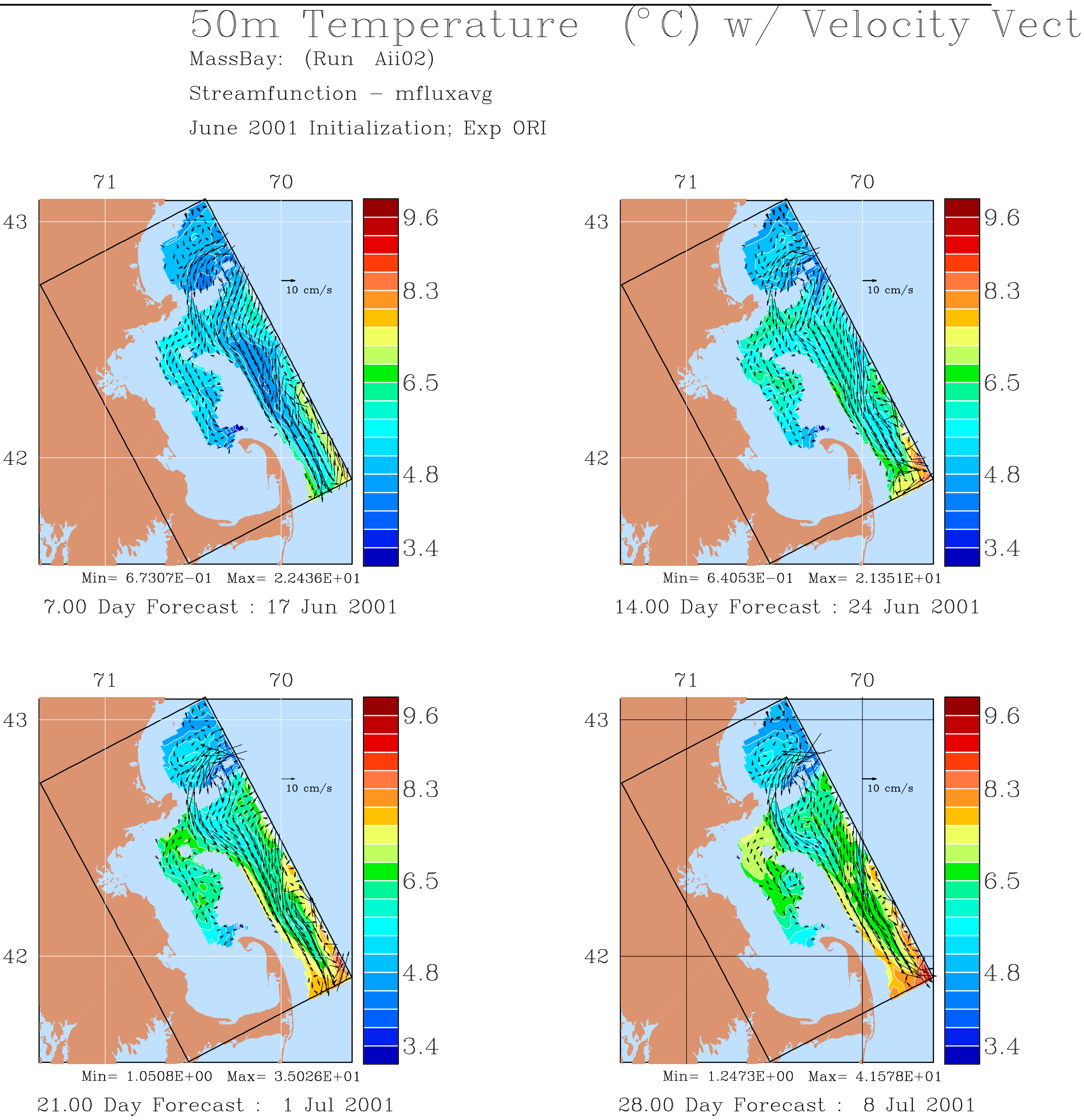


Figure 14 : Pressure formulation momentum fluxes added (CPP option `mfluxavg`). Deep temperature with total velocity vectors.

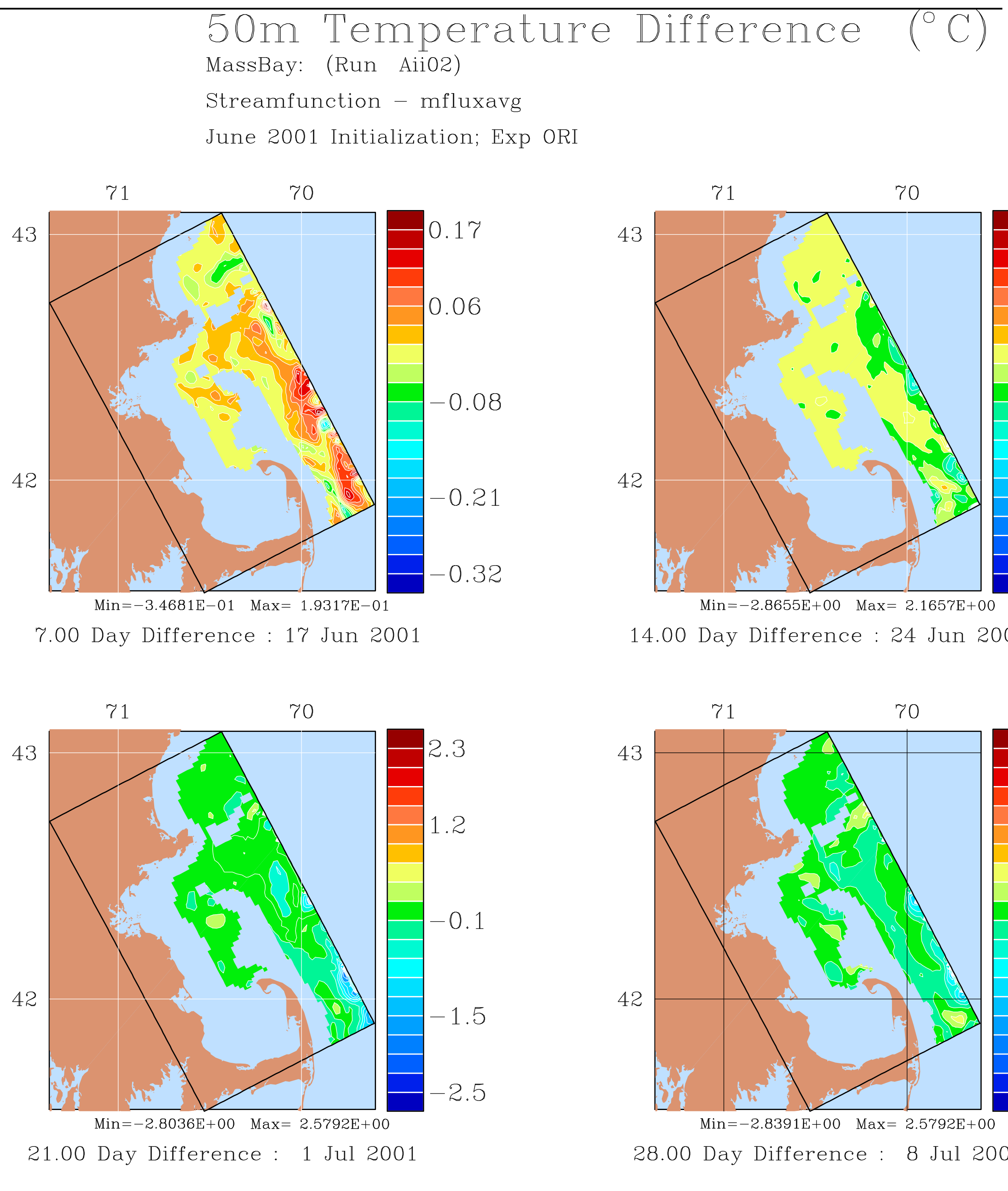


Figure 15 : Deep comparison of baseline simulation to simulation with pressure formulation momentum fluxes added (CPP option `mfluxavg`).

*(iii)* Pressure formulation momentum fluxes, alternative formulation. (CPP options `mflux-avg` + `tfluxes`)

The alternative formulation is a variation in the handling of land masks, specifically the method of preventing the 6–point flux operator from using invalid data under the land mask.

- In the original formulation:
  - In the absence of land masks the operator is coded without reference to masks.
  - In the presence of land masks, each evaluation of the velocity is multiplied by a binary [0,1] mask.
- In the new formulation, the binary mask is tested before each evaluation of the velocity.

The results are as follow.

- The difference fields between cases *(ii)* and *(iii)* are identically zero after 30 days.
- Case *(iii)* is marginally faster than case *(ii)* (approximately 4 cpu minutes in a simulation requiring 3 cpu hours).

Comparing these timing results with those in $P^2S^3$, leads to the following conclusions

- Doing nothing (open domains) is marginally cheaper than anything else.
- Testing (`if` statements) are marginally cheaper than multiplying by a binary mask.

In light of the identity with case *(ii)*, no plots will be presented here.

*(iv)* Addition of Asselin filter. (CPP options `mfluxavg` + `tfluxes` + `AsselinFilt`)

To inhibit the odd–even decoupling of the leap–frog time–stepping, the HOPS PE model has a pair of options

(1) Intermittent revision to forward Euler time–stepping (a first order algorithm).
(2) An Asselin time filter at every time step.

For reason best known to himself, Lozano disabled the Euler time–stepping option when the surface pressure formulation is activated.

A comparison of varying Asselin filter parameter ($\nu$) is presented in figures 16–19. The kinetic energy shows a smaller initial over–shoot in the strongest filter ($\nu$=0.01) tried. The RMS and PCC statistics are also slightly improved in the $\nu$=0.01 case. Those statistics are slightly better than those of *(Aii)*.

The flow fields are somewhat more similar to *(Ai)* than *(Aii)*. The biggest difference is a slight lessening of the northward eastern boundary flow. The temperature difference fields are concentrated external to Massachusetts Bay.

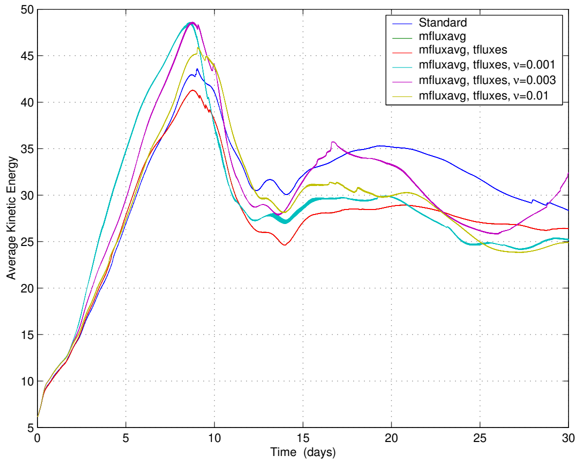


Figure 16 : Kinetic Energy comparison between simulation *(Ai)* – *(Aiv)*. Also examining the effects of changing Asselin filter parameter $\nu$.

**RMS Error** **Pattern Correlation Coefficient**

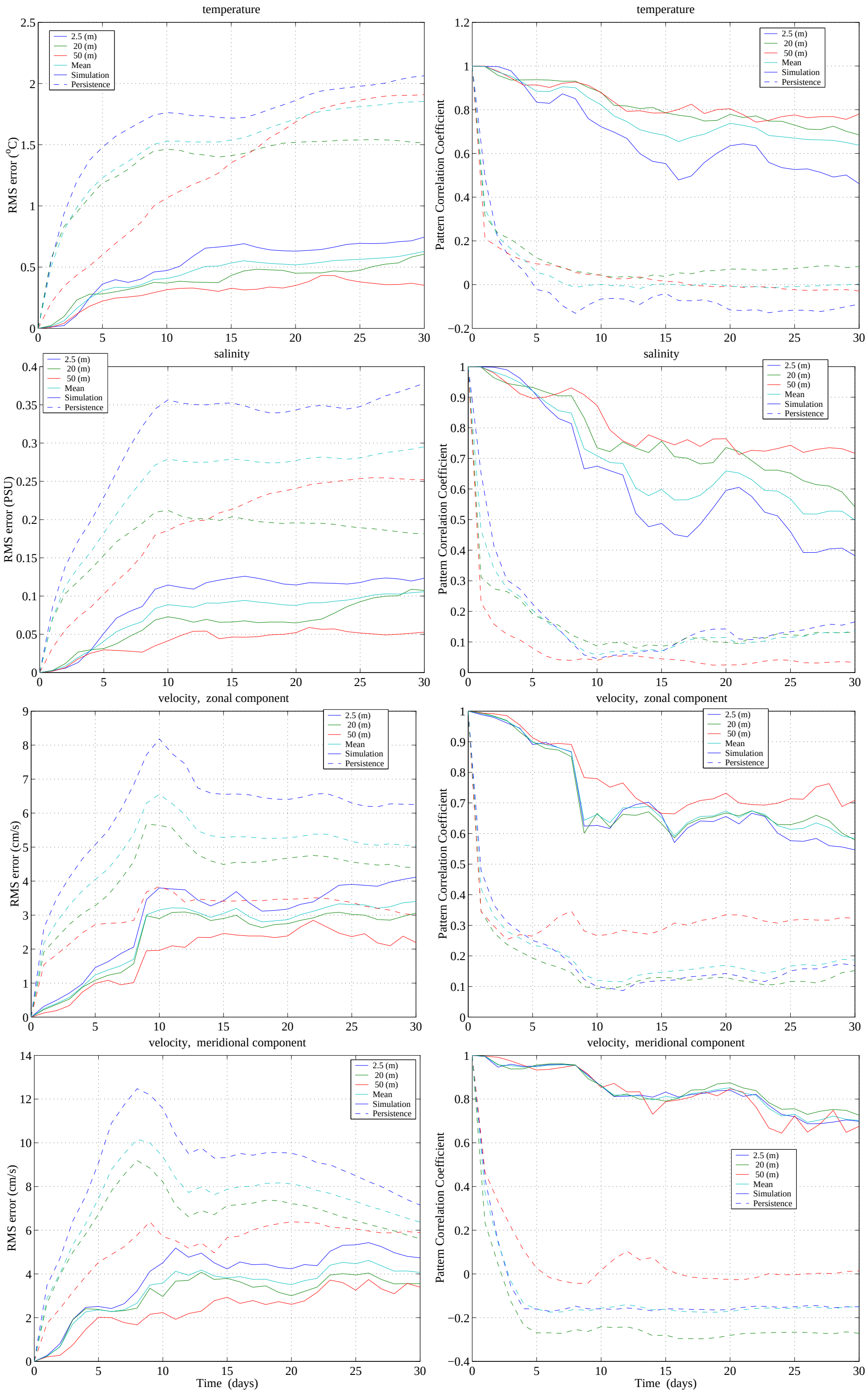


**T**

**S**

**U**

**V**

Figure 17: Comparison of baseline run *(i)* versus alternate 6 point flux algorithm with Asselin filter ($\nu$=0.001) *(iv)*

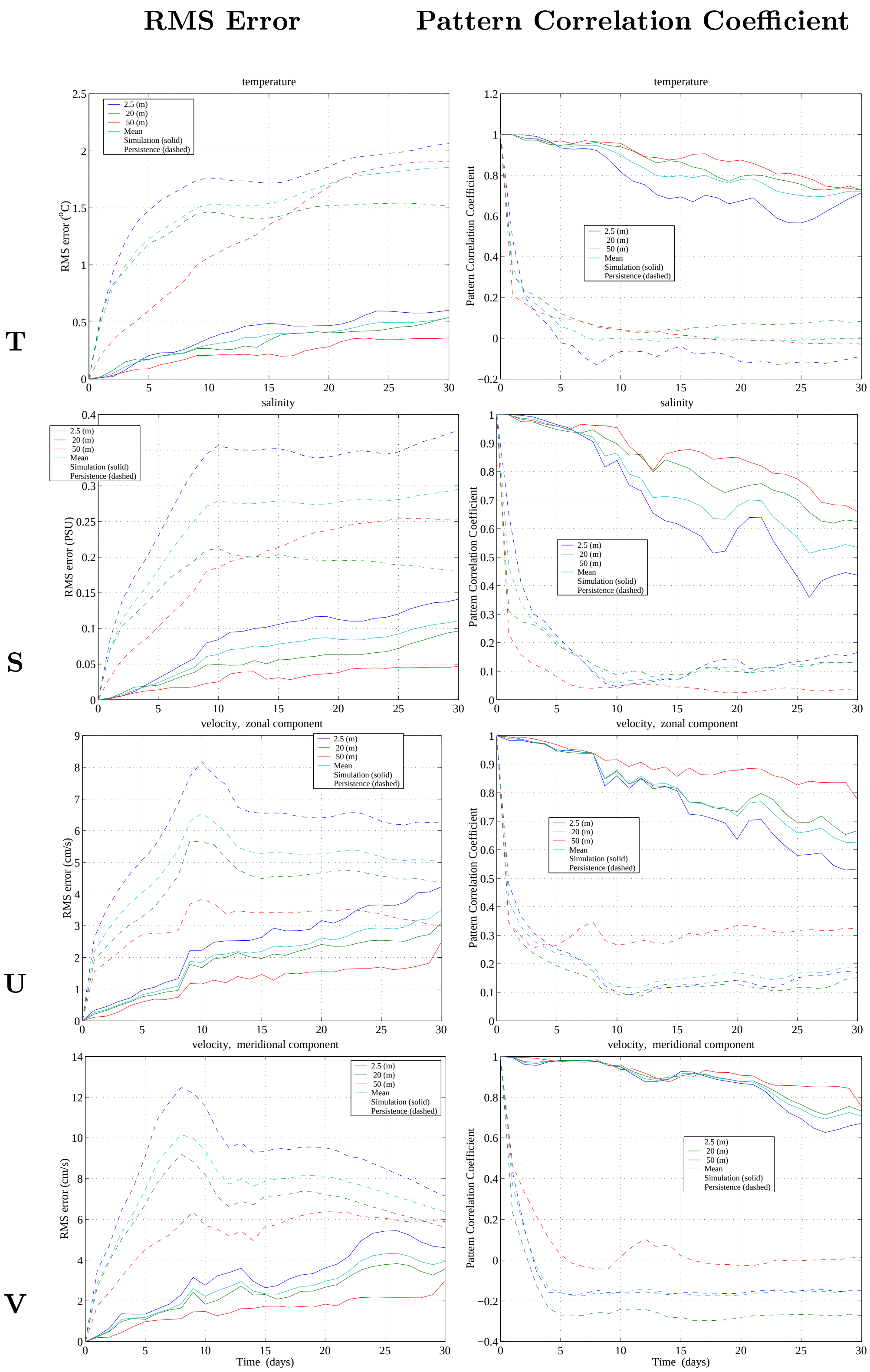


Figure 18: Comparison of baseline run *(i)* versus alternate 6 point flux algorithm with Asselin filter ($\nu$=0.003) *(iv)*

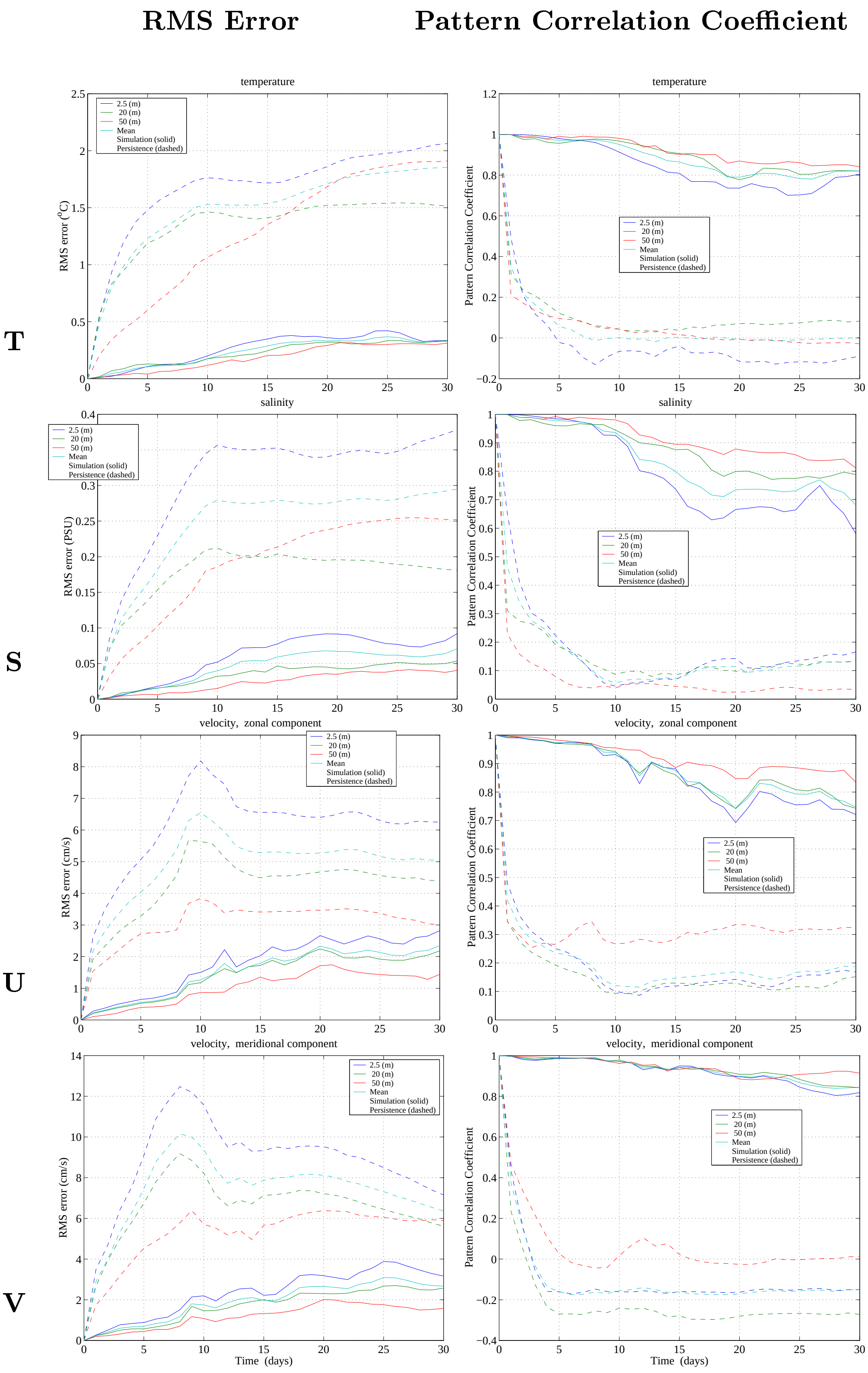


Figure 19: Comparison of baseline run *(i)* versus alternate 6 point flux algorithm with Asselin filter ($\nu$=0.01) *(iv)*

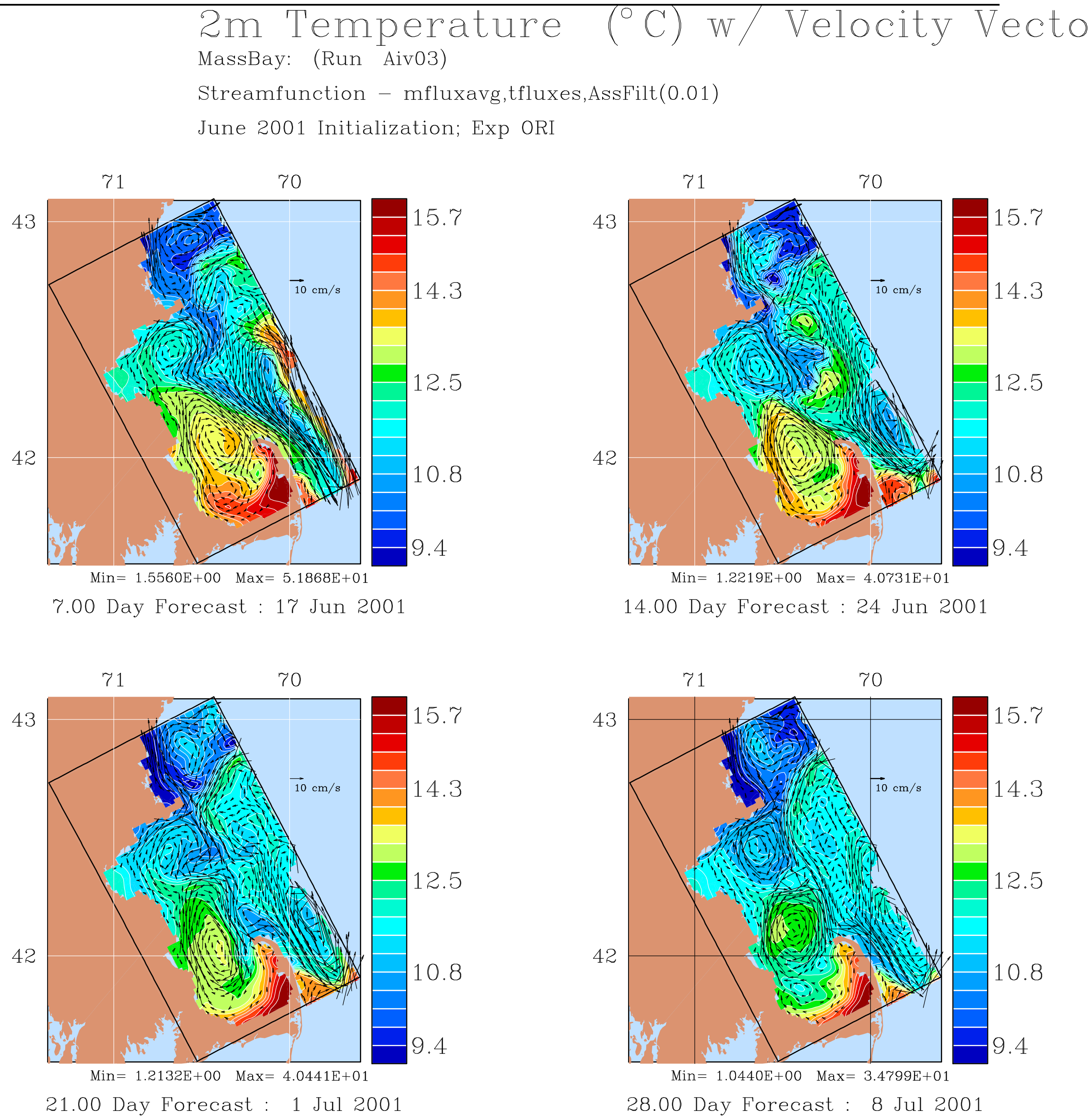


Figure 20 : Alternate pressure formulation momentum fluxes with Asselin filter (CPP options `mfluxavg`, `tfluxes` & `AsselinFilt` with $\nu$=0.01). Near surface temperature with total velocity vectors.

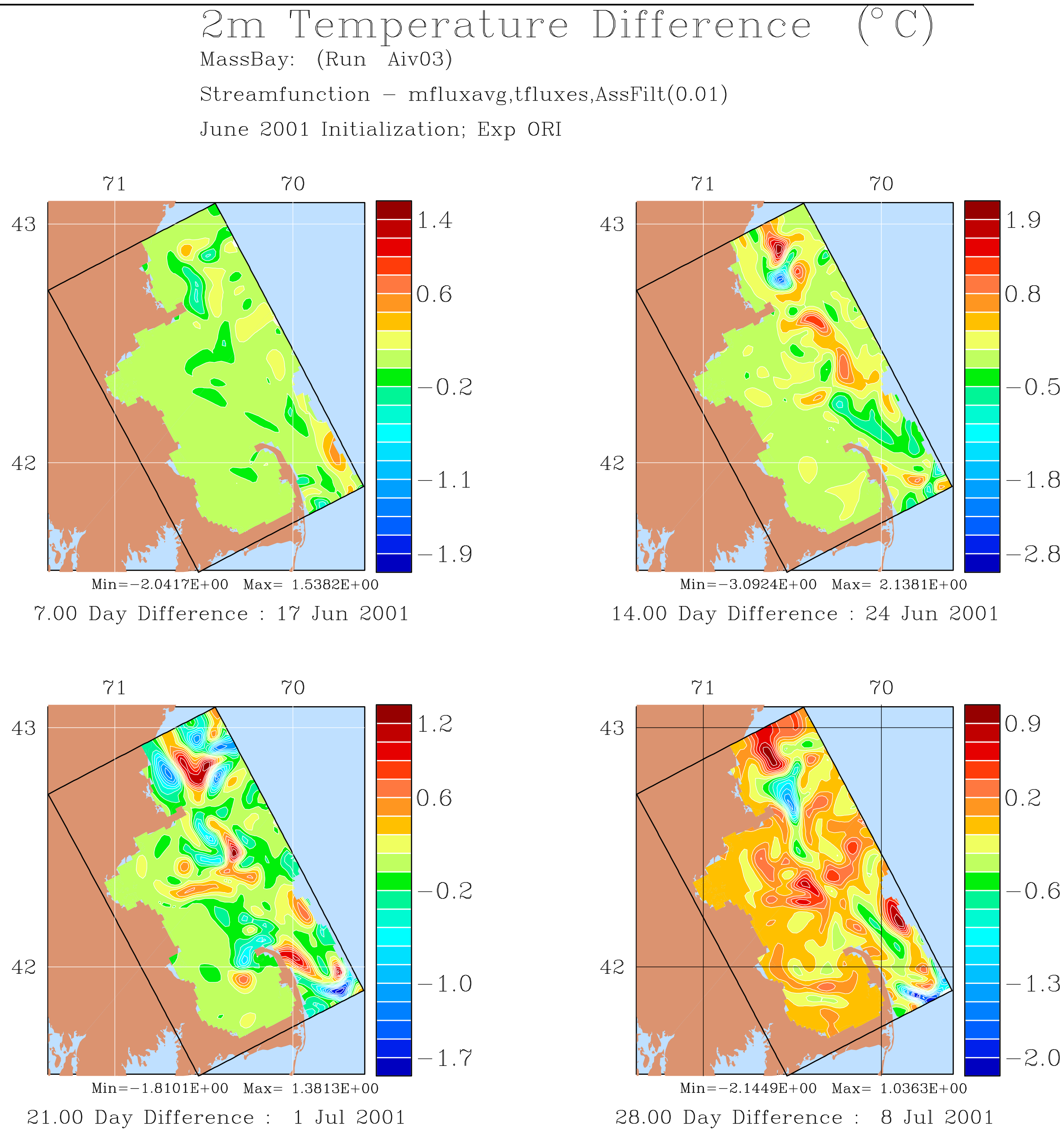


Figure 21 : Near Surface comparison of baseline simulation to simulation with alternate pressure formulation momentum fluxes with Asselin filter (CPP options `mfluxavg`, `tfluxes` & `AsselinFilt` with $\nu$=0.01).

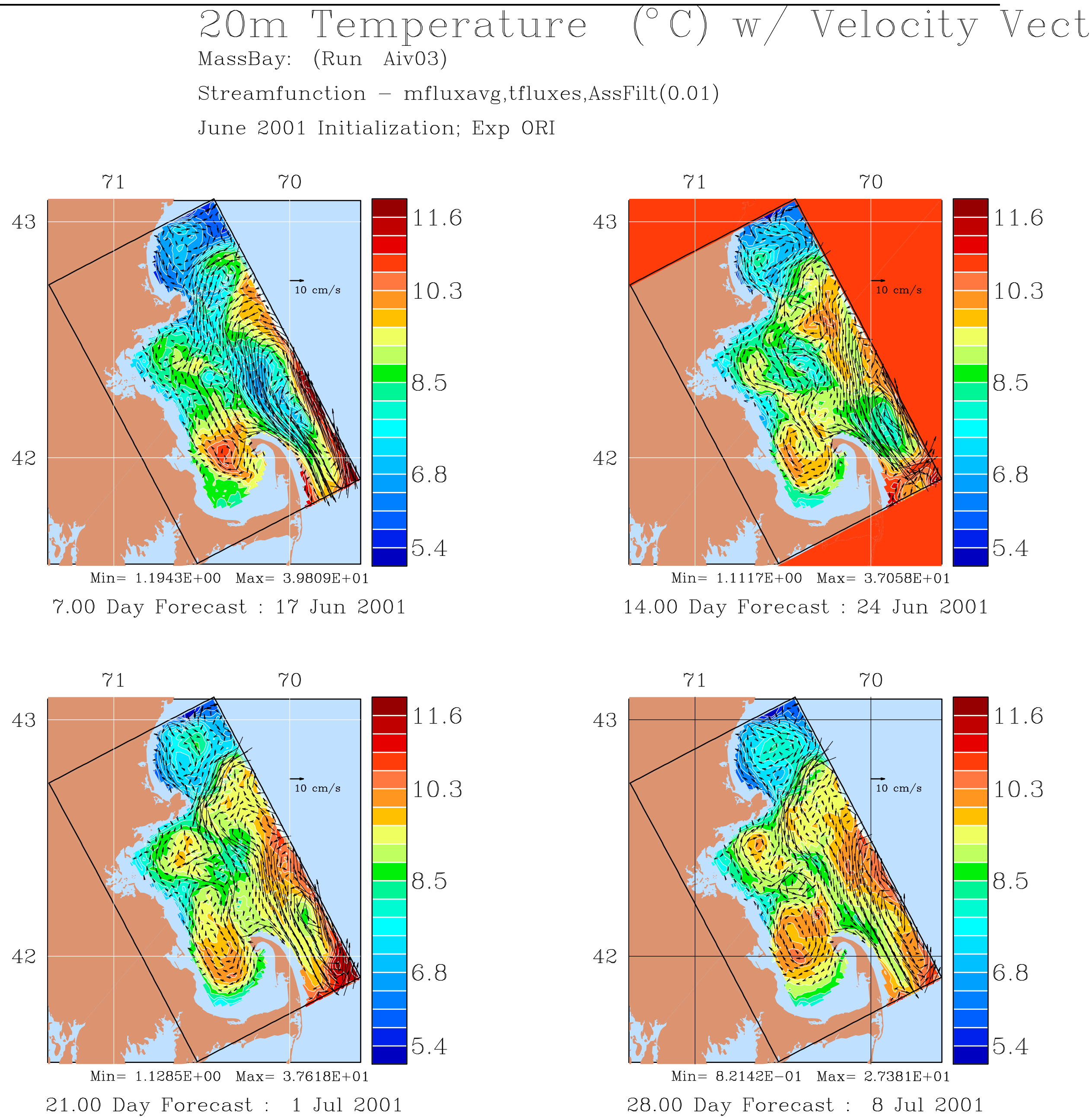


Figure 22 : Alternate pressure formulation momentum fluxes with Asselin filter (CPP options `mfluxavg`, `tfluxes` & `AsselinFilt` with $\nu$=0.01). Mid–level temperature with total velocity vectors.

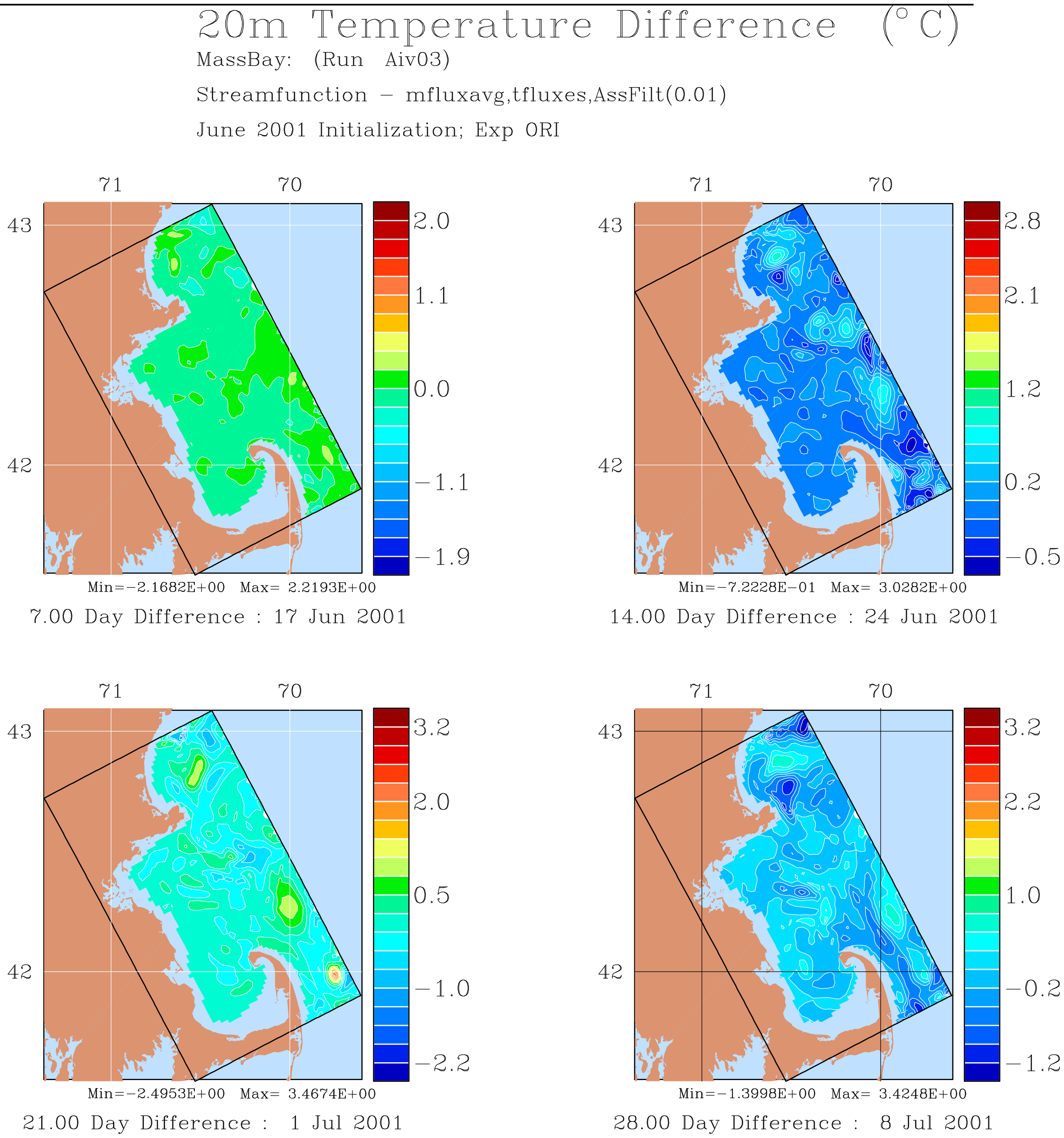


Figure 23 : Mid–level comparison of baseline simulation to simulation with alternate pressure formulation momentum fluxes with Asselin filter (CPP options `mfluxavg`, `tfluxes` & `AsselinFilt` with $\nu$=0.01).

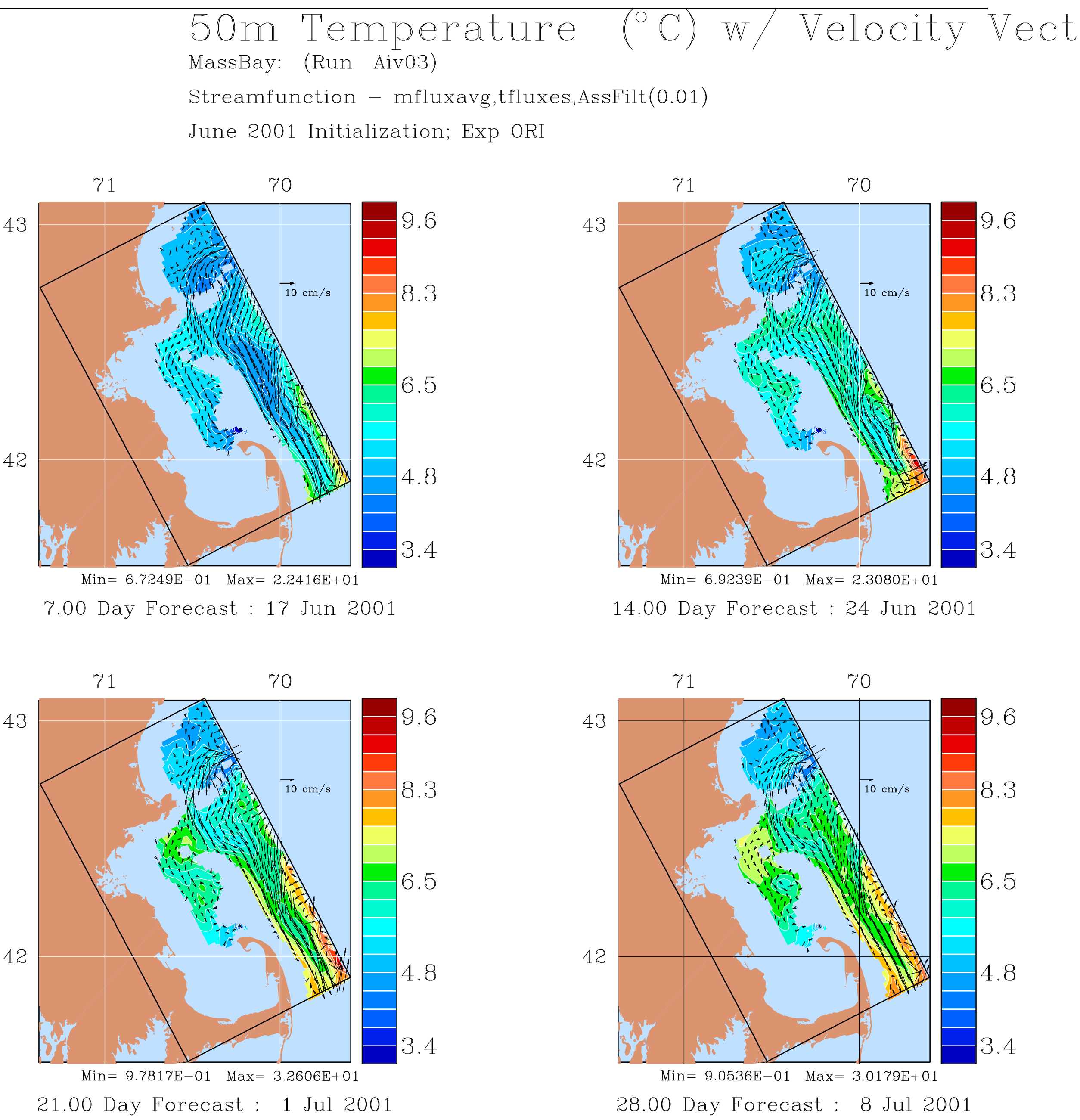


Figure 24 : Alternate pressure formulation momentum fluxes with Asselin filter (CPP options `mfluxavg`, `tfluxes` & `AsselinFilt` with $\nu$=0.01). Deep temperature with total velocity vectors.

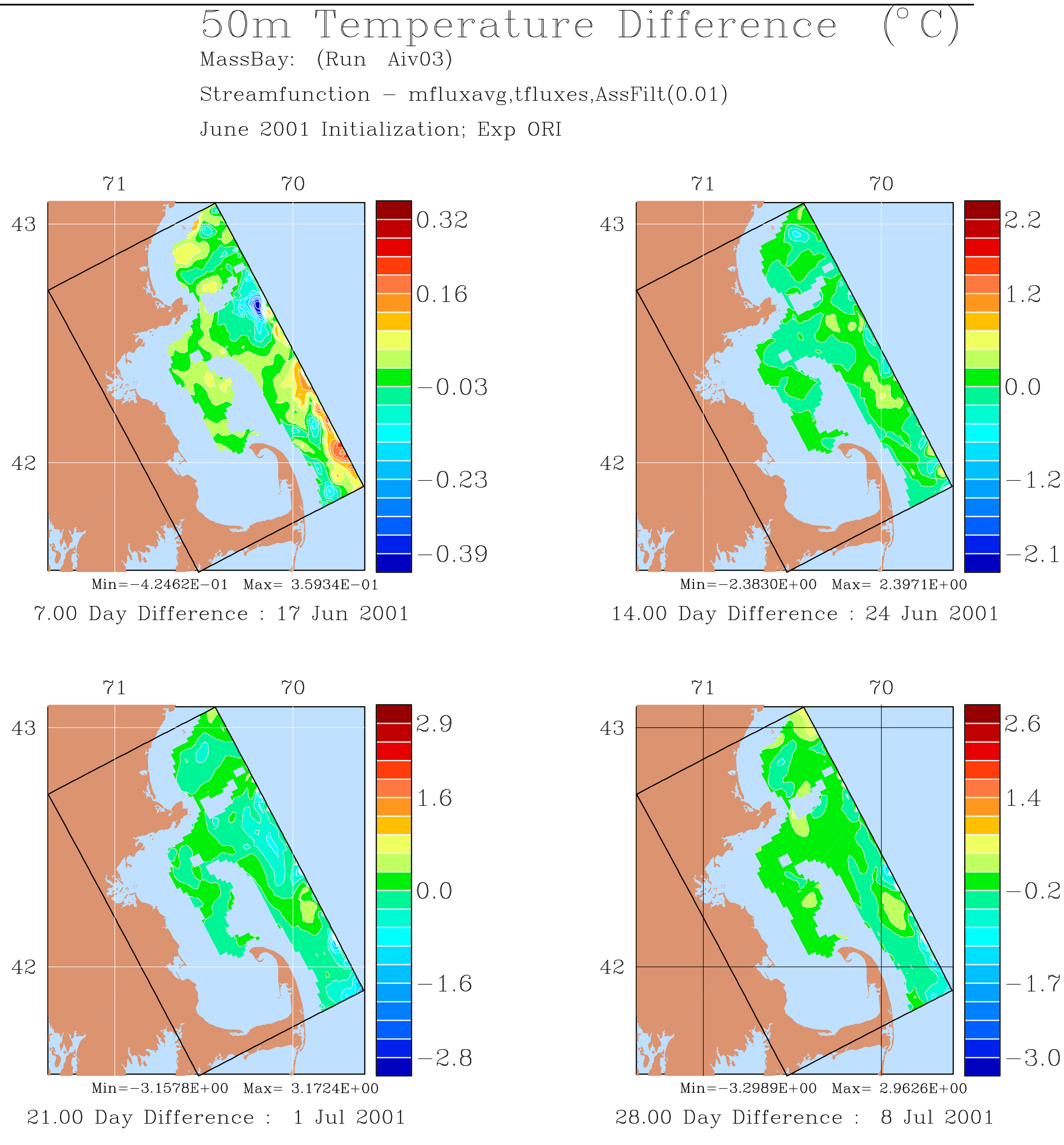


Figure 25 : Deep comparison of baseline simulation to simulation with alternate pressure formulation momentum fluxes with Asselin filter (CPP options `mfluxavg`, `tfluxes` & `AsselinFilt` with $\nu$=0.01).

Table 1: Preconditioning parameter study study for the streamfunction Poisson equation. This example uses left preconditioning and a random field initial guess.

- Unpreconditioned run time: 0.753 (s)

**Speed–up factors**

| *fill* \ $\tau_{\text{small}}$ | $10^{-2}$ | $10^{-3}$ | $10^{-4}$ | $10^{-5}$ | $10^{-6}$ |
|---|---|---|---|---|---|
| **5** | 0.429 | 1.19 | 1.19 | 1.18 | 1.18 |
| **10** | 2.29 | 3.57 | 3.44 | 3.35 | 3.29 |
| **15** | 2.29 | 3.90 | 3.45 | 3.33 | 3.10 |
| **20** | 2.31 | 3.82 | 3.40 | 3.24 | 3.07 |
| **25** | 2.27 | 4.06 | 3.29 | 2.94 | 2.80 |
| **30** | 2.28 | 4.07 | 3.26 | 2.80 | 2.72 |
| **40** | 2.36 | 4.07 | 3.12 | 2.59 | 2.37 |
| **50** | 2.31 | 4.10 | 3.26 | 2.77 | 2.52 |
| **75** | 2.38 | 4.14 | 3.22 | 2.78 | 2.49 |
| **100** | 2.36 | 4.18 | 3.12 | 2.65 | 2.46 |

- Unpreconditioned iteration count: 504

**Number of iterations to converge**

| *fill* \ $\tau_{\text{small}}$ | $10^{-2}$ | $10^{-3}$ | $10^{-4}$ | $10^{-5}$ | $10^{-6}$ |
|---|---|---|---|---|---|
| **5** | 374 | 127 | 127 | 127 | 127 |
| **10** | 50 | 25 | 25 | 25 | 25 |
| **15** | 50 | 17 | 17 | 17 | 17 |
| **20** | 50 | 15 | 12 | 12 | 12 |
| **25** | 50 | 14 | 10 | 10 | 10 |
| **30** | 50 | 14 | 8 | 8 | 8 |
| **40** | 50 | 14 | 8 | 6 | 5 |
| **50** | 50 | 14 | 8 | 5 | 4 |
| **75** | 50 | 14 | 8 | 5 | 4 |
| **100** | 50 | 14 | 8 | 5 | 4 |

*(v)* add Pre–conditioned Conjugate Gradient solver. Compare both solutions and timings.

To more easily and efficiently implement the new Poisson problem for the surface pressure formulation, Lozano & Lanerolle have introduced a sparse matrix, preconditioned conjugate gradient solver (SparsKit).

The first step in using the pre–conditioned conjugate gradient solver is to tune the pre–conditioning parameters. For this experiment, the software to explore the choices in the surface pressure formulation was upgraded to work with the streamfunction formulation. The overall results were identical to those in the surface pressure formulation test in $P^2S^3$.

- The choice of initial guess does **not** greatly affect the speed–up.
- Left pre-conditioning is generally more effective than right pre-conditioning.

The specifics here are:

(1) Balancing the speed–up with economy (program storage requirements), the following pre-conditioning parameters were chosen.
- Left pre-conditioning
- Small value tolerance, $\tau_{\text{small}}$, of $10^{-3}$
- Fill–in bandwidth, $fill$, of 25.

(2) The apparent cost penalty is even more evident here than in the surface pressure $\mathrm{P}^2\mathrm{S}^3$ tunings. The iteration count is reduced by factors of 10–100 while the speed–up peaks at a factor of 4.

Comparing the cumulative PE timings for the Poisson solver over the 30 day simulation:

- Standard HOPS conjugate gradient: 0:12:25.2124 (7%)
- New preconditioned conjugate gradient: 0:20:12.4983 (12%)

This is somewhat less of a penalty than in $\mathrm{P}^2\mathrm{S}^3$ which may suggest that a better ability to explore the pre-conditioning parameter space could have improved the $\mathrm{P}^2\mathrm{S}^3$ run–time.

The kinetic energy reasonably tracks *(Aiv)*, except for an excursion around day 18. The RMS and PCC statistics are generally similar to *(Aiv)*. In the surface flow, the northern gyre in Massachusetts Bay is getting pinched by MCC inflow, relative to the previous simulations. This intrusion is also evident in the mid–level flows. Otherwise the flow fields are very similar to *(Aiv)*. The main temperature differences occur external to the Bay, over Stellwagen Bank and off Race Point. There are more secondary difference patterns in the Bay proper than in previous simulations.

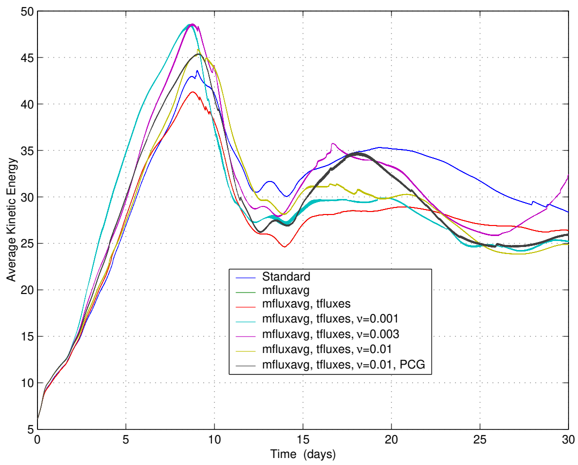


Figure 26 : Kinetic Energy comparison between simulations *(Ai)* – *(Av)*. Also examining the effects of changing Asselin filter parameter $\nu$.

**RMS Error** **Pattern Correlation Coefficient**

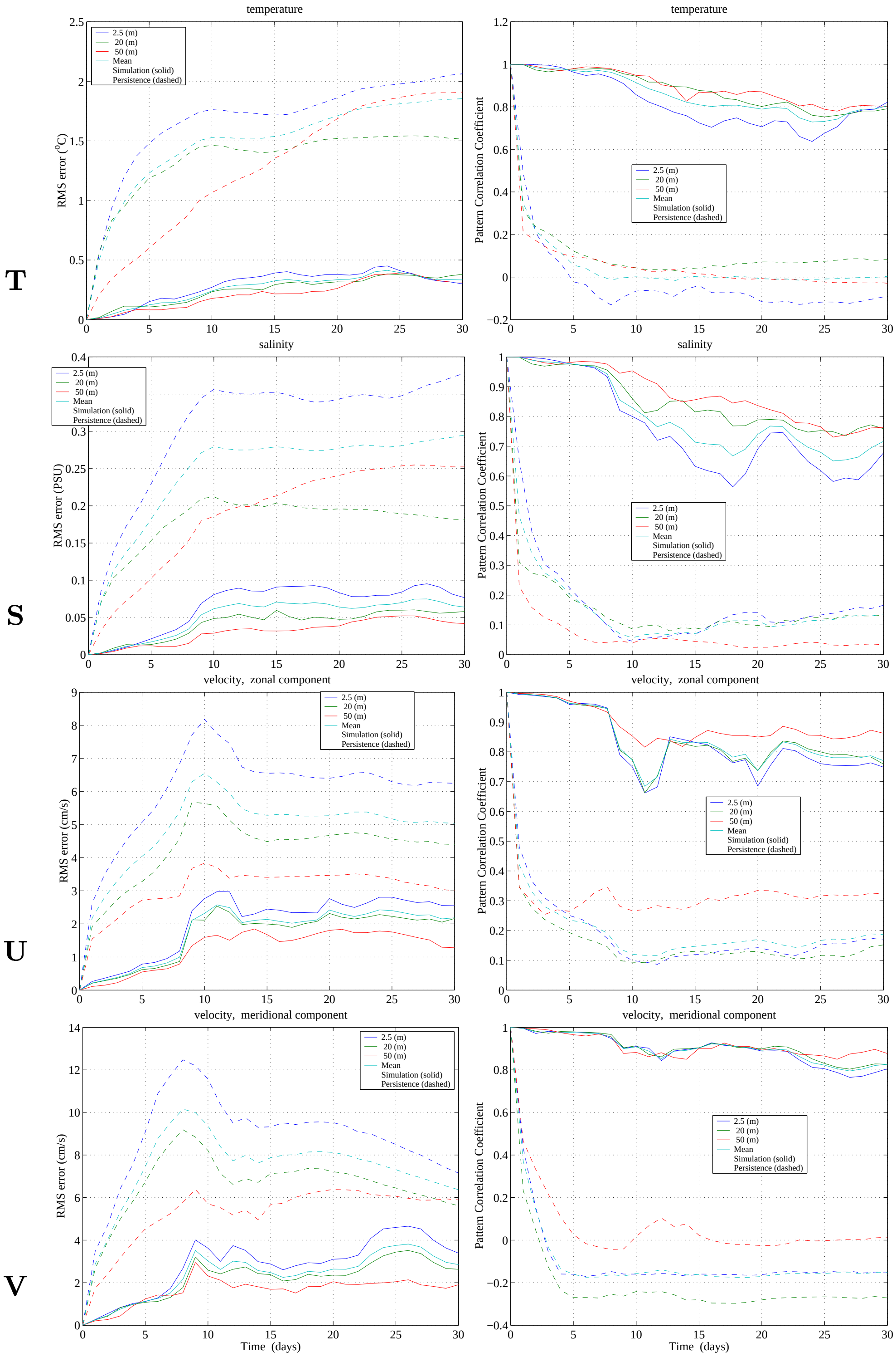


Figure 27: Comparison of baseline run *(i)* versus alternate 6 point flux algorithm with Asselin filter ($\nu$=0.01) and Pre–Conditioned Conjugate Gradient solver *(v)*

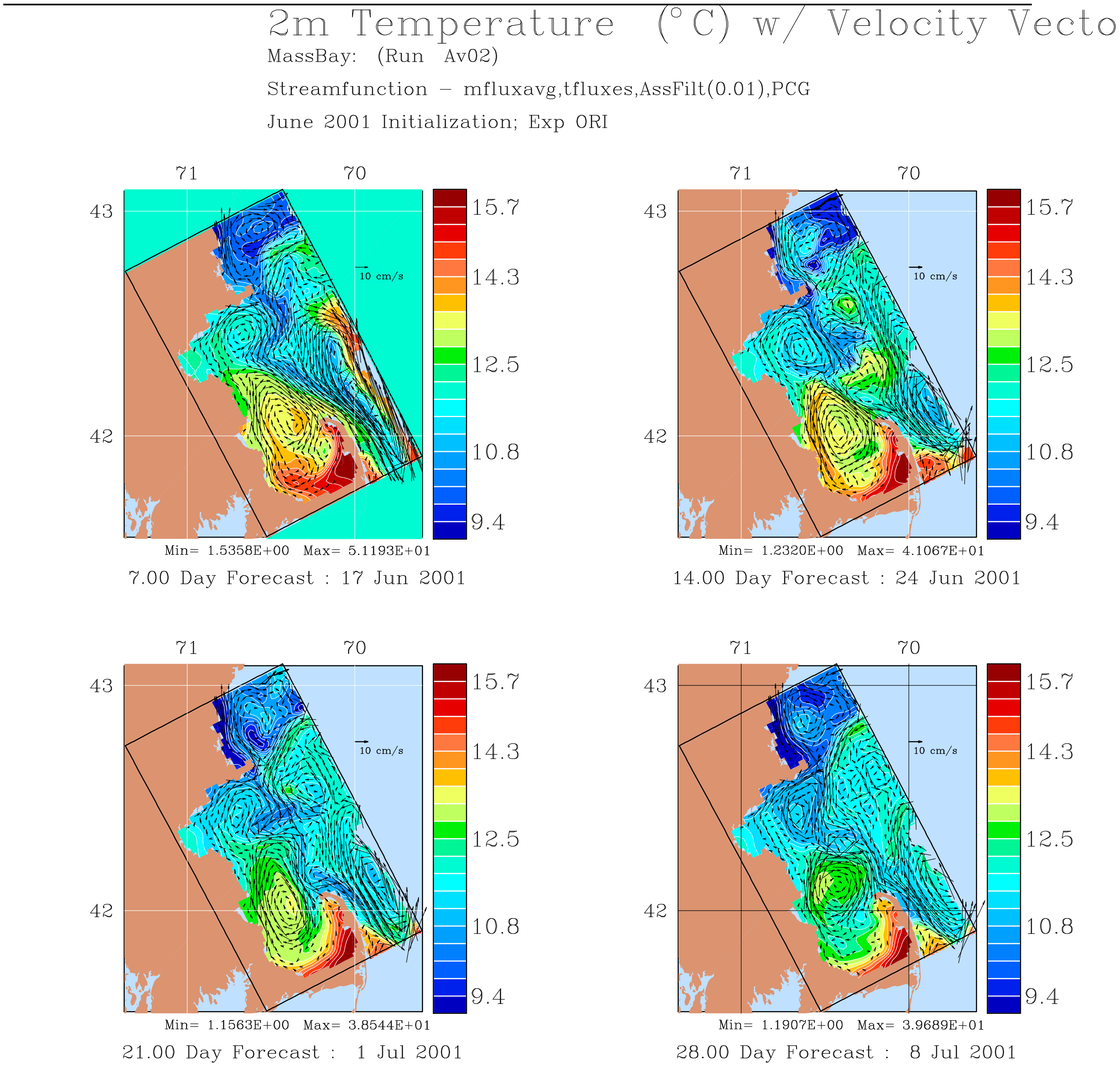


Figure 28 : Alternate pressure formulation momentum fluxes with Asselin filter & pre–conditioned conjugate gradient solver (CPP options `mfluxavg`, `tfluxes`, `AsselinFilt` with $\nu$=0.01 & `pcg5`). Near surface temperature with total velocity vectors.

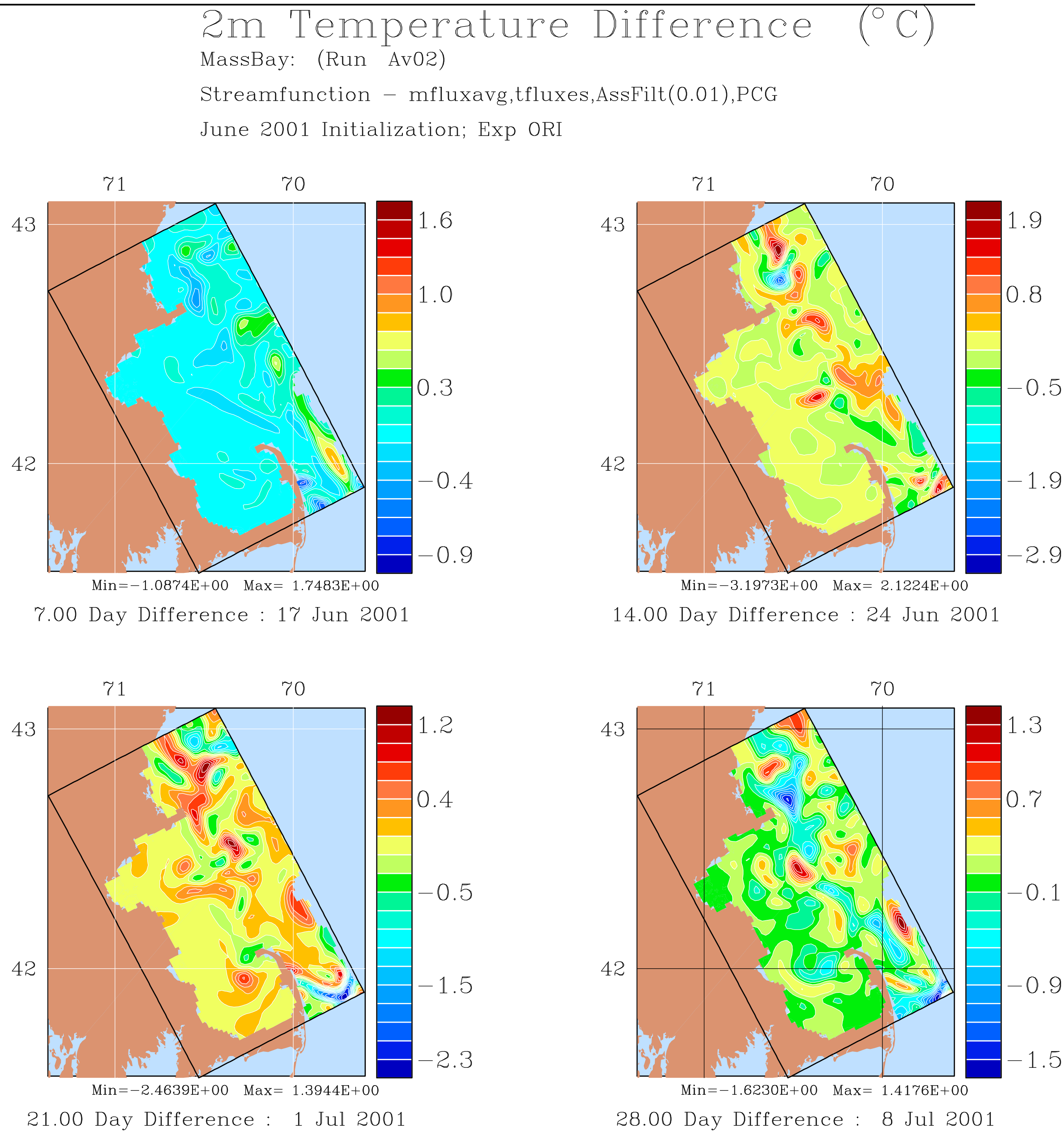


Figure 29 : Near Surface comparison of baseline simulation to simulation with alternate pressure formulation momentum fluxes with Asselin filter & pre–conditioned conjugate gradient solver (CPP options `mfluxavg`, `tfluxes`, `AsselinFilt` with $\nu$=0.01 & `pcg5`).

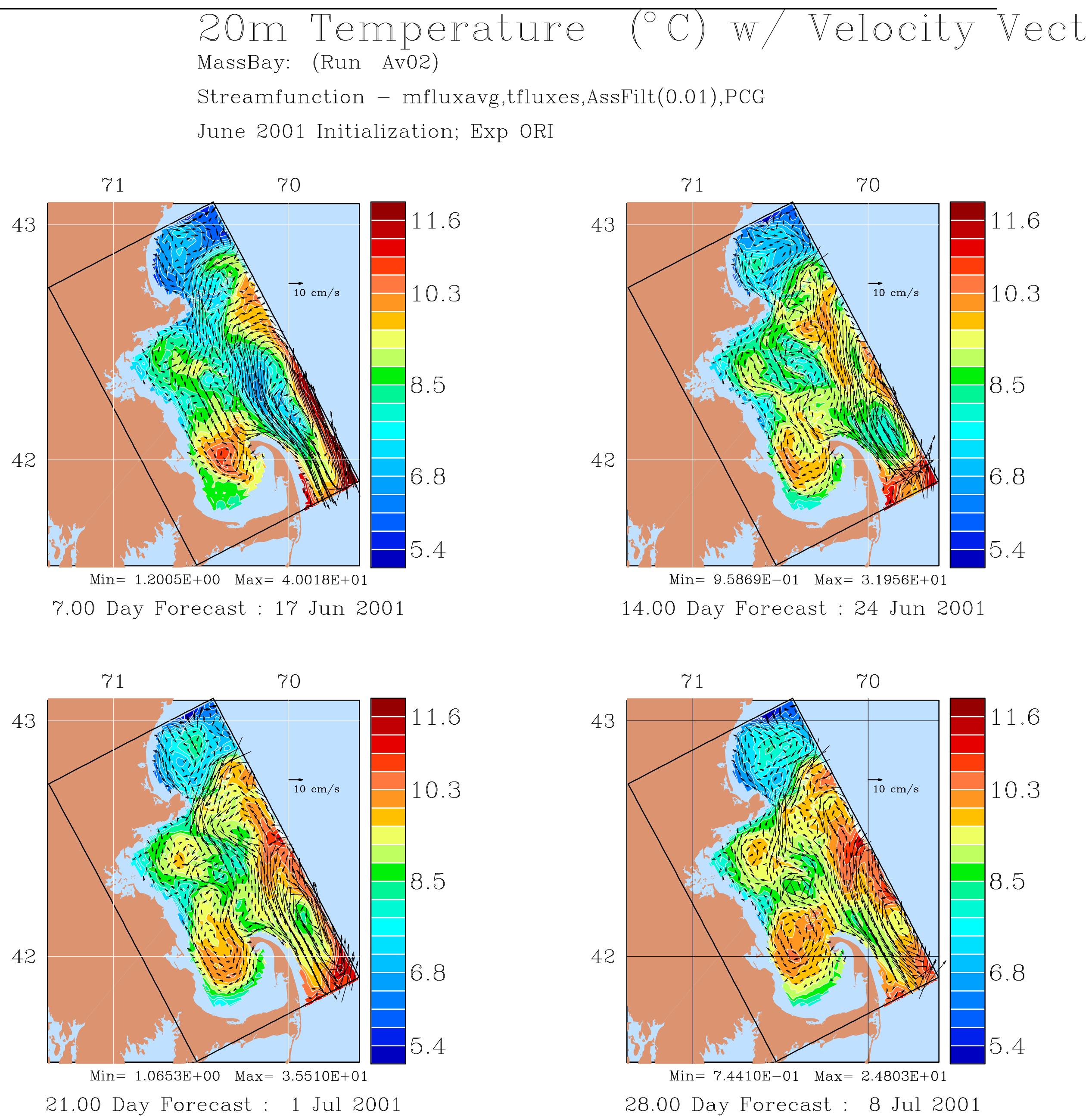


Figure 30 : Alternate pressure formulation momentum fluxes with Asselin filter & pre–conditioned conjugate gradient solver (CPP options `mfluxavg`, `tfluxes`, `AsselinFilt` with $\nu$=0.01 & `pcg5`). Mid–level temperature with total velocity vectors.

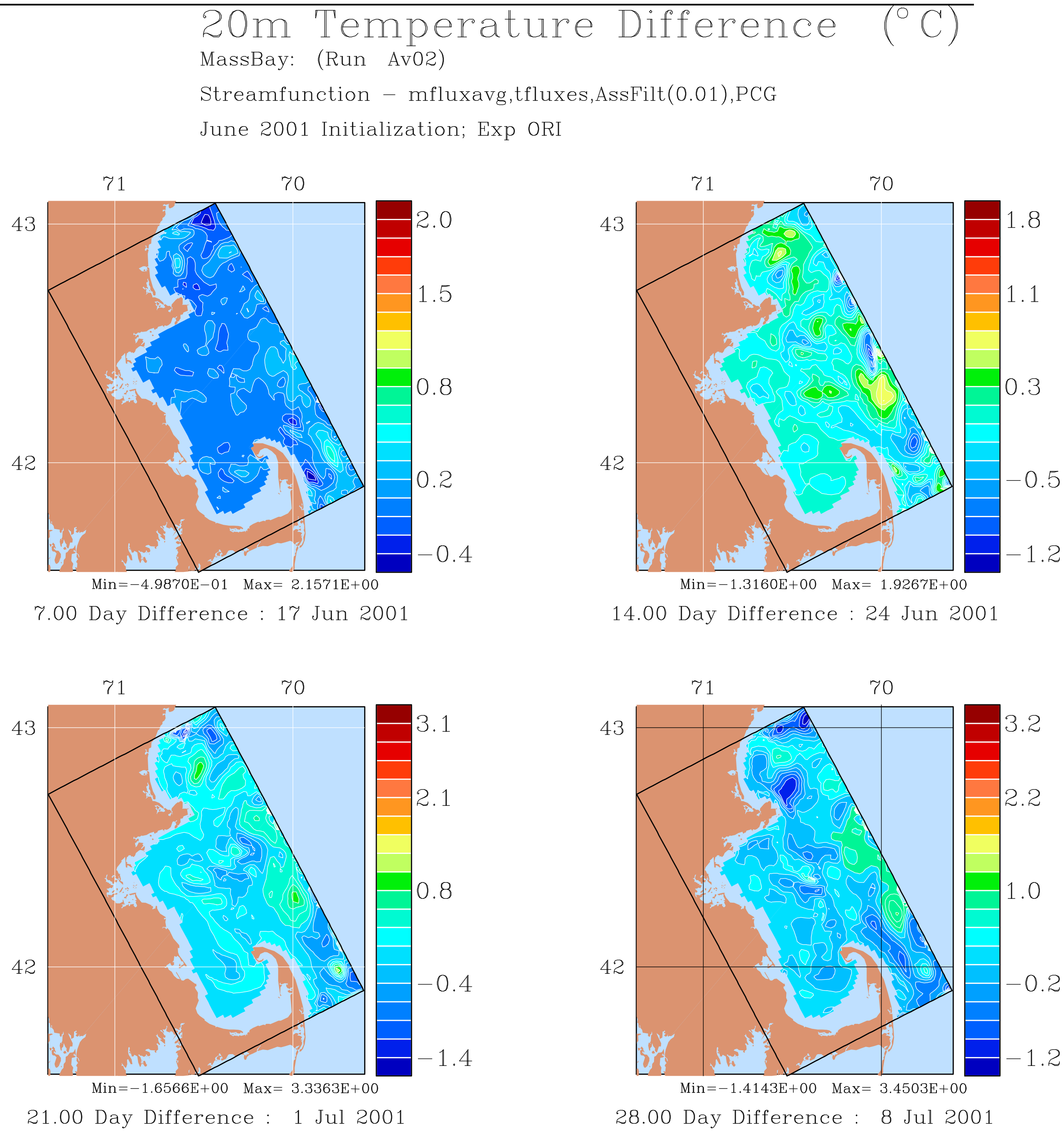


Figure 31 : Mid–level comparison of baseline simulation to simulation with alternate pressure formulation momentum fluxes with Asselin filter & pre–conditioned conjugate gradient solver (CPP options `mfluxavg`, `tfluxes`, `AsselinFilt` with $\nu$=0.01 & `pcg5`).

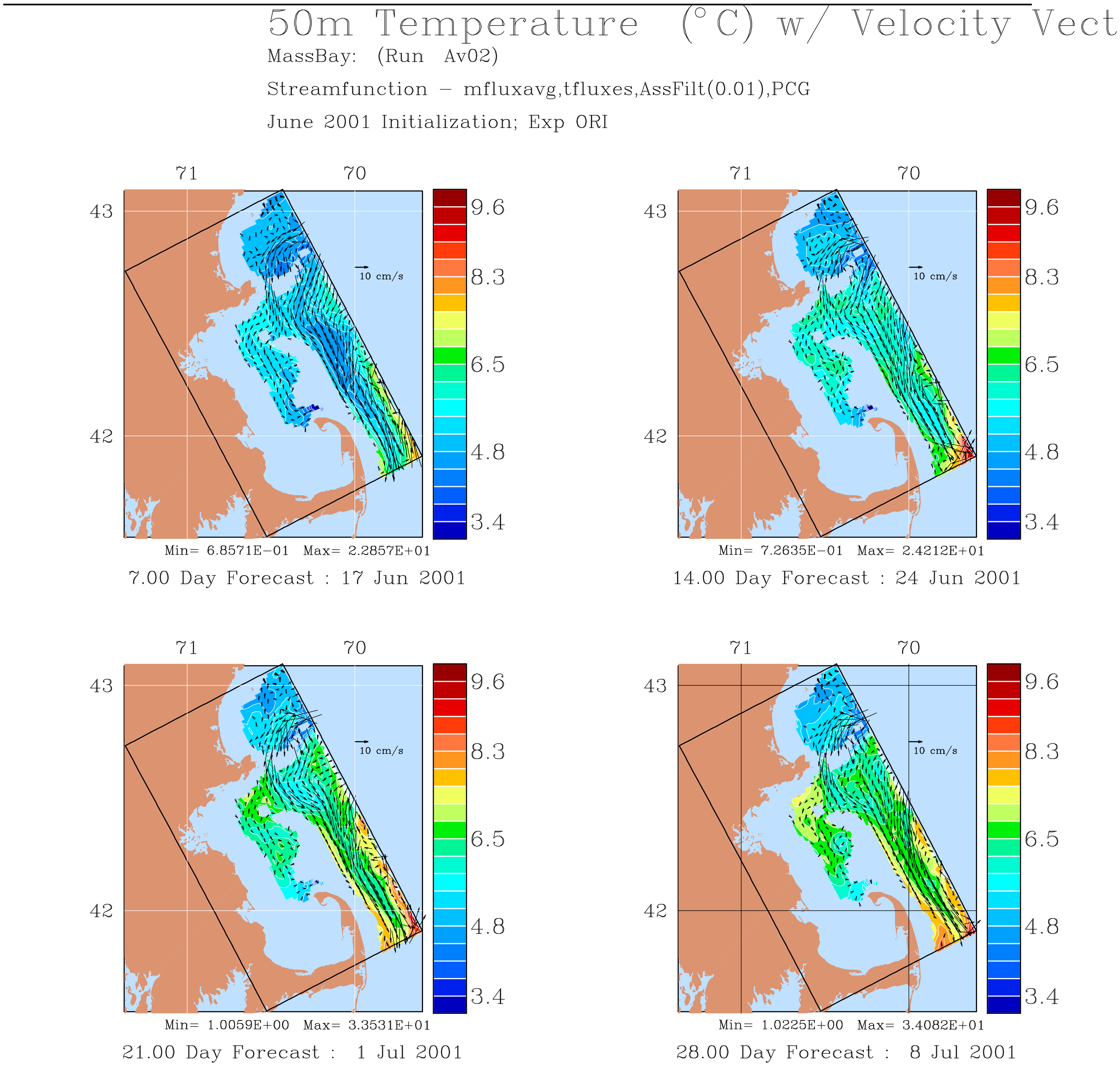


Figure 32 : Alternate pressure formulation momentum fluxes with Asselin filter & pre–conditioned conjugate gradient solver (CPP options `mfluxavg`, `tfluxes`, `AsselinFilt` with $\nu$=0.01 & `pcg5`). Deep temperature with total velocity vectors.

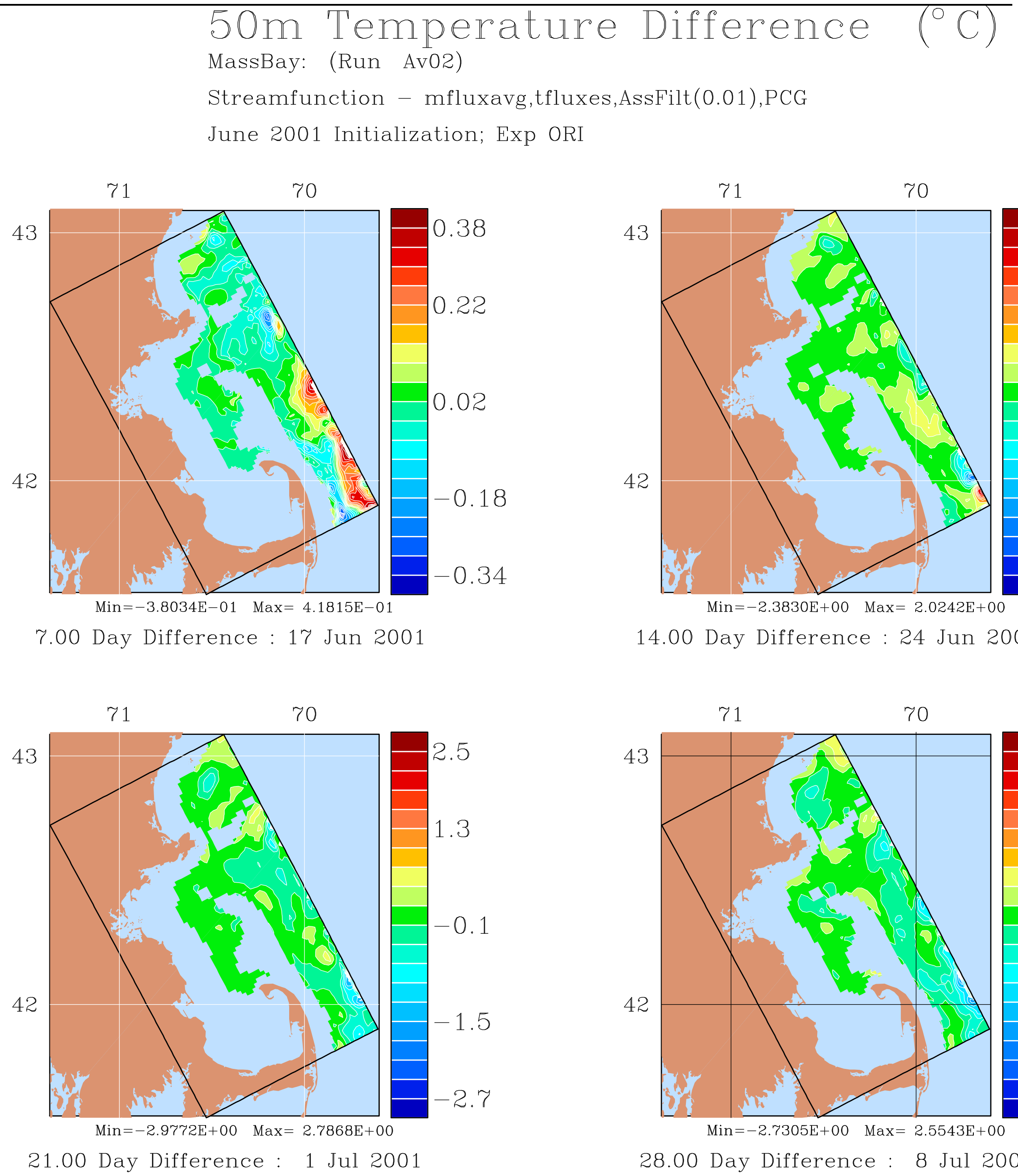


Figure 33 : Deep comparison of baseline simulation to simulation with alternate pressure formulation momentum fluxes with Asselin filter & pre–conditioned conjugate gradient solver (CPP options `mfluxavg`, `tfluxes`, `AsselinFilt` with $\nu$=0.01 & `pcg5`).

*(B) Surface Pressure formulation – Rigid Lid*

Initialization Procedure

The construction of initial conditions for the surface pressure has been discussed in the $P^2S^3$ test. We merely proceed here with the comparison of the various options.

*(i)* Surface Streamfunction (`psurf` = 0)
*(ii)* Surface Streamfunction & Velocity (`psurf` = 1)
*(iii)* Surface Streamfunction & the Barotropic Equation (`psurf` = 1 & CPP option `bctest2`)
*(iv)* Smooth Approximation (`psurf` = 2)

A discussion, which has been delayed until now, is the assurance of continuity, in the presence of land masks, of the integrated boundary conditions *(ii)* & *(iii)*. Figure 34 (to the right) presents a simplified diagram of the issue, in which the boundary values of the surface pressure are denoted by $\mathrm{Ps}_i$ and the estimated values of the tangential derivatives of surface pressure between adjacent boundary nodes are denoted by $\mathrm{f}_i$. These estimated values come from $P^2S^3$ equation (5) for case *(ii)* or $P^2S^3$ equation (4) for case *(iii)*. The method for constructing the boundary values is:

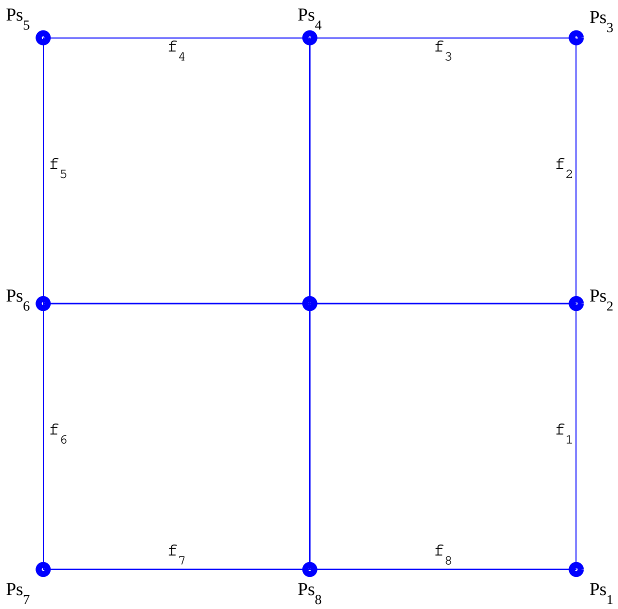


(1) Assign an arbitrary value for the first point $\mathrm{Ps}_1$
(2) Numerically integrate the tangential derivatives along the boundary.

$$\hat{P}s_i = \begin{cases} Ps_1 + \alpha_1 f_1\, \delta\mathcal{S}_1 & i = 2 \\ \hat{P}s_{i-1} + \alpha_{i-1} f_{i-1}\, \delta\mathcal{S}_{i-1} & 3 \leq i \leq N \end{cases}$$

where $\alpha_i$ is $\pm 1$ depending on whether the local direction of integration agrees with the local direction of the tangential derivative and $\delta\mathcal{S}_i$ is the length element.

(3) Construct a correction function. First compute a second estimate of the value at point 1 by continuing step (2).

$$\hat{P}s_1 = \hat{P}s_N + \alpha_N f_N\, \delta\mathcal{S}_N$$

In general $\hat{P}s_1 \neq Ps_1$. A correction function, proportional to the local magnitude of the tangential derivative, is obtained from

$$\delta Ps_i = \frac{Ps_1 - \hat{P}s_1}{\sum_{j=1}^{N} \|f_j\| \delta\mathcal{S}_j} \|f_i\| \delta\mathcal{S}_i$$

(4) Re–integrate the tangential derivatives, including the correction.

$$Ps_i = Ps_{i-1} + \alpha_{i-1} f_{i-1}\, \delta\mathcal{S}_{i-1} + \delta Ps_{i-1} \quad 2 \leq i \leq N$$

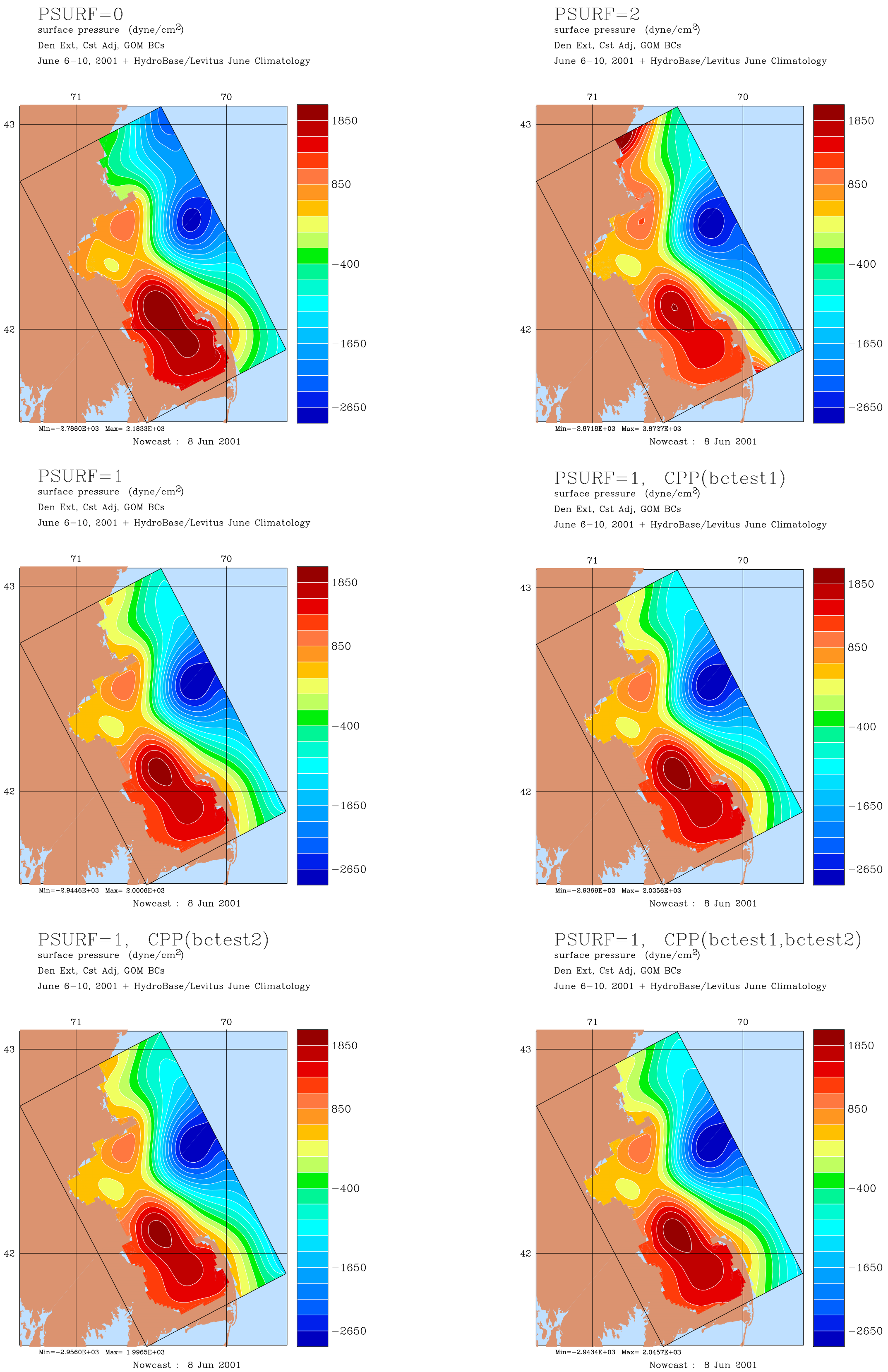


Figure 35 : Comparison of surface pressure initialization schemes in the coastal ocean.

The issue of the land mask comes about in assigning sensible values of $f_i$ under the mask. For the transport streamfunction case these values are set to zero, giving a constant value for the transport streamfunction under the mask and along the coast. For the surface pressure case, no such simple constraint exists on the tangential derivatives. As a result, the default action of `PE_initial` in the presence of land is to ignore the correction algorithm (steps 3 & 4). A CPP option `bctest1` was included to force this correction, arbitrarily assigning zero to values of $f_i$ under the mask.

A comparison of these initialization schemes is presented in figure 35. The first first row contains the results of the cases without boundary conditions derived from integration *(i)* & *(iv)*. The second row contains case *(ii)*, both standard and with the correction algorithm. The third row contains case *(iii)*, both standard and with the correction algorithm. The first observation is all schemes produce similar gross features. Case *(iv)* produces spurious highs at the ends of the coastlines. In fact, if the plotting package is allowed to select the contours, these highs become the dominant features. Looking at cases *(ii)* & *(iii)* without the correction algorithm in the southeast corner shows the surface pressure pinching in the corner. This is expected as the integration algorithm arbitrarily starts in the southeast corner. The other three initializations are suitable candidates for testing in the PE model.

Tuning Preconditioning Parameters

The tuning of the pre-conditioning parameters for conjugate gradient solver proceeded as in $P^2S^3$. The resulting statistics are briefly presented in table 2.

The general observations of this study are the same as in $P^2S^3$:

- The choice of initial guess does **not** greatly affect the speed–up.
- Left pre-conditioning is generally more effective than right pre-conditioning.

Balancing the speed–up with economy (program storage requirements), the following pre-conditioning parameters were chosen.

- Left pre-conditioning
- Small value tolerance, $\tau_{\text{small}}$, of $10^{-4}$
- Fill–in bandwidth, $fill$, of 20.

The pre–conditioning speeds up the solver by a factor of 4–5 but the number of iterations is reduced by a factor of 20–100. This reinforces the notion of a significant cost associated with pre-conditioning.

*(i)* Surface pressure initialization. (`psurf` = 0)

**PE Run Parameters**

| | **Shapiro Filter** | **BC** |
|---|---|---|
| $P_s$ | 16 1 1 | Orlanski |
| **RHS** | | Constant Extrapolation |
| $\hat{U}$ | 2 2 1 | |

The rigid–lid surface pressure simulations used identical parameters to the streamfunction *(v)* simulation with the parameters at right, chosen by sensitivity studies, and the semi-implicit coriolis parameter set to `0.5` according to Lyon's stability analyses. The parameters in the table were tuned in case *(iii)* to bring about the greatest similarity between the surface pressure formulation

Table 2: Preconditioning parameter study for the surface pressure Poisson equation. This example uses left preconditioning and a random field initial guess.

- Unpreconditioned run time: 1.42 (s)

**Speed–up factors**

| *fill* \ $\tau_{\text{small}}$ | $10^{-2}$ | $10^{-3}$ | $10^{-4}$ | $10^{-5}$ | $10^{-6}$ |
|---|---|---|---|---|---|
| **5** | 4.283E-02 | 4.180E-02 | 4.155E-02 | 4.121E-02 | 4.136E-02 |
| **10** | 3.589E-02 | 2.808E-02 | 2.793E-02 | 2.760E-02 | 2.760E-02 |
| **15** | 3.562E-02 | 4.11 | 5.85 | 5.58 | 5.31 |
| **20** | 3.562E-02 | 5.49 | 6.59 | 5.21 | 4.76 |
| **25** | 3.554E-02 | 5.71 | 6.25 | 5.68 | 4.74 |
| **30** | 3.564E-02 | 5.70 | 6.54 | 6.20 | 5.13 |
| **40** | 3.563E-02 | 5.65 | 6.54 | 6.18 | 4.90 |
| **50** | 3.571E-02 | 5.69 | 6.69 | 6.06 | 4.85 |
| **75** | 3.583E-02 | 5.67 | 6.65 | 6.17 | 4.91 |
| **100** | 3.570E-02 | 5.85 | 6.67 | 6.25 | 4.87 |

- Unpreconditioned iteration count: 718

**Number of iterations to converge**

| *fill* \ $\tau_{\text{small}}$ | $10^{-2}$ | $10^{-3}$ | $10^{-4}$ | $10^{-5}$ | $10^{-6}$ |
|---|---|---|---|---|---|
| **5** | 6000 | 6000 | 6000 | 6000 | 6000 |
| **10** | 6000 | 6000 | 6000 | 6000 | 6000 |
| **15** | 6000 | 29 | 16 | 15 | 15 |
| **20** | 6000 | 19 | 10 | 12 | 12 |
| **25** | 6000 | 18 | 9 | 8 | 8 |
| **30** | 6000 | 18 | 8 | 5 | 5 |
| **40** | 6000 | 18 | 8 | 5 | 4 |
| **50** | 6000 | 18 | 8 | 5 | 4 |
| **75** | 6000 | 18 | 8 | 5 | 4 |
| **100** | 6000 | 18 | 8 | 5 | 4 |

KE and the transport streamfunction formulation KE. Case *(iii)* was chosen since it was the most prone to CFL violations.

The results of the rigid–lid, surface pressure formulation simulation from a "surface streamfunction" initialization are presented in figures 36–44. The kinetic energy (figure 36) shows a sharp divergence from the streamfunction KE, far outside the envelope of the streamfunction KE results (figure 26). This can be expected for a couple of reasons. First, this domain has shallow topography so that the pressure formulation is not expected to mimic the streamfunction formulation results. Second the run parameters were chosen so that case *(Biii)* had its closest match to the streamfunction results. On the plus side, the kinetic energy is bounded and not yet showing signs of run–away growth.

In a similar vein, the skill metric comparison is the worst to date. The tracers still show some favorable skill compared to persistence (except for the surface salinity PCC in the last 2 weeks). The velocity RMS difference is generally larger than persistence. Only the meridional velocity component PCC shows any skill compared to persistence.

The surface velocity fields external to Massachusetts Bay show more coherence, without the questionable strong northward coastal current north of Cape Ann. At the mouth of Mass. Bay, a MCC–type stream is present, skirting the mouth. Interior to Mass. Bay, the northern gyre is suppressed and the southern gyre is squeezed to the west of the MCC-type stream. The surface temperature has a wide spread cooling in the entire region north of Cape Ann and in the descending stream. This is probably the recurring northern boundary issue (from past Mass. Bay simulations) showing up in this simulation.

Similar general observations can be made for the mid–level fields. In addition, the southern Mass. Bay gyre no longer closes at mid–depth and the relative cooling covers virtually the entire domain. The deep fields exhibit similar comparisons as the mid–level fields.

One new feature in this simulation is the noise present in the surface pressure field. The surface pressure is shown in figure 44. The overall pattern is reasonable, but a high frequency fluctuation is superimposed. This was not observed in the jet or $P^2S^3$ simulations. This is probably due to a combination of geometry and dynamics, as geometry alone should have corrupted the initial fields (figure 35).

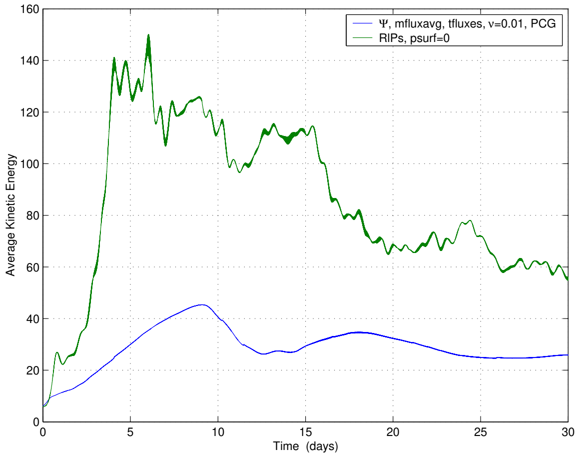


Figure 36 : Kinetic Energy comparison between simulations *(Av)* & *(Bi)*.

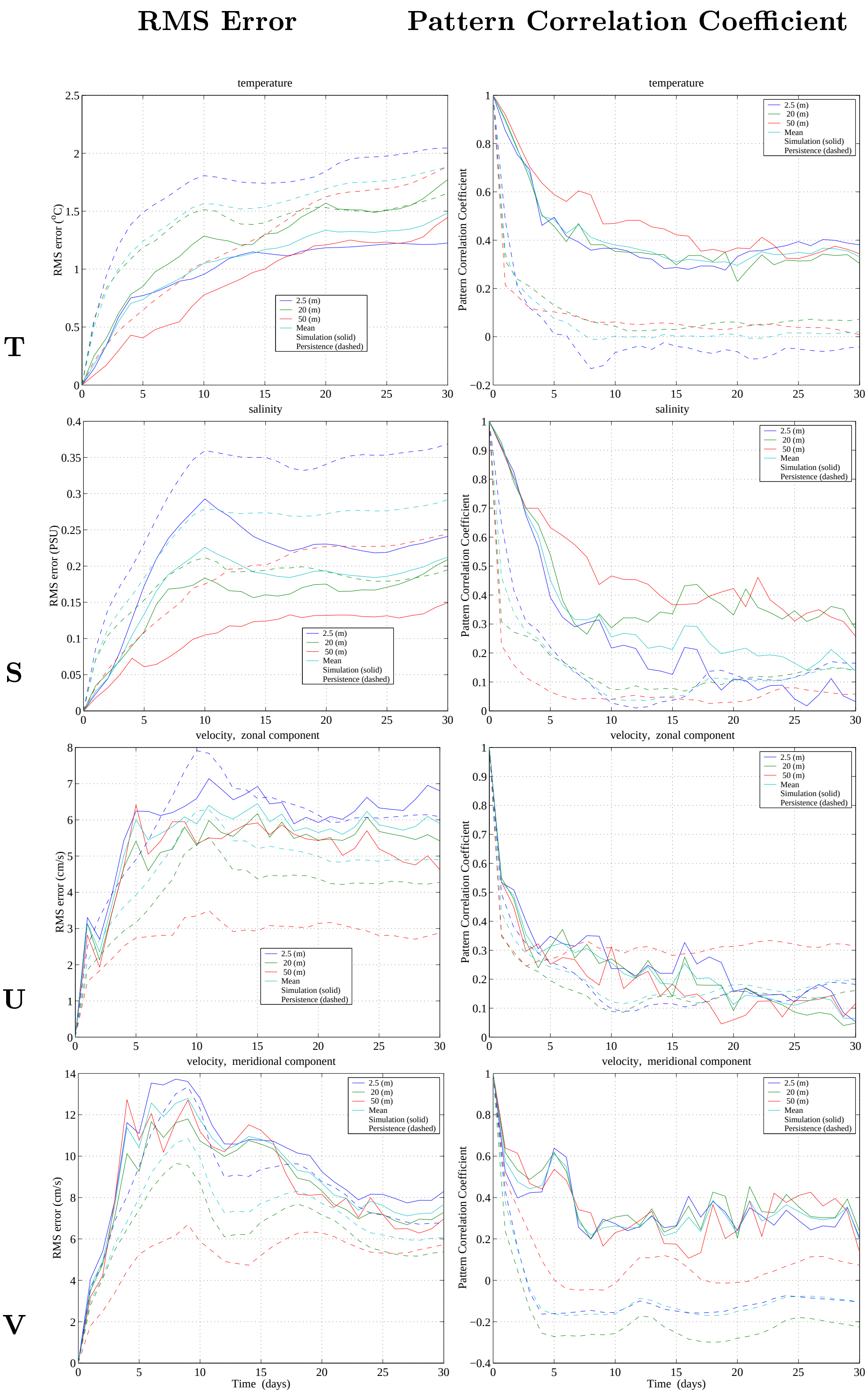


Figure 37: Comparison of most similar streamfunction simulation *(Av)* to rigid–lid, surface pressure formulation simulation from “surface streamfunction” initial conditions *(Bi)*.

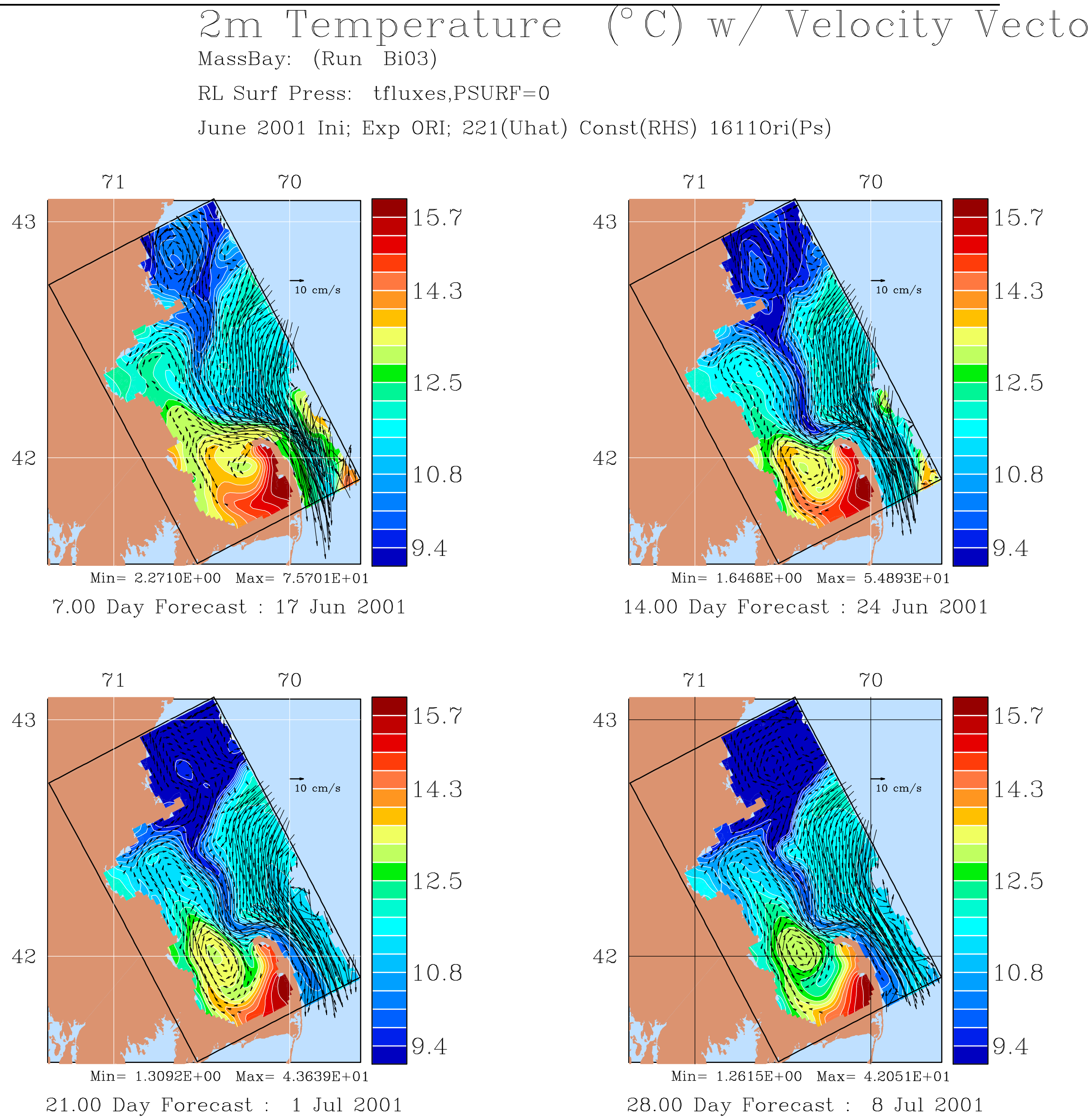


Figure 38 : Rigid–lid, surface pressure formulation simulation from "surface streamfunction" initial conditions (`psurf` $= 0$). Near surface temperature with total velocity vectors.

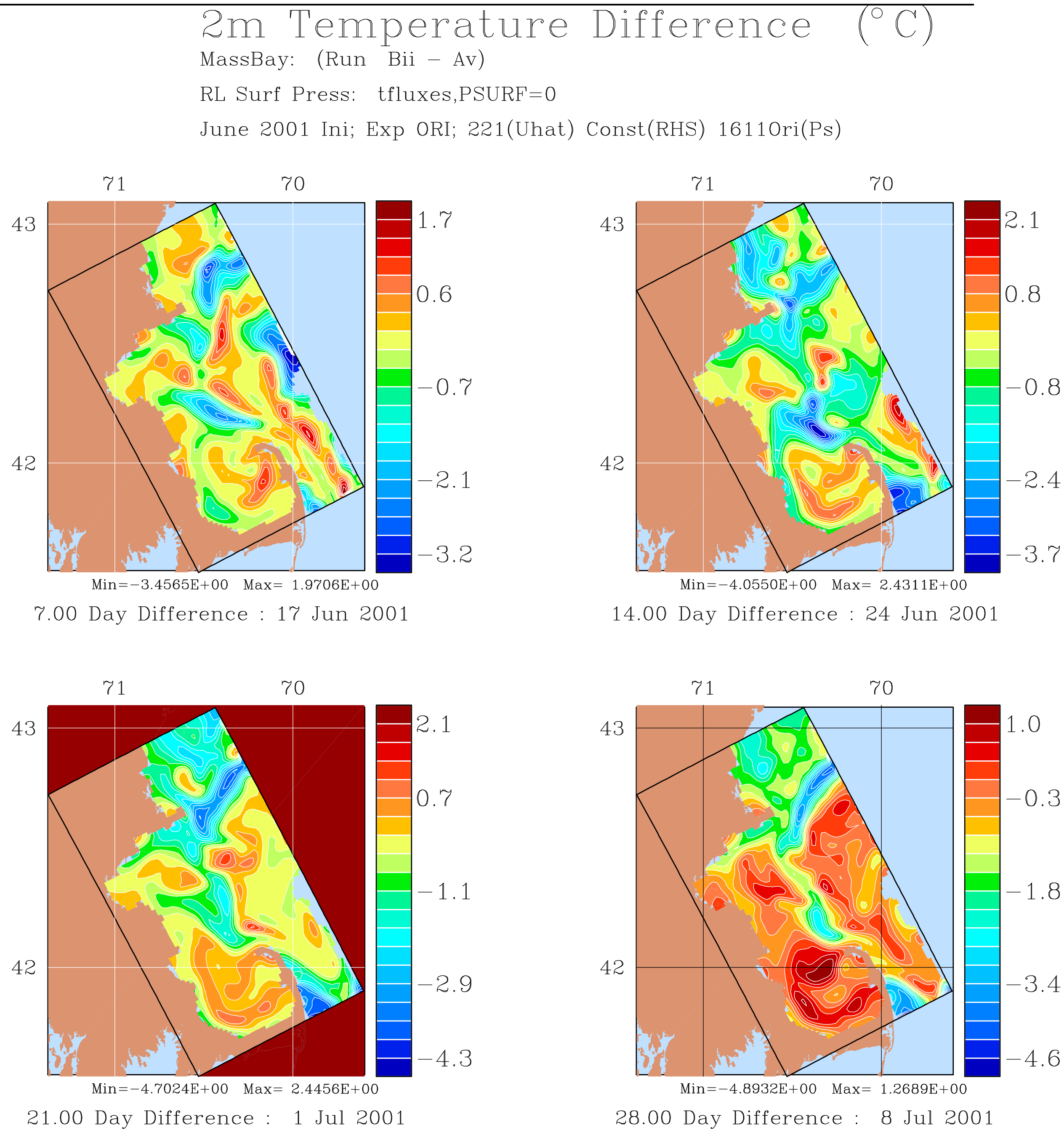


Figure 39 : Near Surface comparison of most similar streamfunction simulation *(Av)* to rigid–lid, surface pressure formulation simulation from “surface streamfunction” initial conditions *(Bi)*.

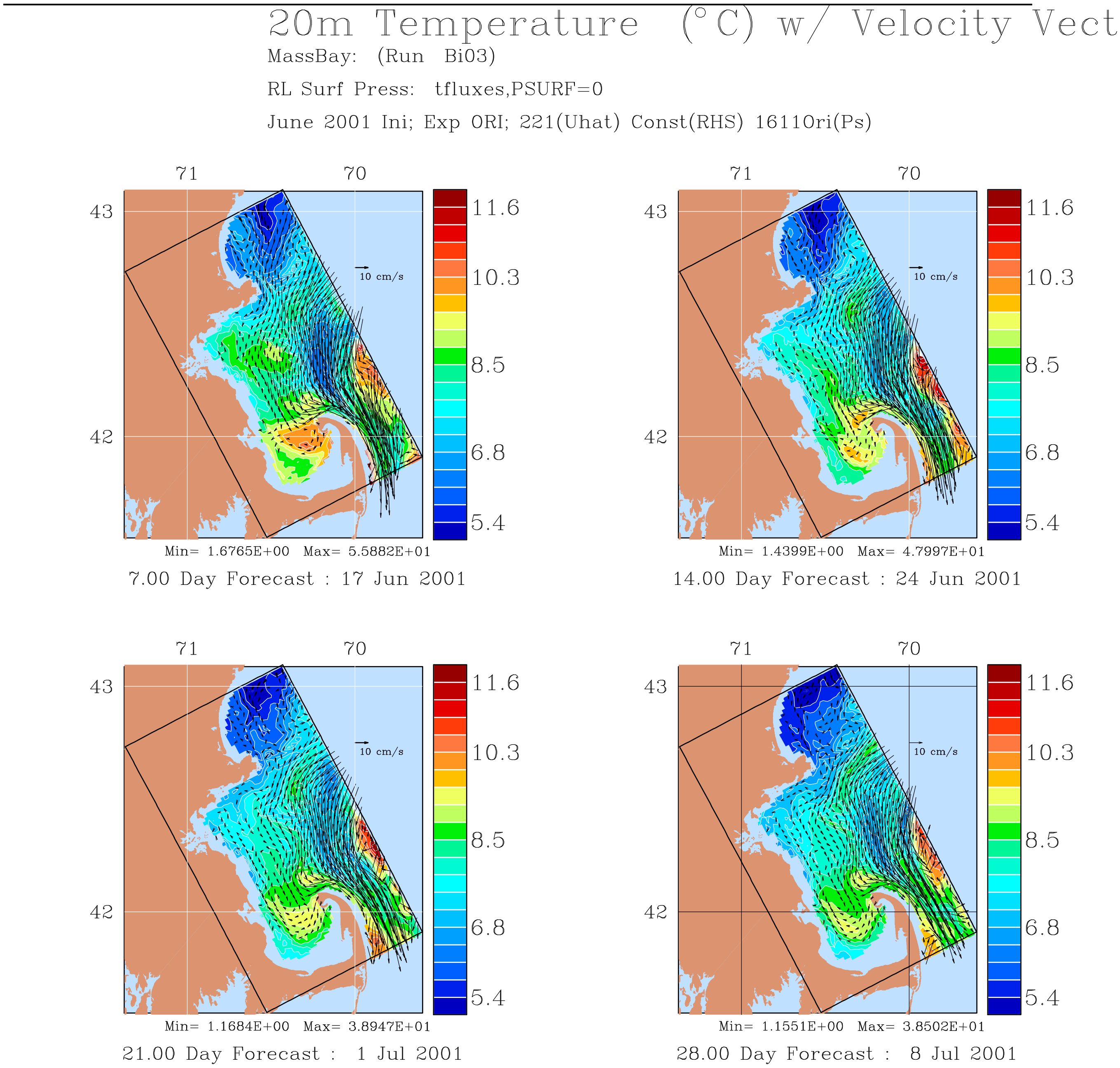


Figure 40 : Rigid–lid, surface pressure formulation simulation from "surface streamfunction" initial conditions (`psurf` = 0). Mid–level temperature with total velocity vectors.

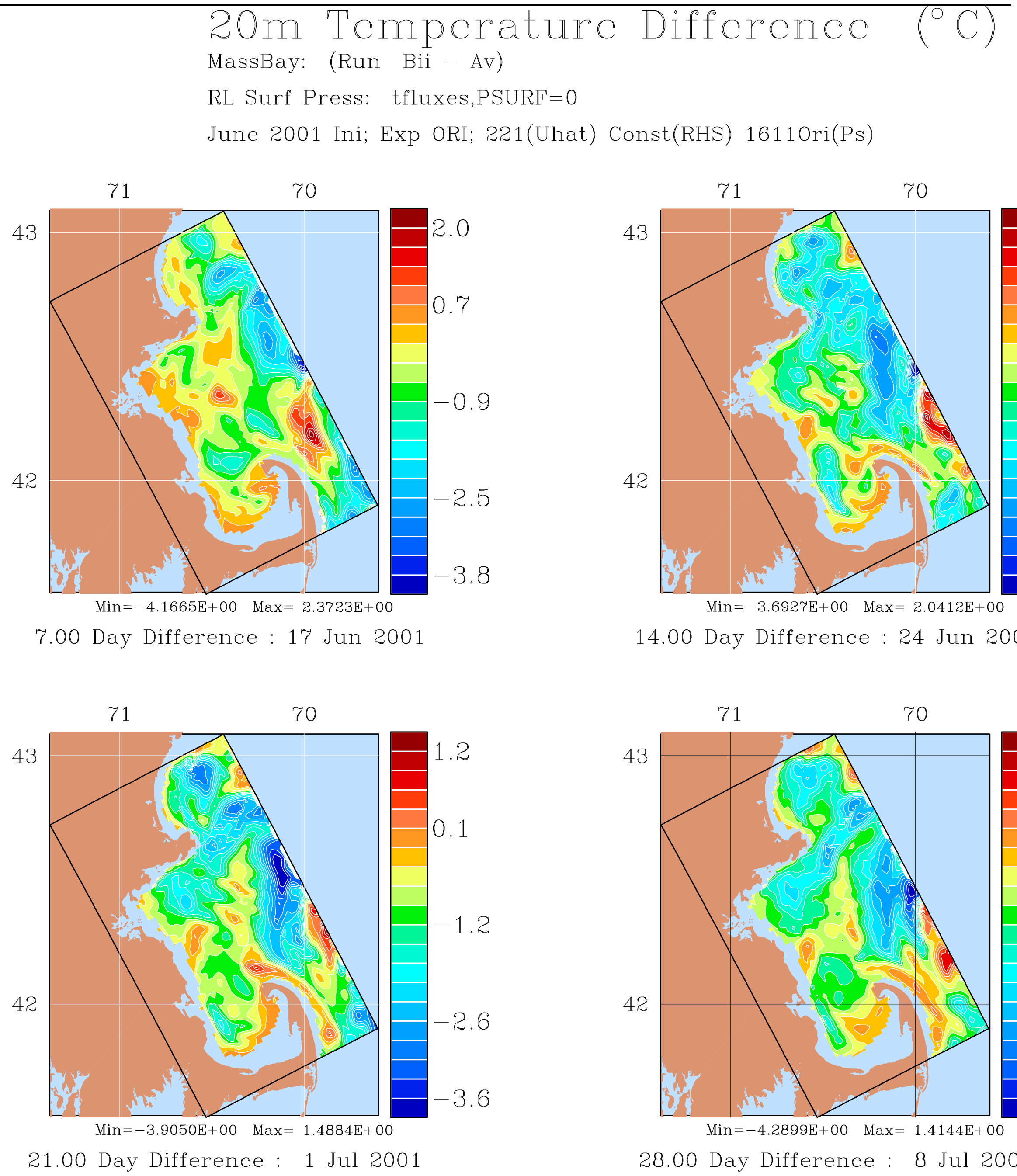


Figure 41 : Mid–level comparison of most similar streamfunction simulation *(Av)* to rigid–lid, surface pressure formulation simulation from "surface streamfunction" initial conditions *(Bi)*.

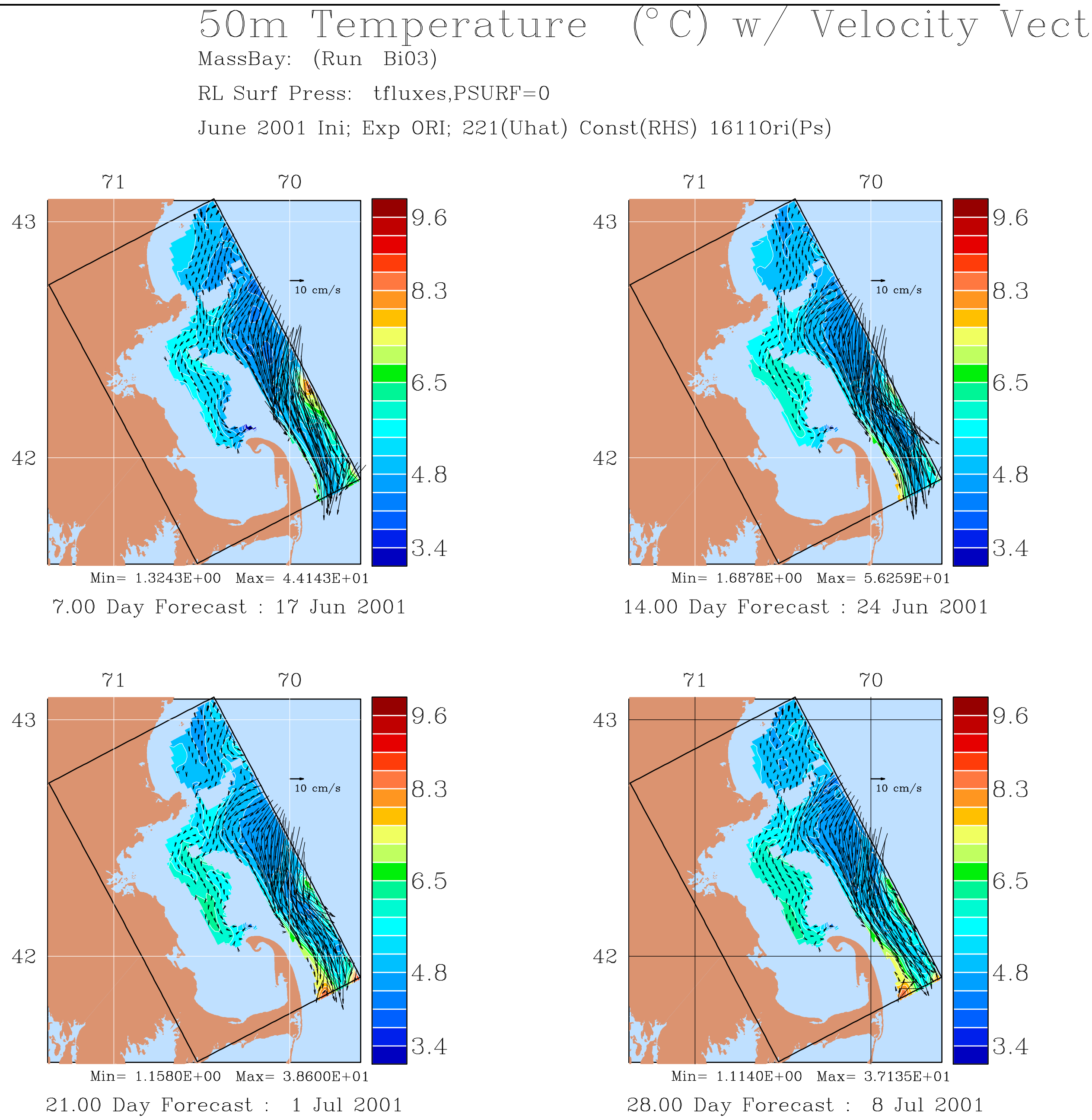


Figure 42 : Rigid–lid, surface pressure formulation simulation from "surface streamfunction" initial conditions (`psurf` = 0). Deep temperature with total velocity vectors.

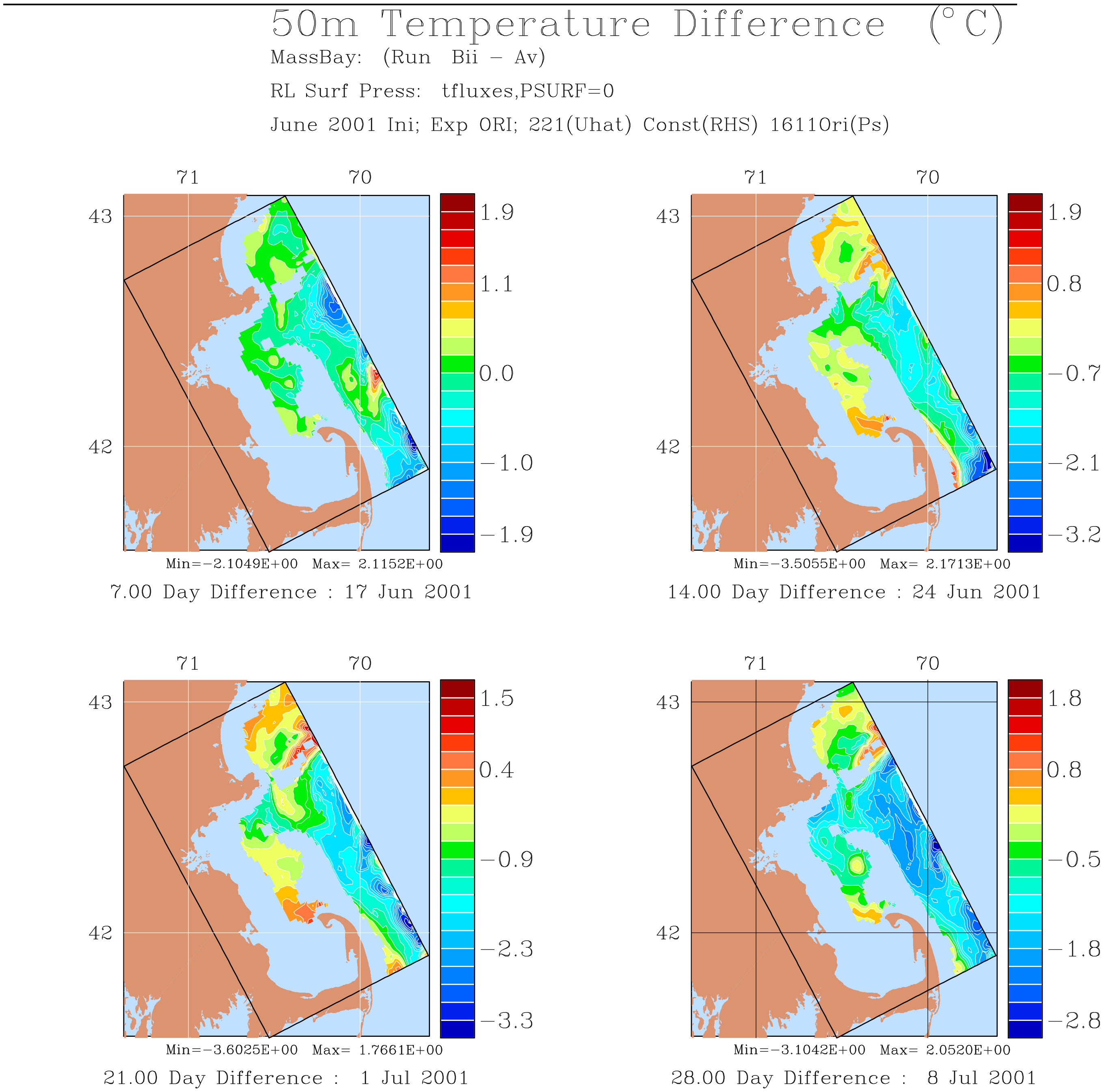


Figure 43 : Deep comparison of most similar streamfunction simulation *(Av)* to rigid–lid, surface pressure formulation simulation from "surface streamfunction" initial conditions *(Bi)*.

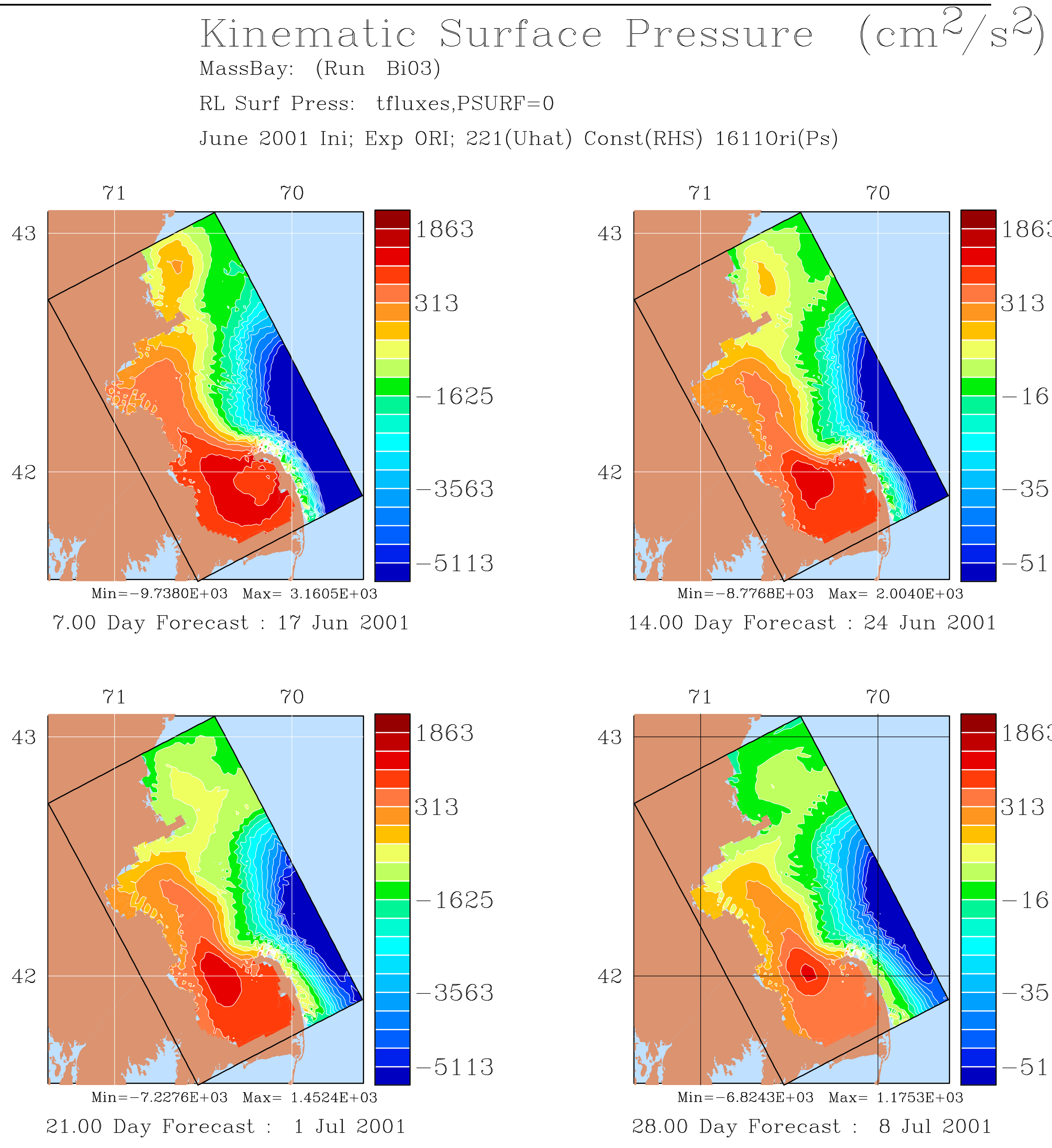


Figure 44 : Rigid–lid, surface pressure formulation simulation from "surface streamfunction" initial conditions (`psurf` = 0). Noisy kinematic surface pressure.

*(ii)* Surface Streamfunction & Velocity (`psurf` = 1)

The results of this simulation are presented in figures 45–53. The kinetic energy has less initial growth in the beginning of the simulation than *(Bi)* but more at the end. The skill metrics are very similar to those of *(Bi)* with the same overall conclusions.

The surface fields are again similar to those of *(Bi)*. In this simulation, the inflow along the eastern boundary extends further north, which pushes more of the questionable cold water into northern Mass. Bay. North of Cape Ann, a more pronounce gyre produces stronger northward flows along the coast. The outflow at the southern boundary is closer to Cape Cod. Similar comparisons occur in the mid–level and deep fields.

The surface pressure fields have a similar noise level to those of *(Bi)*. Here, the high in Cape Cod Bay is intensified, the exterior low is extended to the southern boundary and a significant high appears north of Cape Ann.

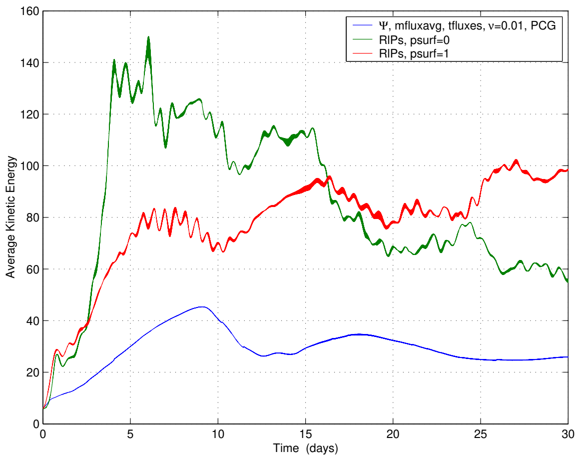


Figure 45 : Kinetic Energy comparison between simulations *(Av)* & *(Bi–ii)*.

**RMS Error** **Pattern Correlation Coefficient**

T

S

U

V

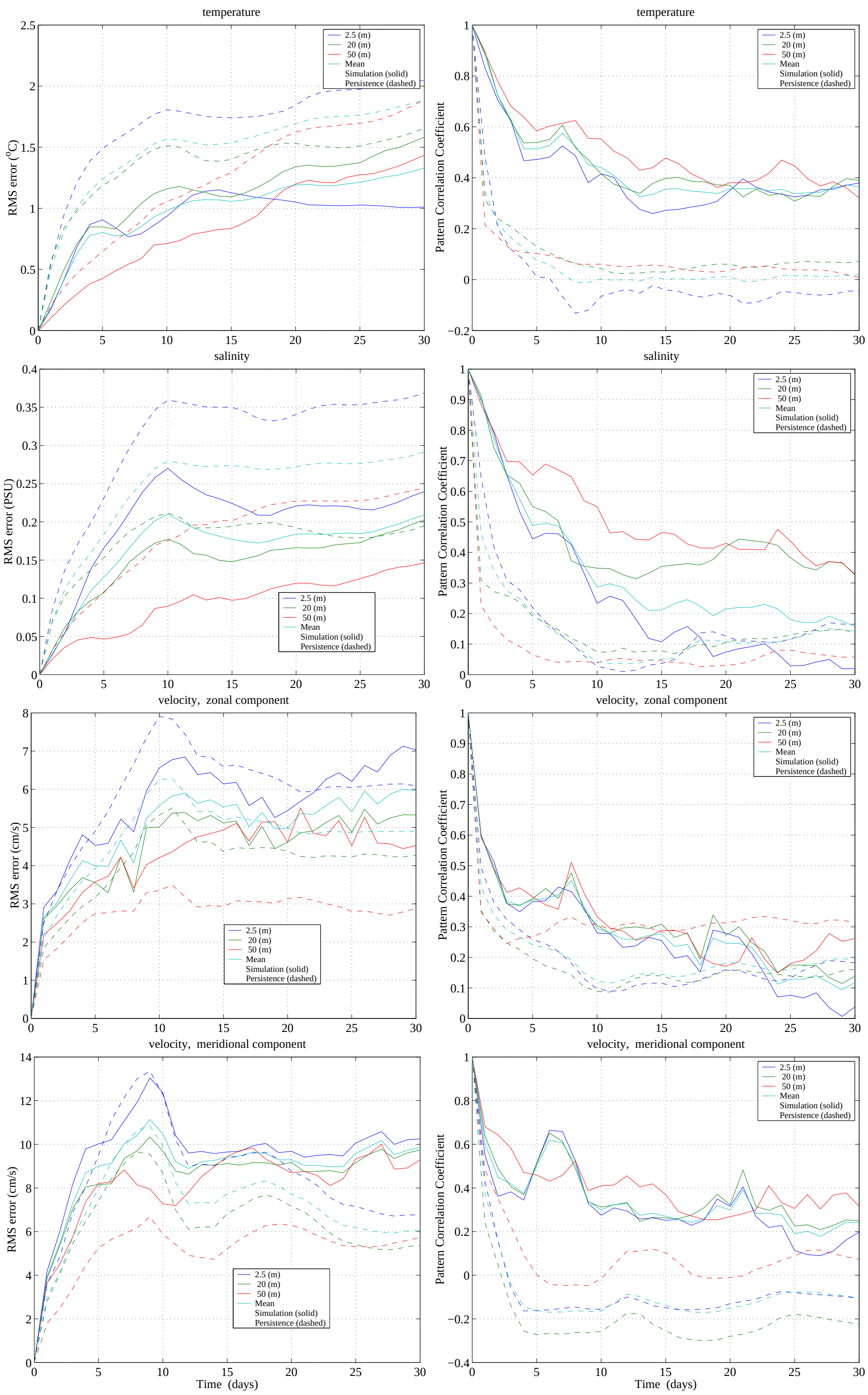


Figure 46: Comparison of most similar streamfunction simulation *(Av)* to rigid–lid, surface pressure formulation simulation from "surface streamfunction with boundary velocity" initial conditions *(Bii)*.

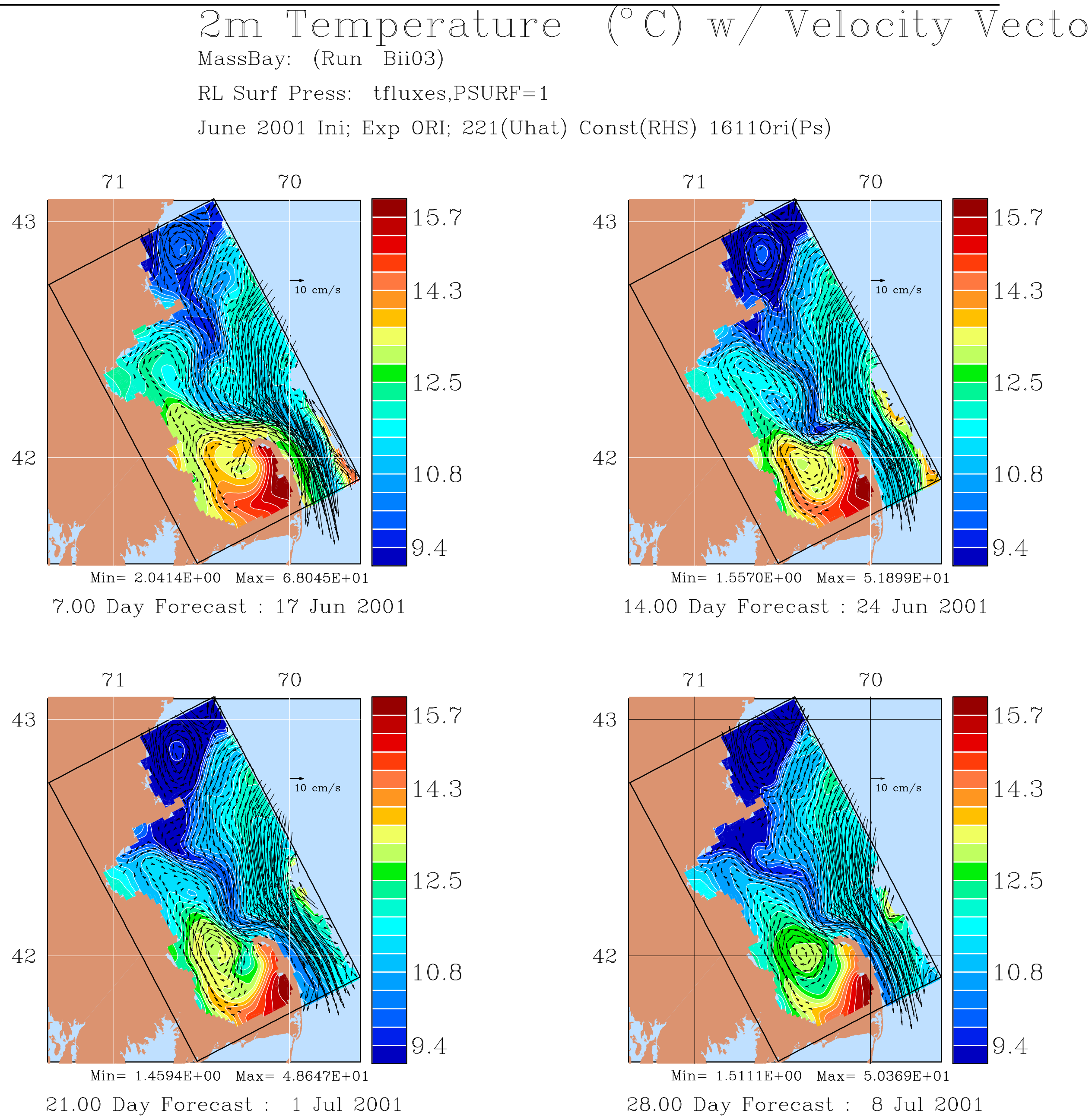


Figure 47 : Rigid–lid, surface pressure formulation simulation from "surface streamfunction with boundary velocity" initial conditions (psurf = 1). Near surface temperature with total velocity vectors.

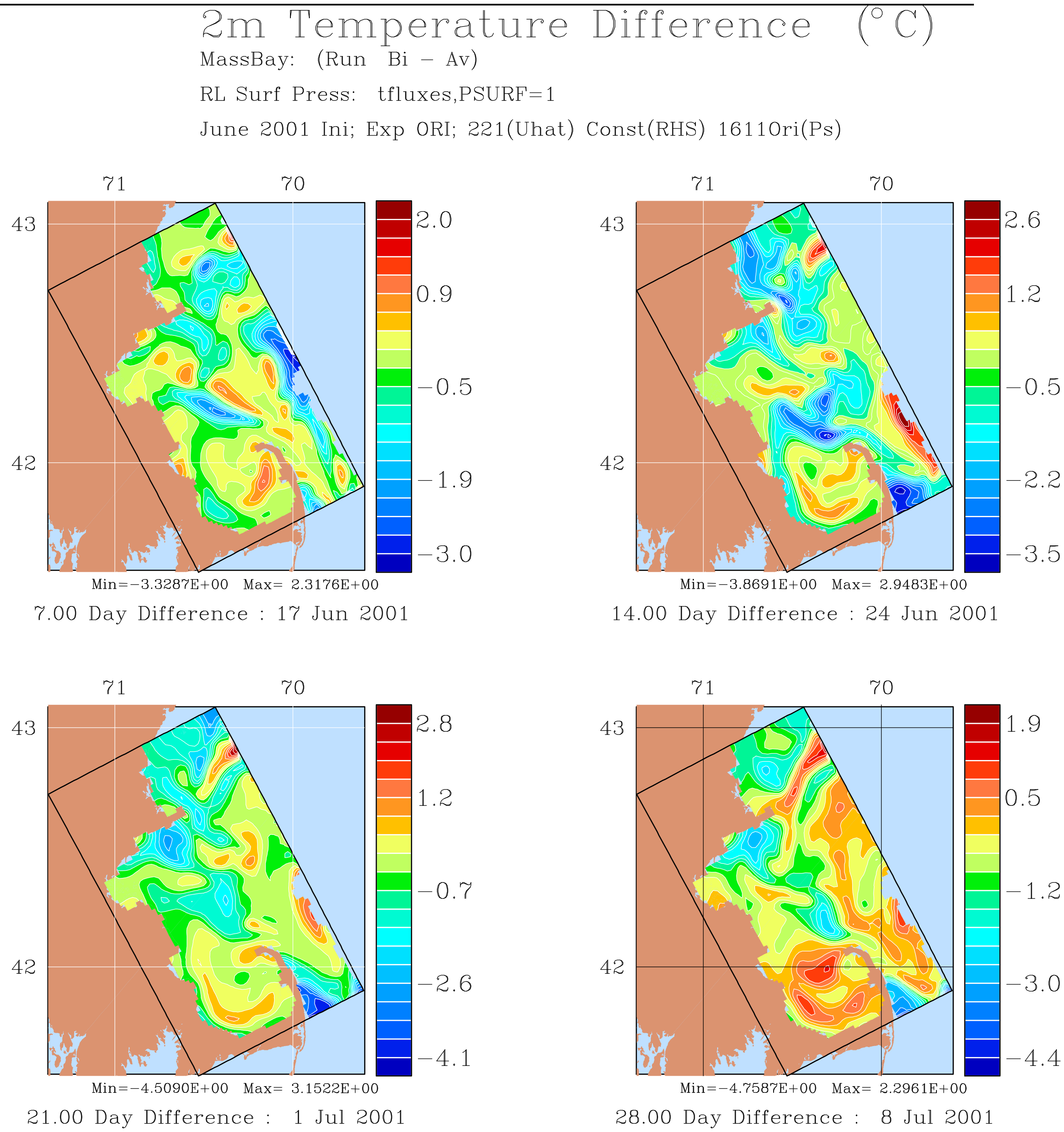


Figure 48 : Near Surface comparison of most similar streamfunction simulation *(Av)* to rigid–lid, surface pressure formulation simulation from “surface streamfunction with boundary velocity” initial conditions *(Bii)*.

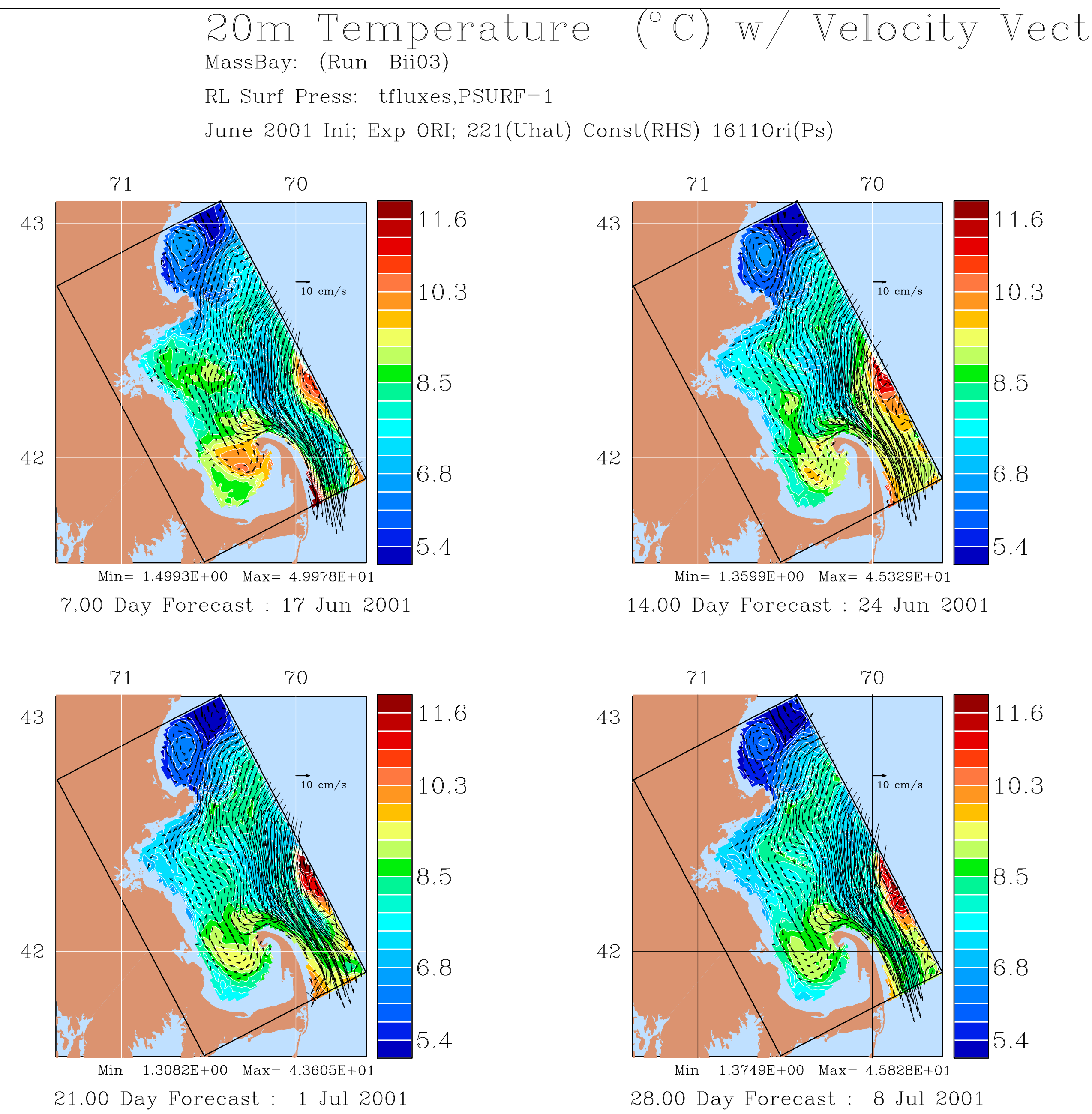


Figure 49 : Rigid–lid, surface pressure formulation simulation from "surface streamfunction with boundary velocity" initial conditions (`psurf` = 1). Mid–level temperature with total velocity vectors.

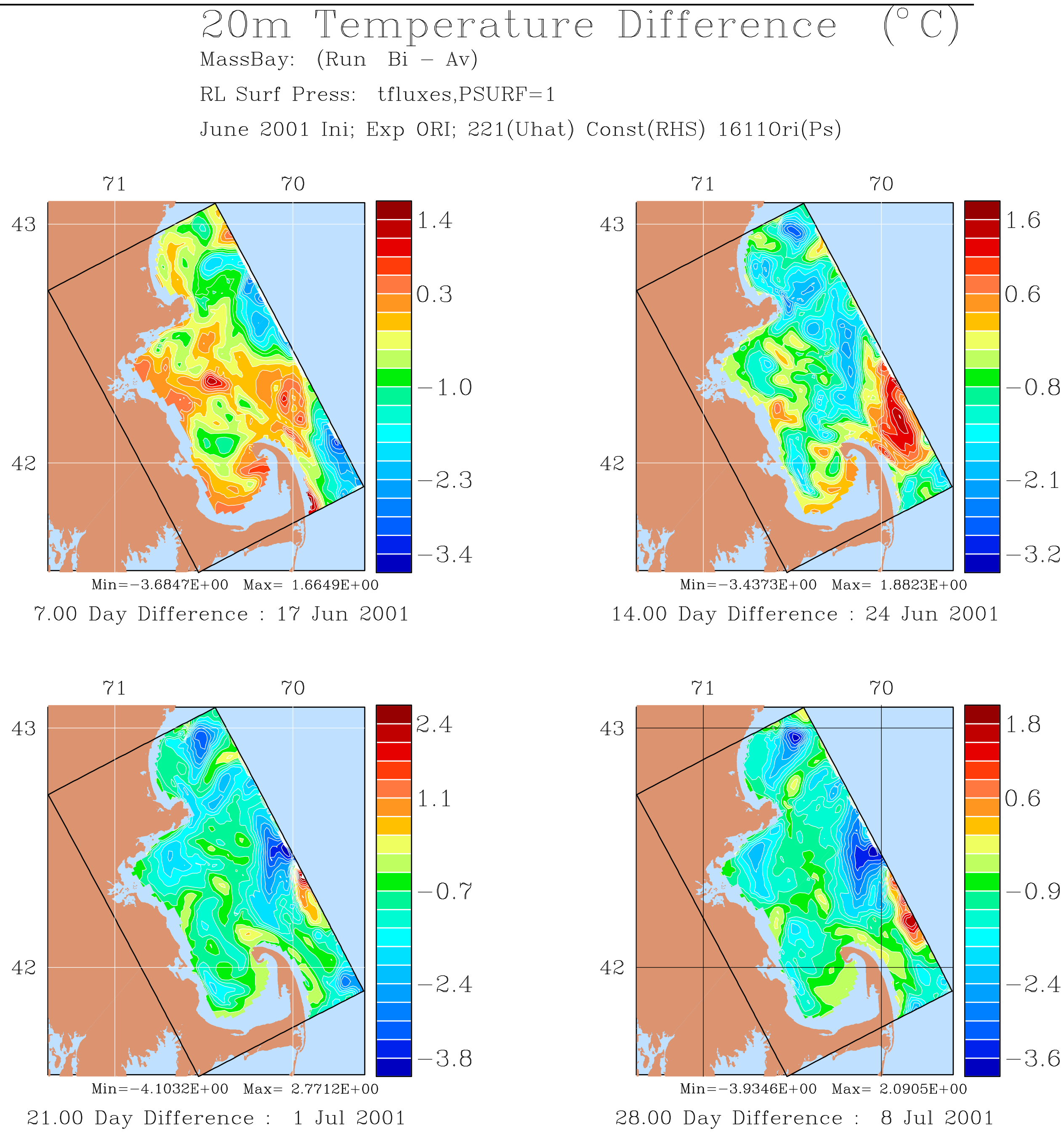


Figure 50 : Mid–level comparison of most similar streamfunction simulation *(Av)* to rigid–lid, surface pressure formulation simulation from “surface streamfunction with boundary velocity” initial conditions *(Bii)*.

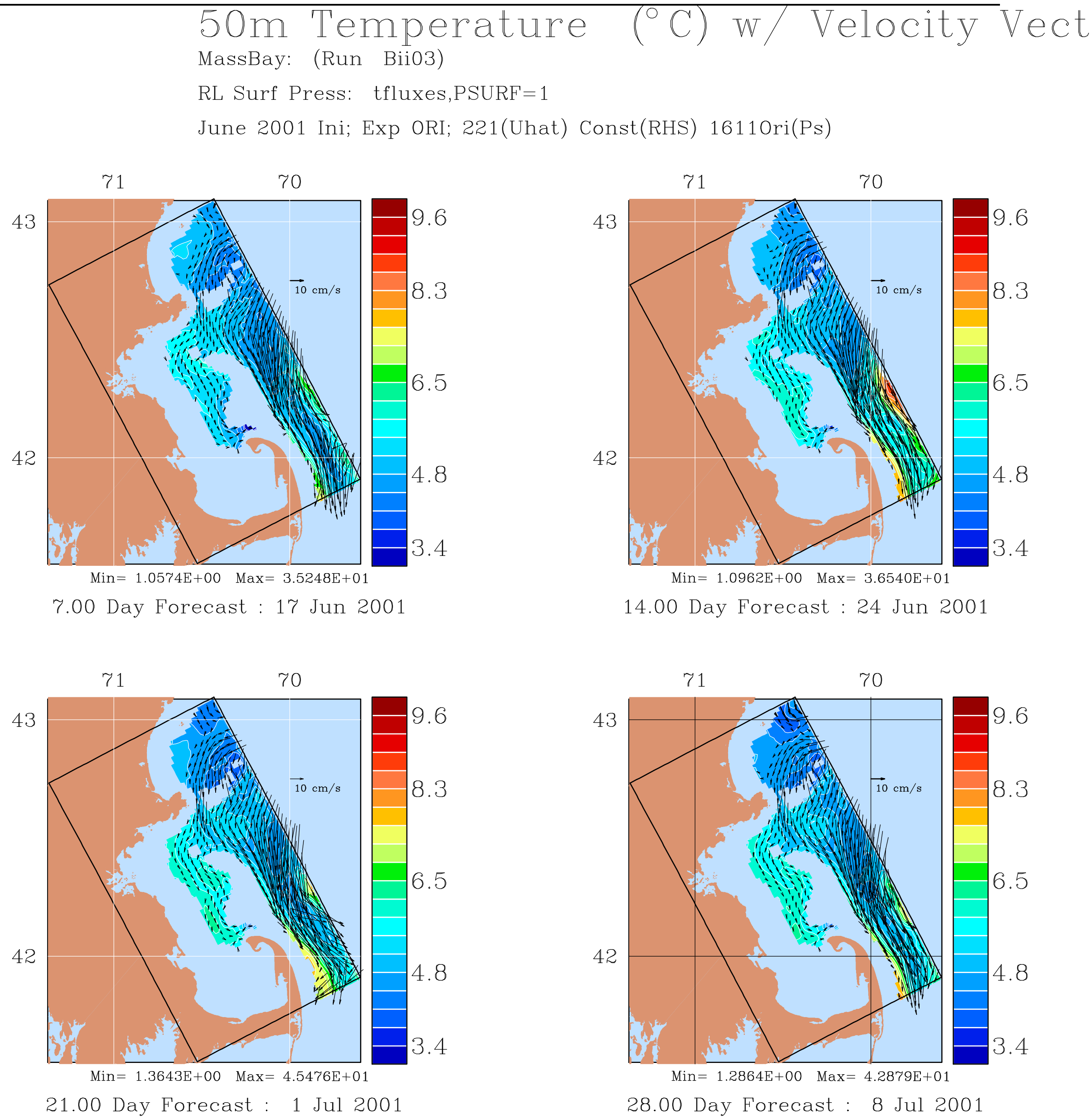


Figure 51 : Rigid–lid, surface pressure formulation simulation from "surface streamfunction with boundary velocity" initial conditions (`psurf` = 1). Deep temperature with total velocity vectors.

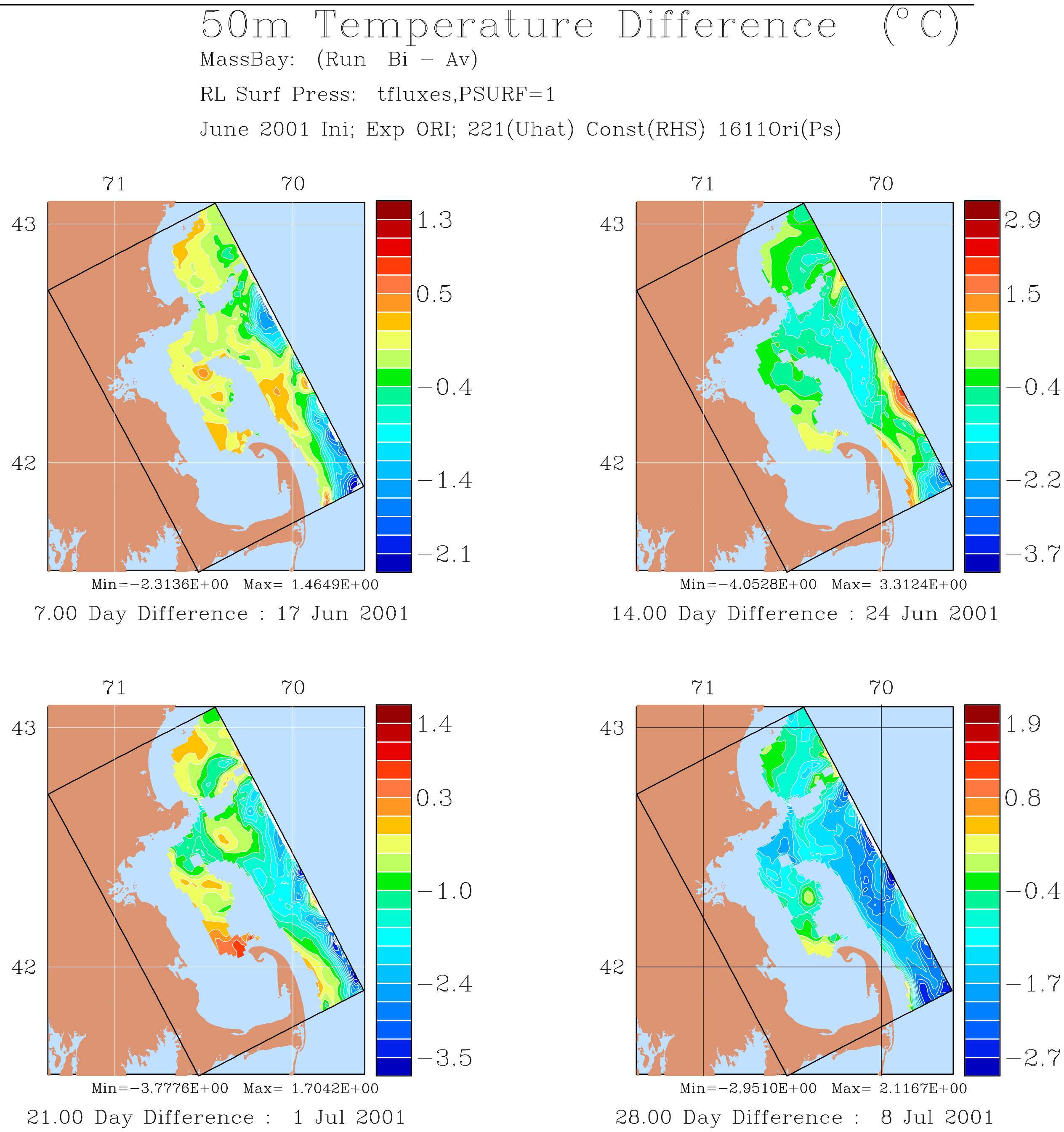


Figure 52 : Deep comparison of most similar streamfunction simulation *(Av)* to rigid–lid, surface pressure formulation simulation from "surface streamfunction with boundary velocity" initial conditions *(Bii)*.

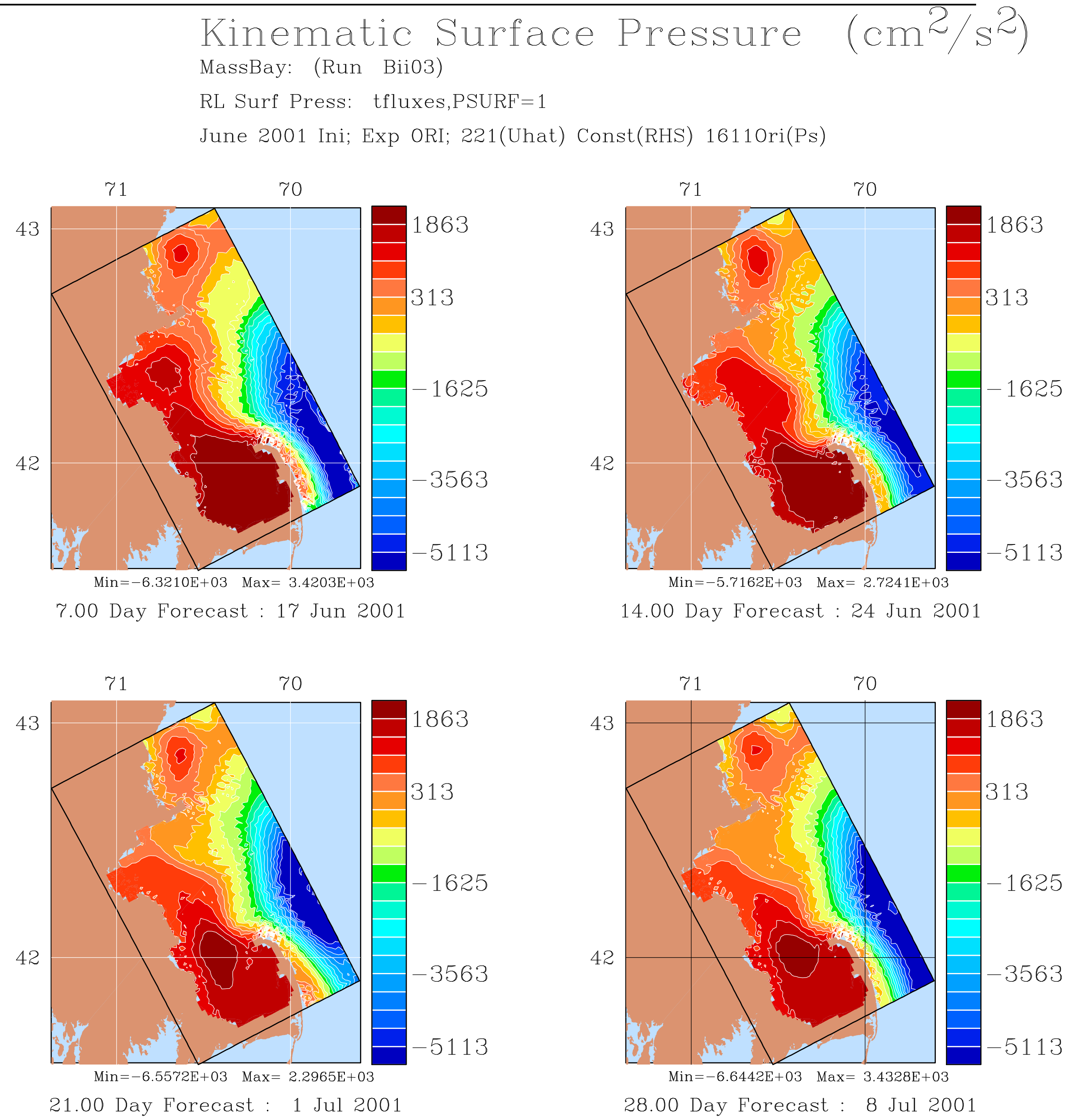


Figure 53 : Rigid–lid, surface pressure formulation simulation from "surface streamfunction with boundary velocity" initial conditions (`psurf` = 1). Noisy kinematic surface pressure.

*(iii)* Surface Streamfunction & the Barotropic Equation (`psurf` $= 1$ & CPP option `bctest2`)

The results of this simulation are presented in figures 45–53. The kinetic energy has the slower initial growth of *(Bii)* and the slower final growth of *(Bi)*. The skill metrics are similar to those of *(Bi)* & *(Bii)*.

The flow fields are very similar to those of *(Bii)*, with the exception that the southern outflow is not so near to Cape Cod.

Again, the surface pressure is very similar to that of *(Bii)*, with the exception that the exterior low does not extend to the southern boundary.

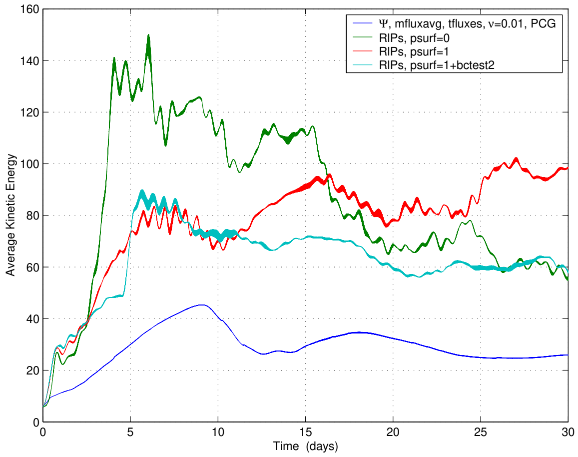


Figure 54 : Kinetic Energy comparison between simulations *(Av)* & *(Bi–iii)*.

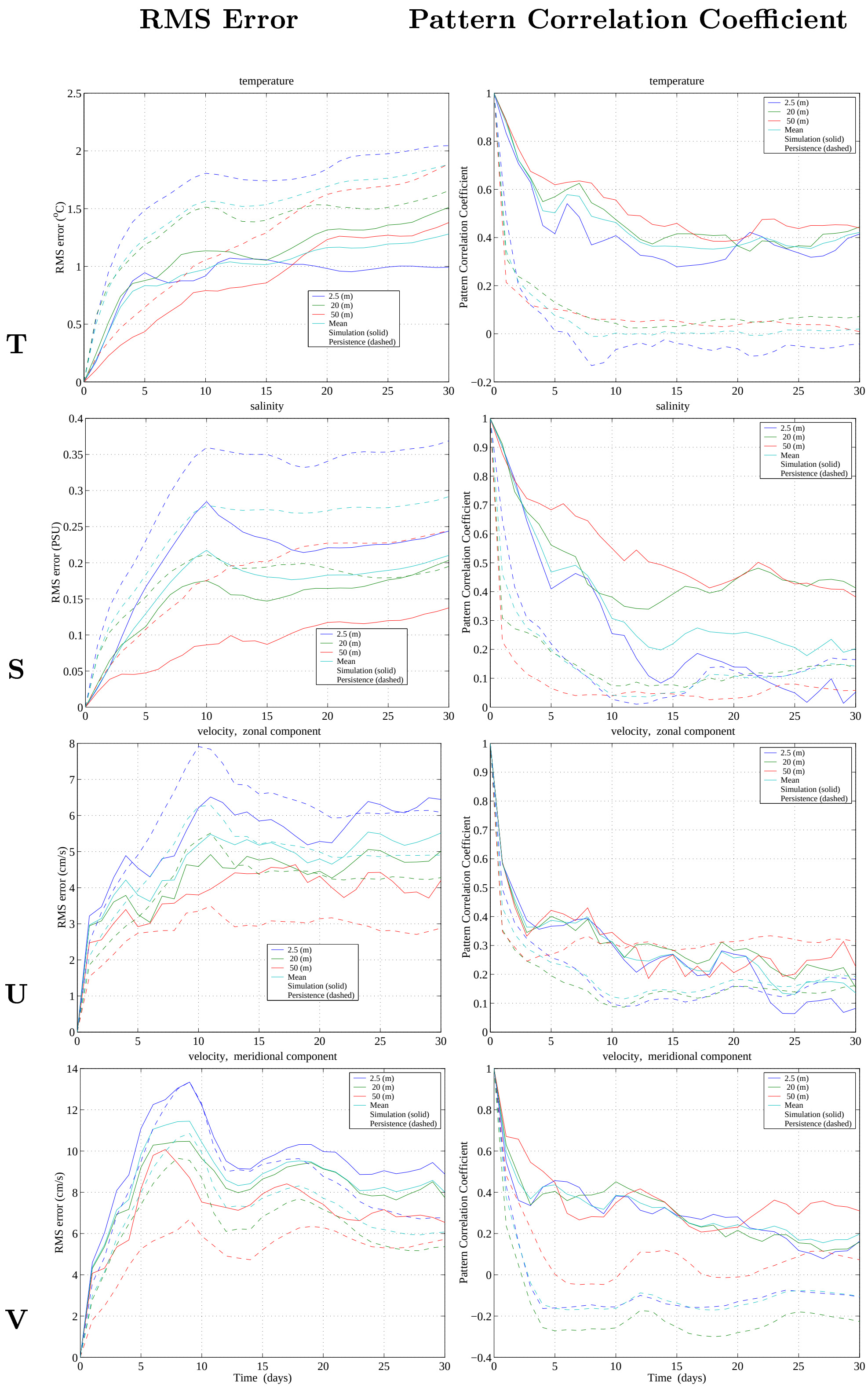


Figure 55: Comparison of most similar streamfunction simulation *(Av)* to rigid–lid, surface pressure formulation simulation from "surface streamfunction with boundary barotropic equation" initial conditions *(Biii)*.

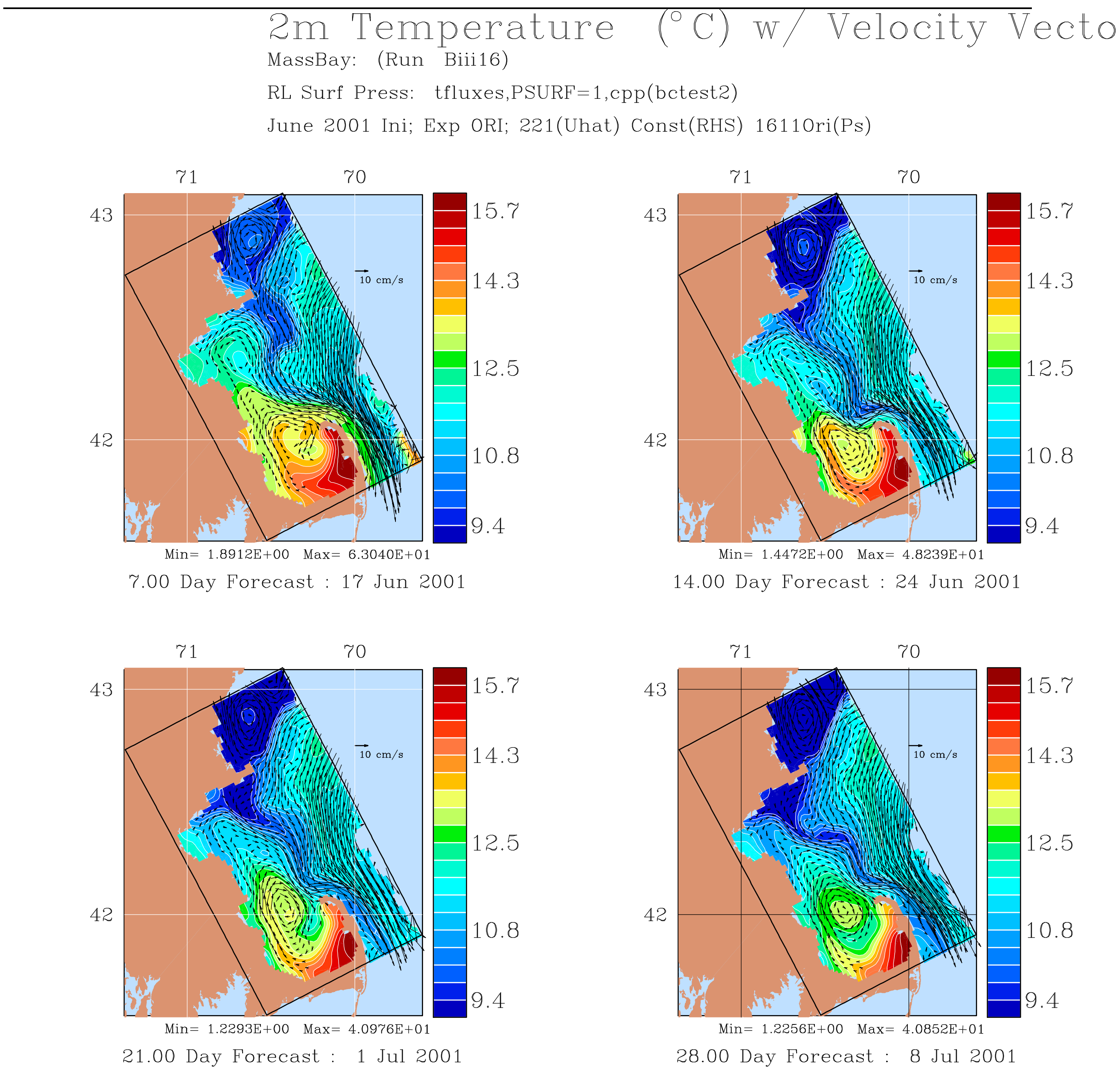


Figure 56 : Rigid–lid, surface pressure formulation simulation from "surface streamfunction with boundary barotropic equation" initial conditions (`psurf` = 1 & CPP option `bctest2`). Near surface temperature with total velocity vectors.

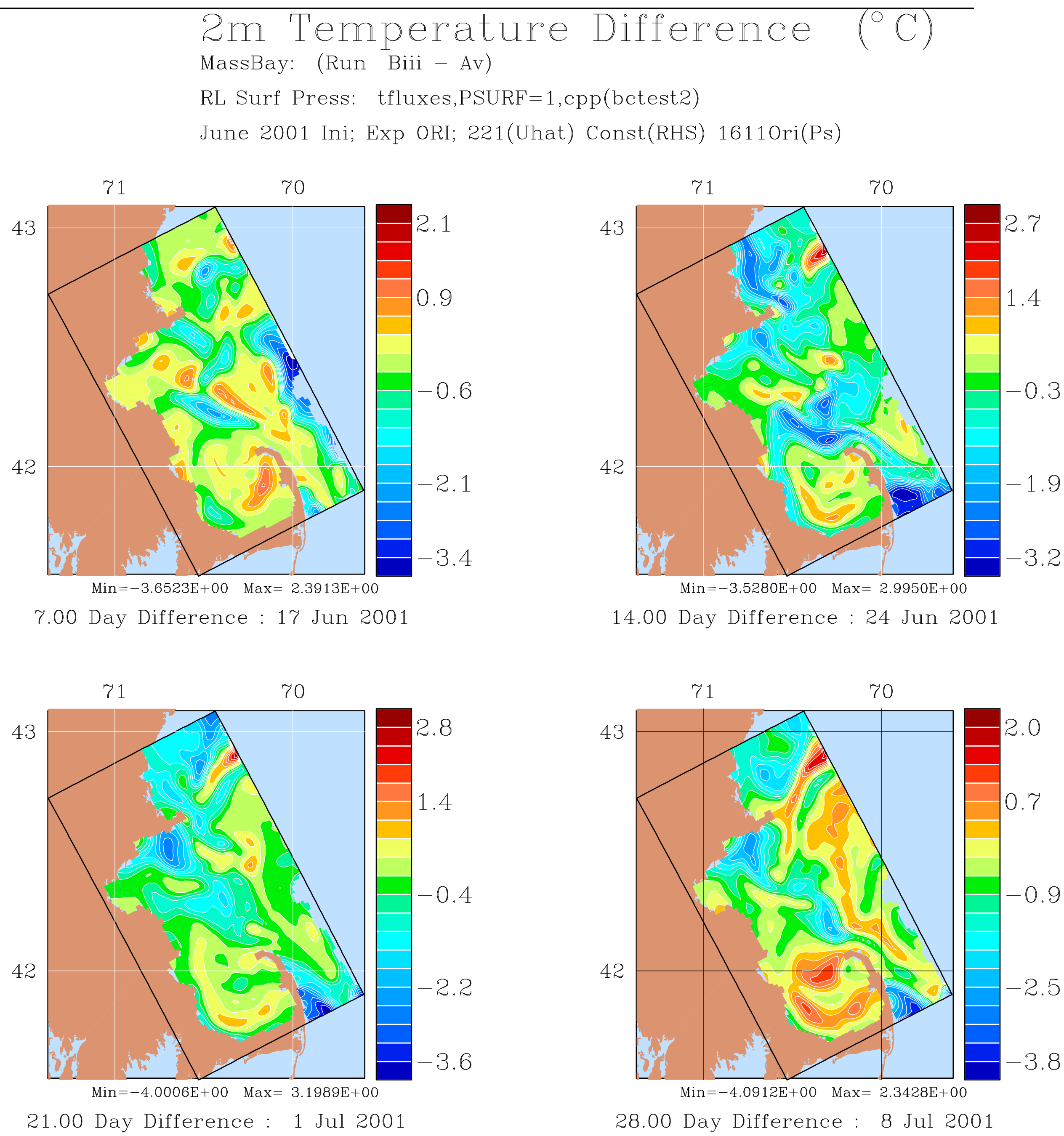


Figure 57 : Near Surface comparison of most similar streamfunction simulation *(Av)* to rigid–lid, surface pressure formulation simulation from "surface streamfunction with boundary barotropic equation" initial conditions *(Biii)*.

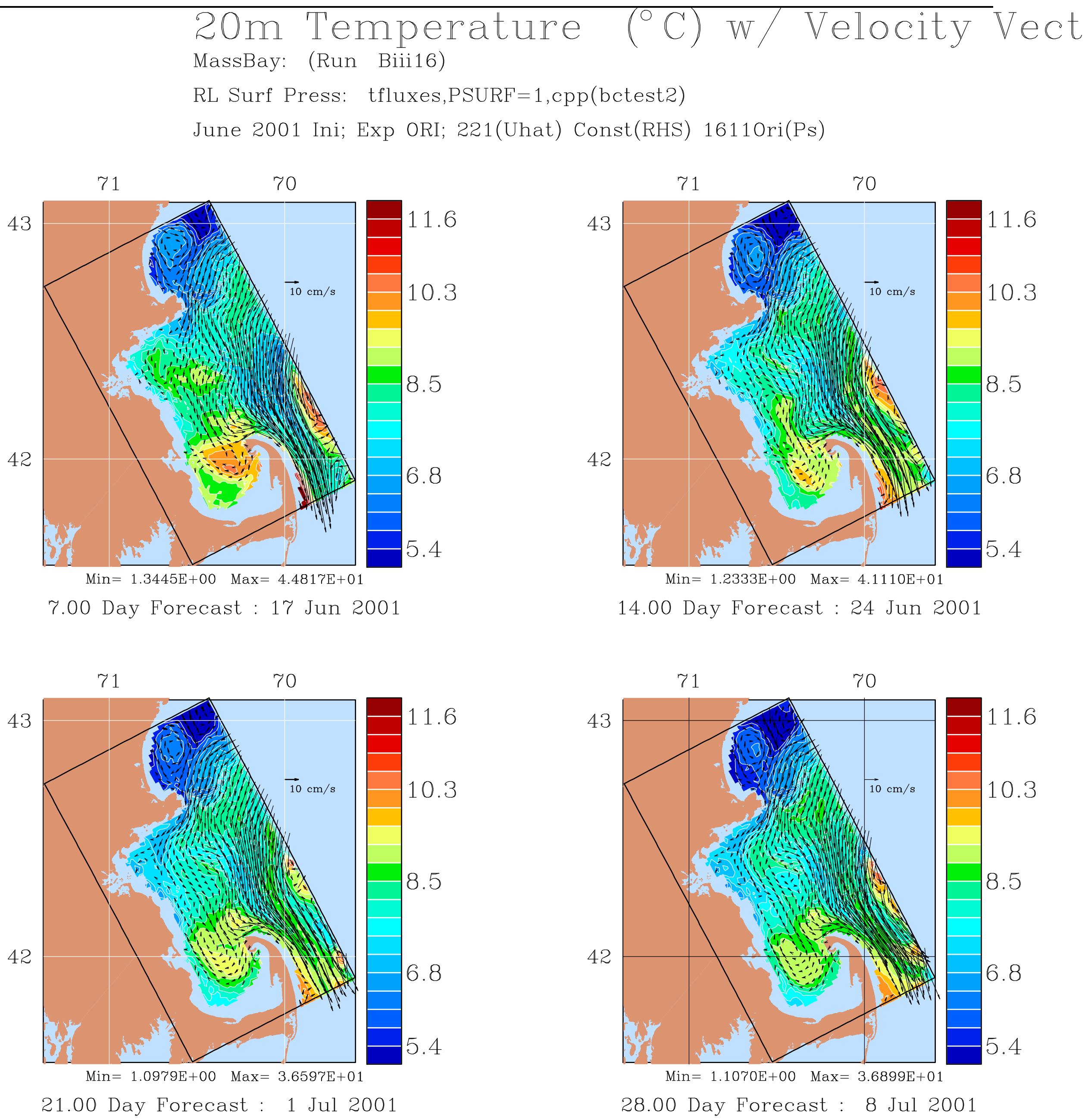


Figure 58 : Rigid–lid, surface pressure formulation simulation from "surface streamfunction with boundary barotropic equation" initial conditions (`psurf` = 1 & CPP option `bctest2`). Mid–level temperature with total velocity vectors.

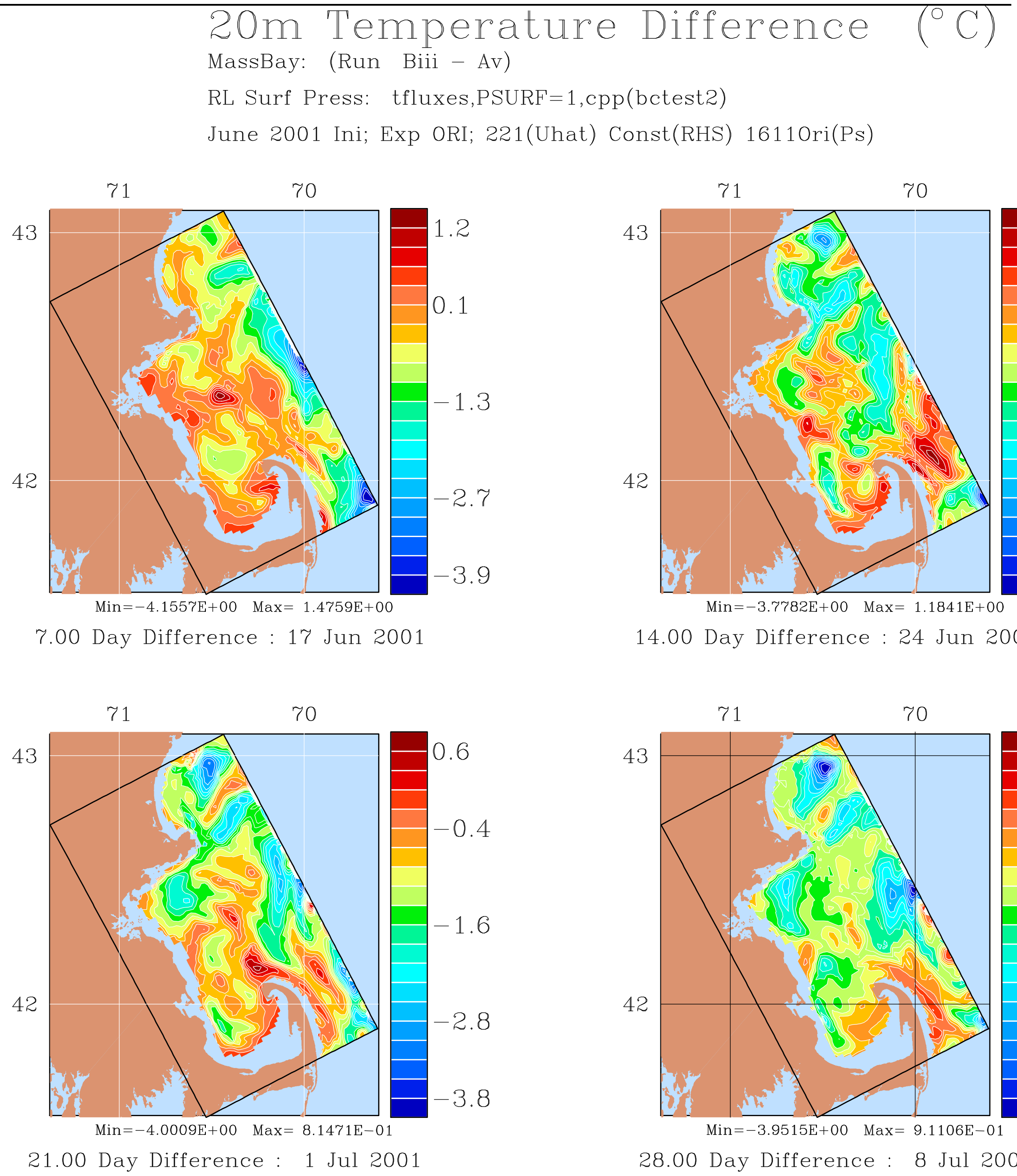


Figure 59 : Mid–level comparison of most similar streamfunction simulation *(Av)* to rigid–lid, surface pressure formulation simulation from “surface streamfunction with boundary barotropic equation” initial conditions *(Biii)*.

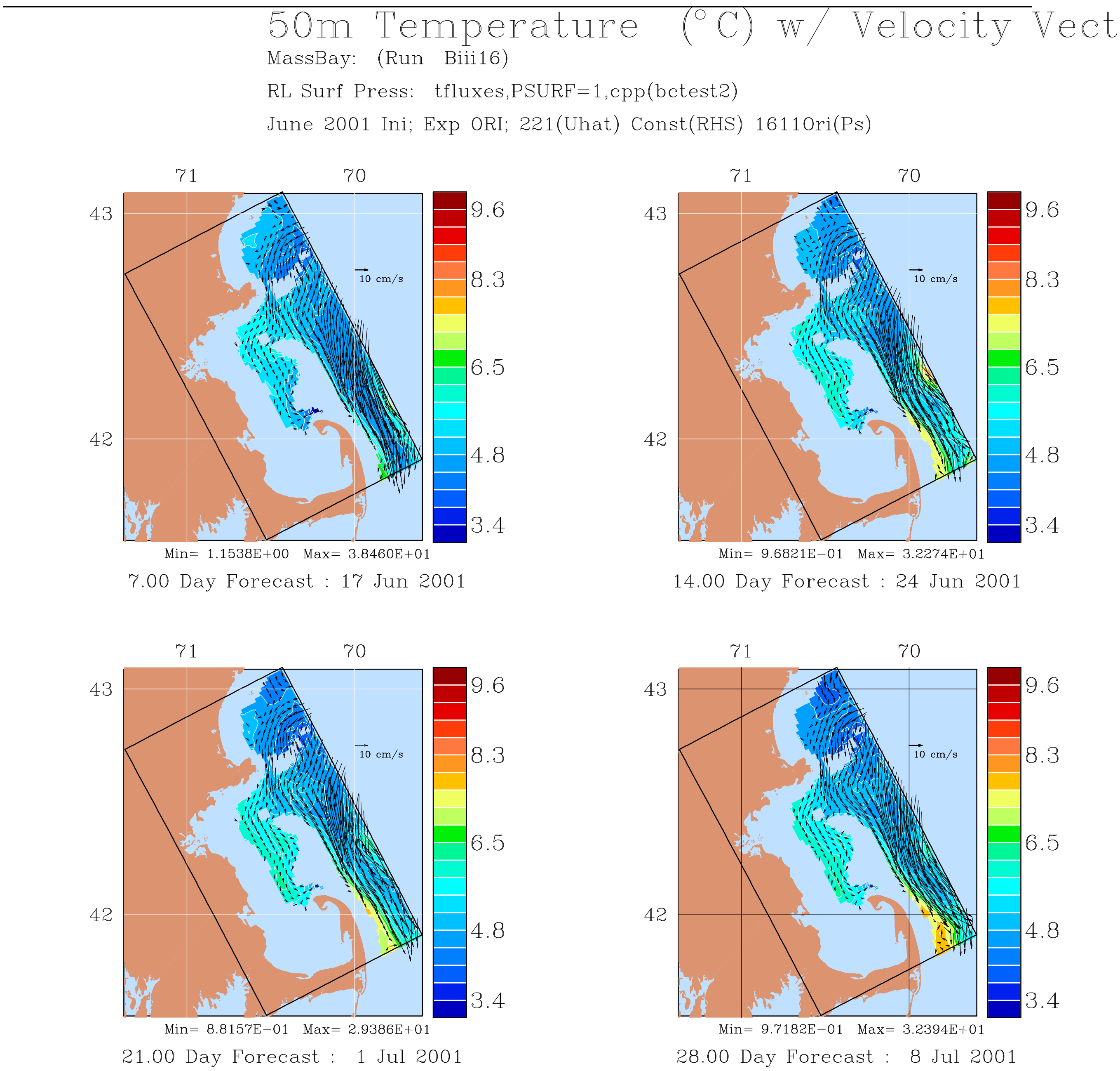


Figure 60 : Rigid–lid, surface pressure formulation simulation from "surface streamfunction with boundary barotropic equation" initial conditions (`psurf` = 1 & CPP option `bctest2`). Deep temperature with total velocity vectors.

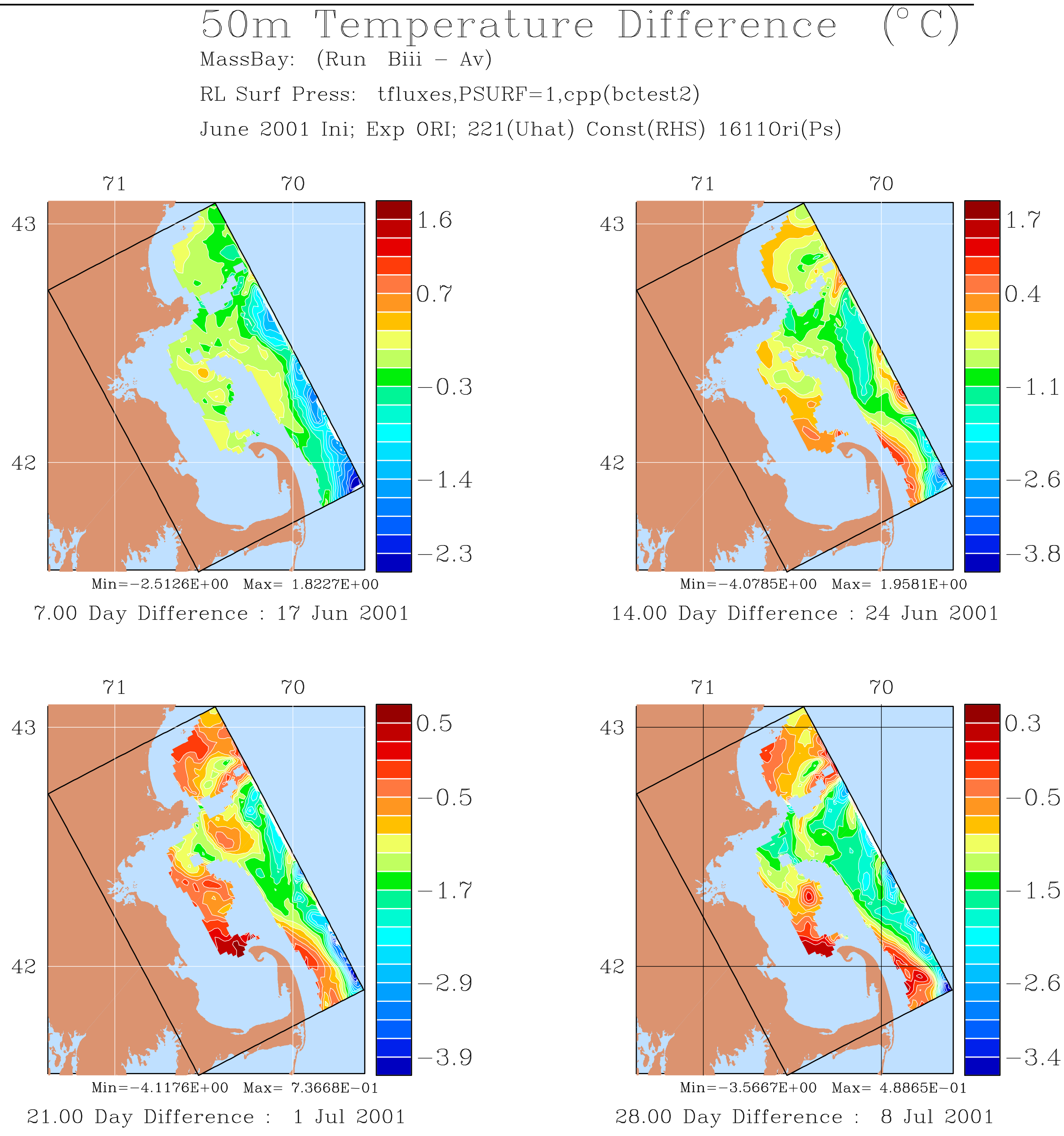


Figure 61 : Deep comparison of most similar streamfunction simulation *(Av)* to rigid–lid, surface pressure formulation simulation from "surface streamfunction with boundary barotropic equation" initial conditions *(Biii)*.

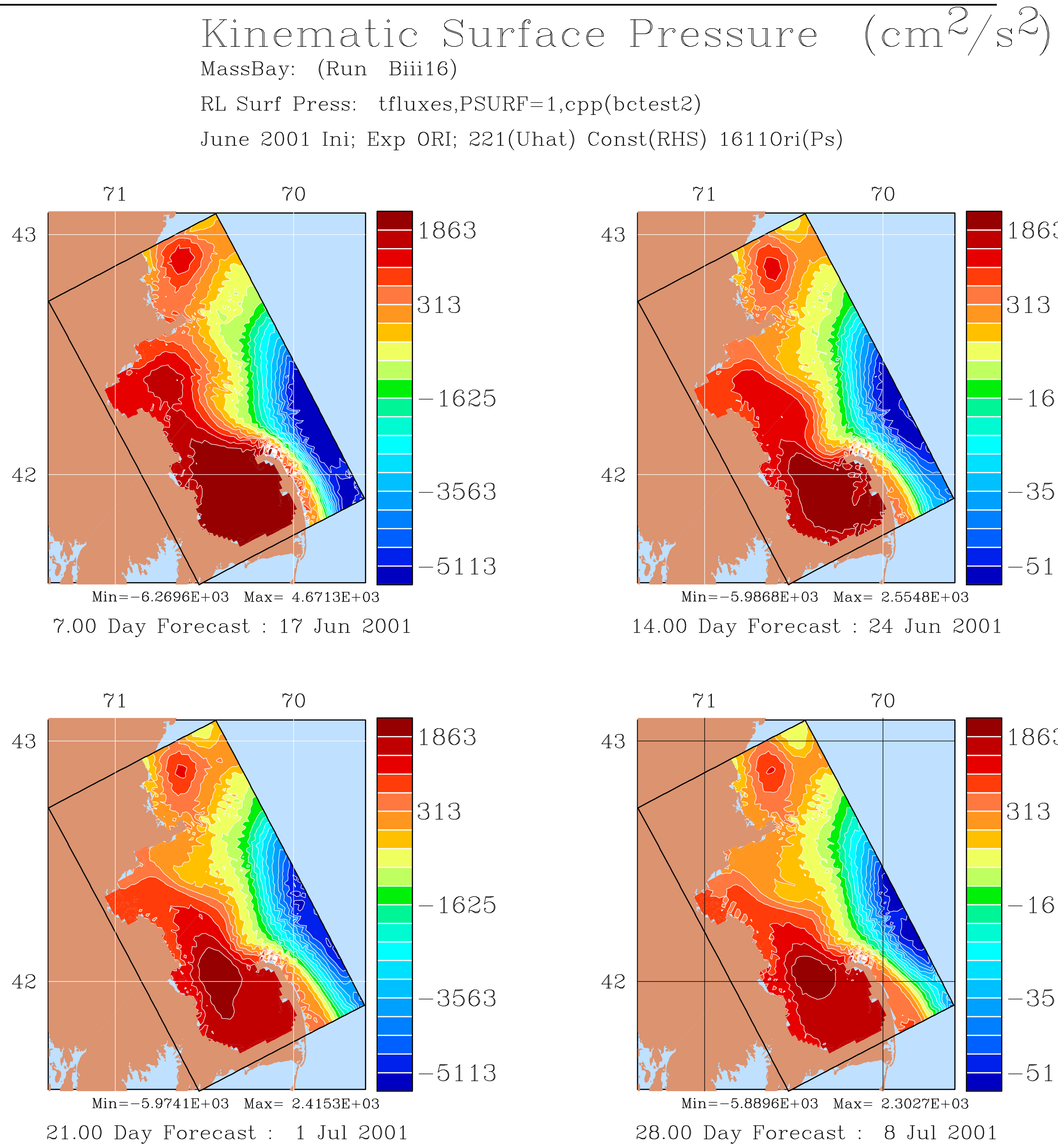


Figure 62 : Rigid–lid, surface pressure formulation simulation from "surface streamfunction with boundary barotropic equation" initial conditions (`psurf` = 1 & CPP option `bctest2`). Noisy kinematic surface pressure.

*(C) Surface Pressure formulation – Free Surface* *(i–iv)* as in *(B)*.

All three simulations in the rigid–lid surface pressure tests are repeated here with free surface codes, with the coriolis semi-implicit parameter set to $\frac{1}{3}$, following the stability results of Smith & Dukowicz. As in the periodic jet and $P^2S^3$ tests, neither the plotting codes nor the skill metric routines account for the time variability of the vertical coordinates.

*(i)* Surface pressure initialization. (`psurf` = 0)

The free surface results and comparisons to rigid–lid surface pressure formulation results are presented in figures 63–71. The kinetic energy experiences less initial growth in the free surface case, then tracks the final 10 days of the rigid–lid case well. The RMS and PCC skill metrics consistently show better agreement between the 2 pressure formulations than between either and the streamfunction formulation.

The surface flow patterns are very similar to the rigid–lid surface pressure case, with lesser initial peak velocities and developing somewhat more advection of the questionable cold water from north of Cape Ann. This plume becomes one of the dominant features in the difference fields. The mid–level flows show similar features, with the plume being more subtle. The major temperature differences occur external to the Bay. The deep flows are very similar in the two tests, with slightly smaller velocities in the northern area of the free surface test and a slightly less coherent southern outflow too. The peak temperature differences occur in the southern portion of the exterior of the domain.

The surface pressure shows similar overall patterns and similar noise to the rigid–lid case. In the free surface case, however, a wave seems to be coming off of the exterior of Cape Cod.

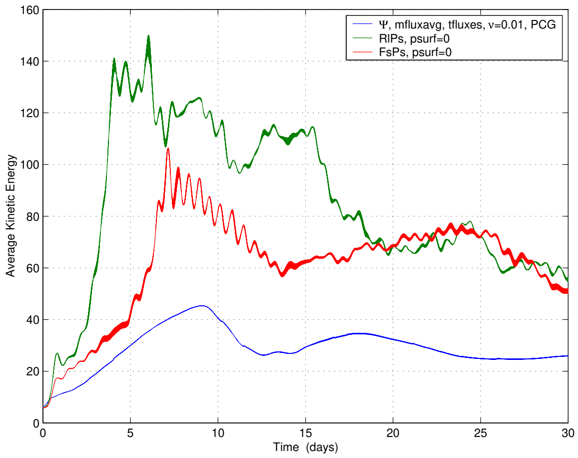


Figure 63 : Kinetic Energy comparison between simulations *(Av)*, *(Bi)* & *(Ci)*.

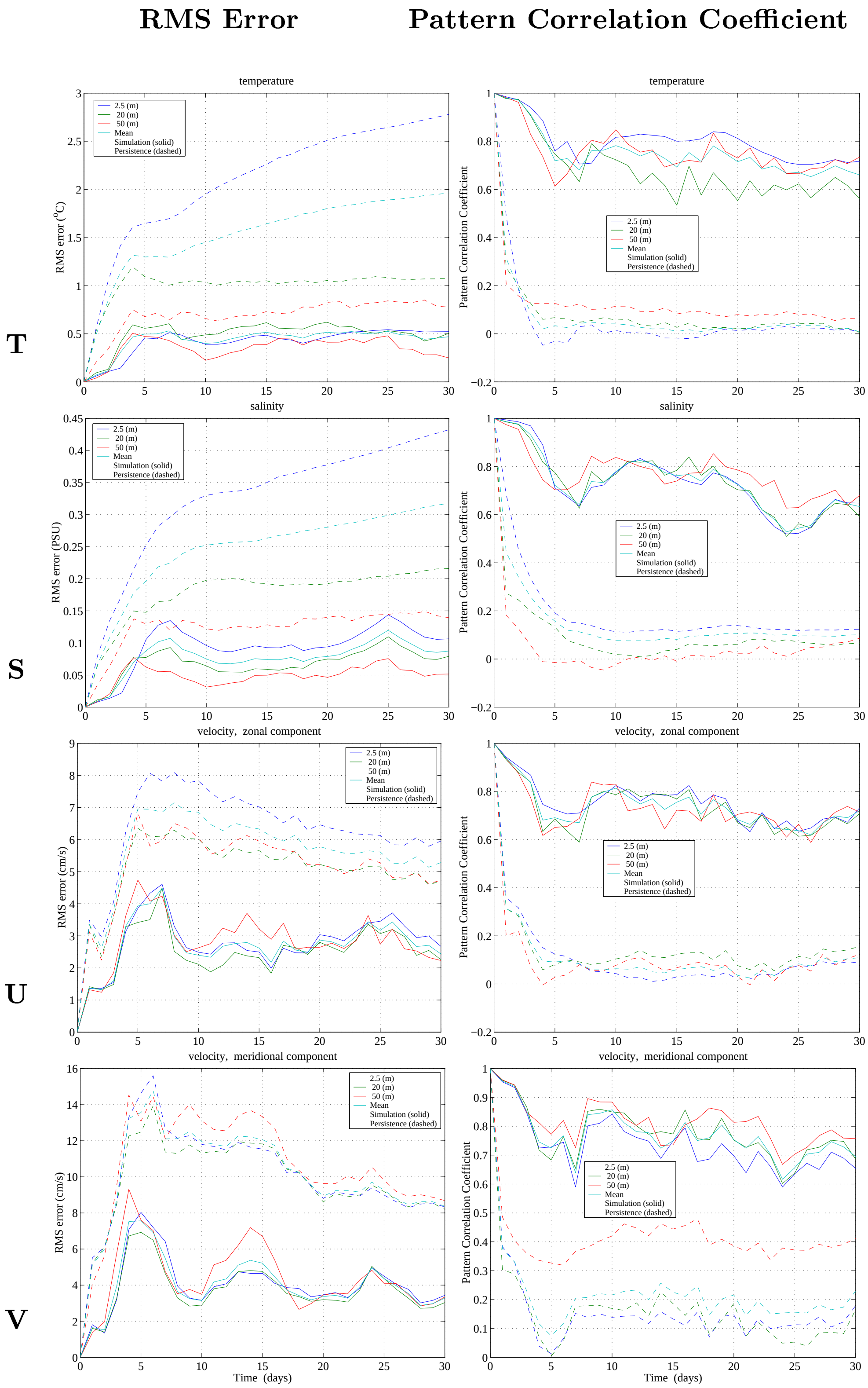


Figure 64: Comparison of rigid–lid, surface pressure formulation simulation *(Bi)* to free surface, surface pressure formulation simulation *(Ci)*. Both from "surface streamfunction" initial conditions

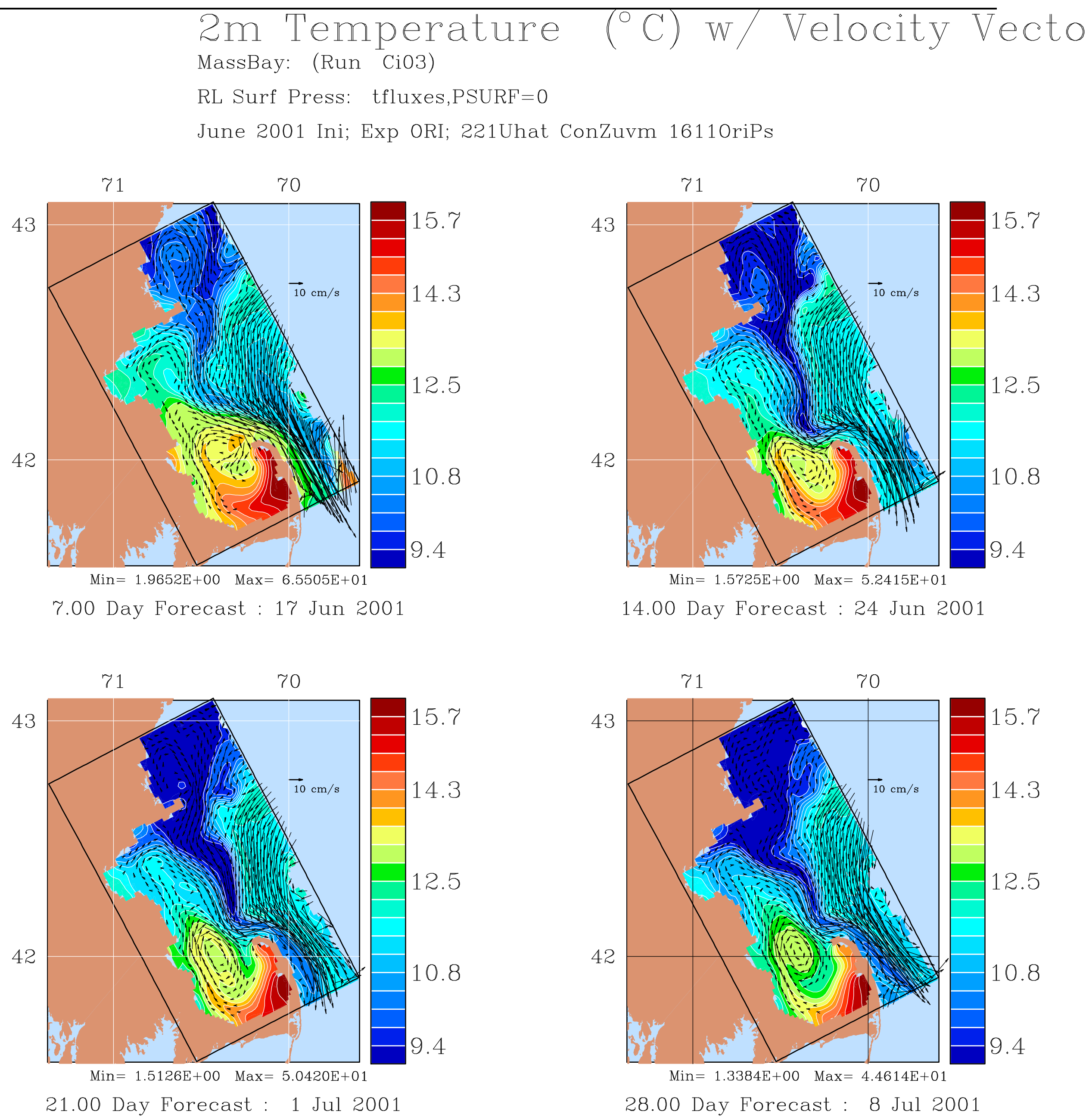


Figure 65 : Free surface, surface pressure formulation simulation from "surface stream-function" initial conditions (psurf = 0). Near surface temperature with total velocity vectors.

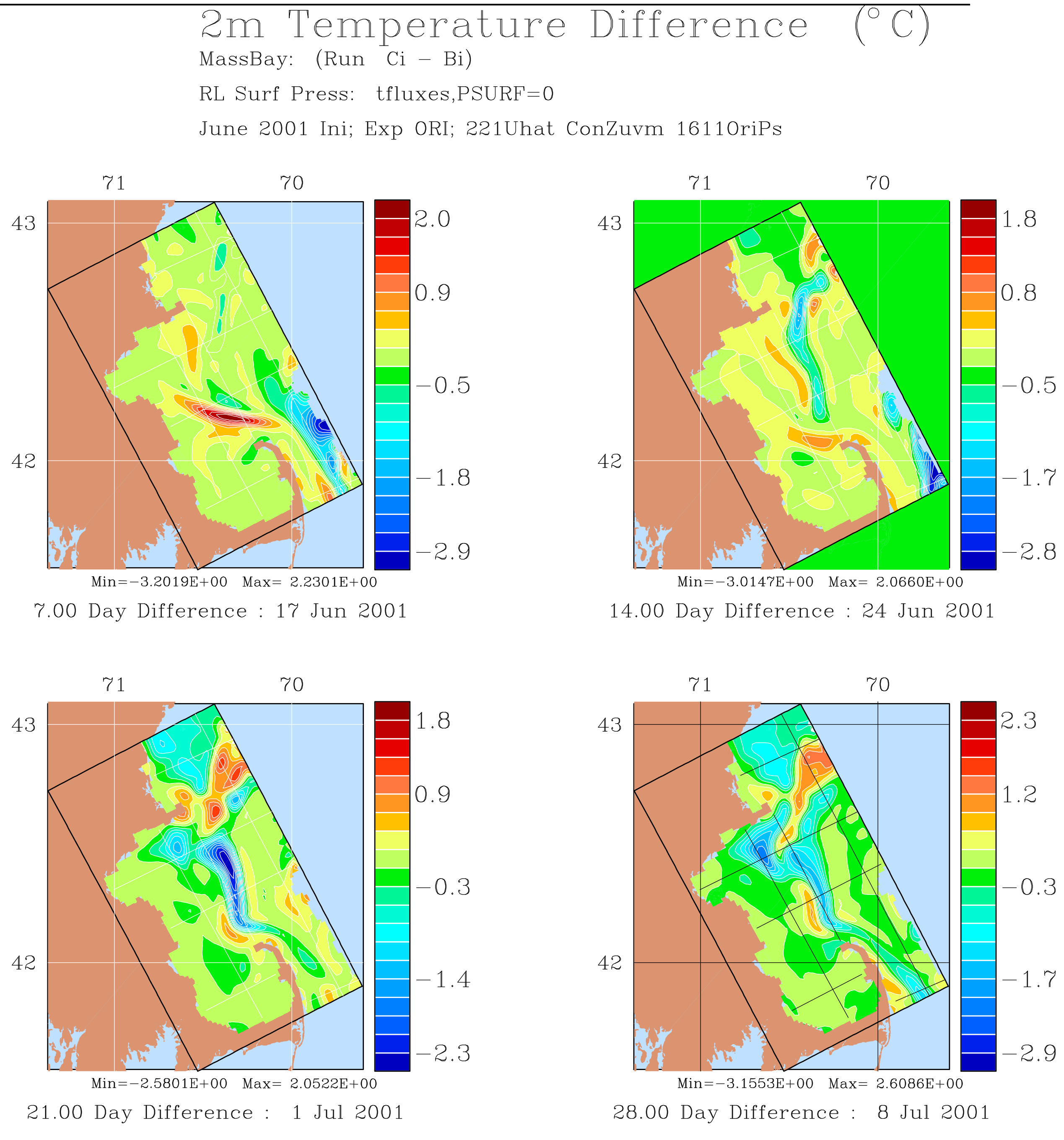


Figure 66 : Near Surface comparison of rigid–lid, surface pressure formulation simulation *(Bi)* to free surface, surface pressure formulation simulation *(Ci)*. Both from "surface streamfunction" initial conditions

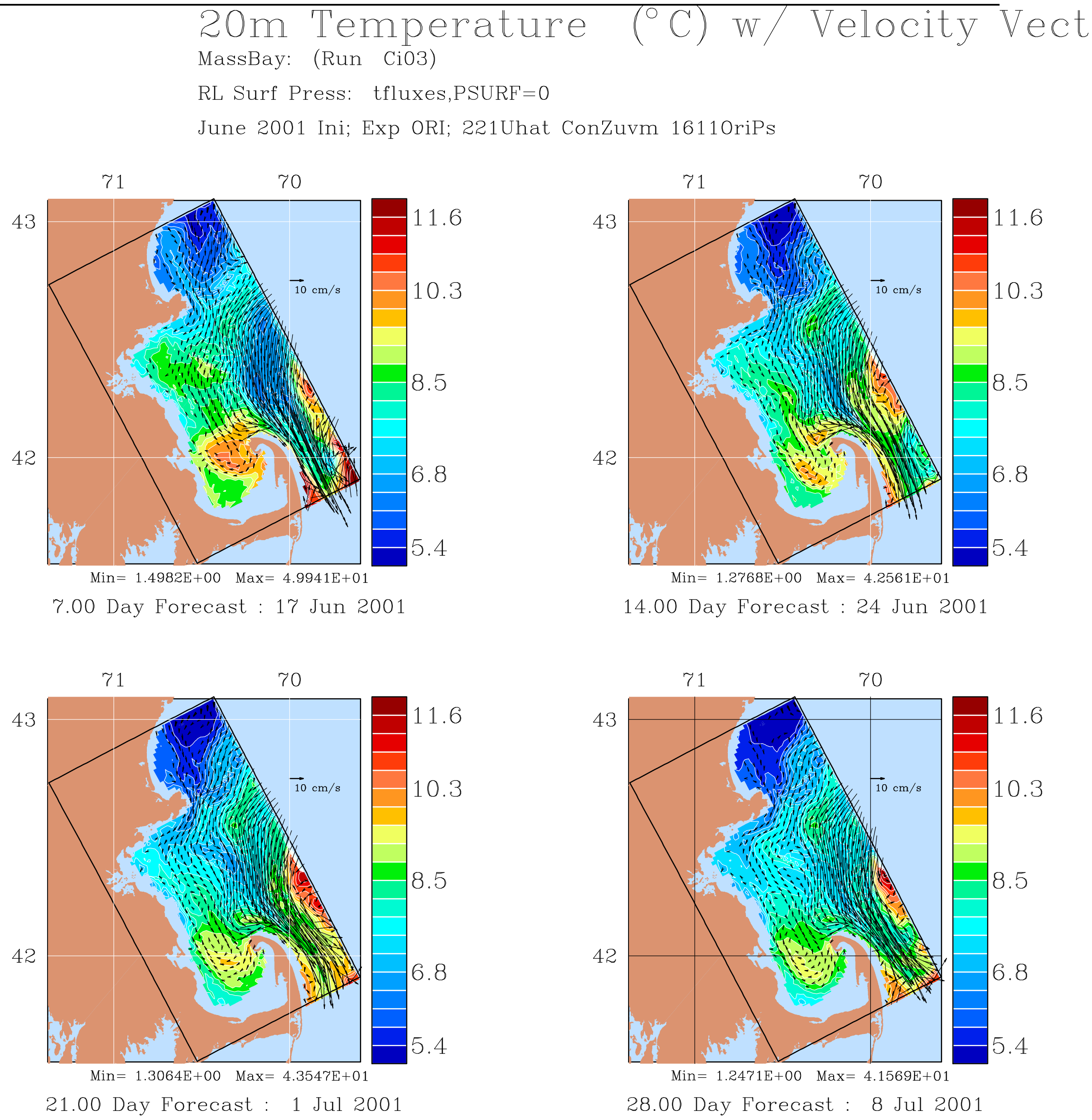


Figure 67 : Free surface, surface pressure formulation simulation from “surface streamfunction” initial conditions (`psurf` = 0). Mid–level temperature with total velocity vectors.

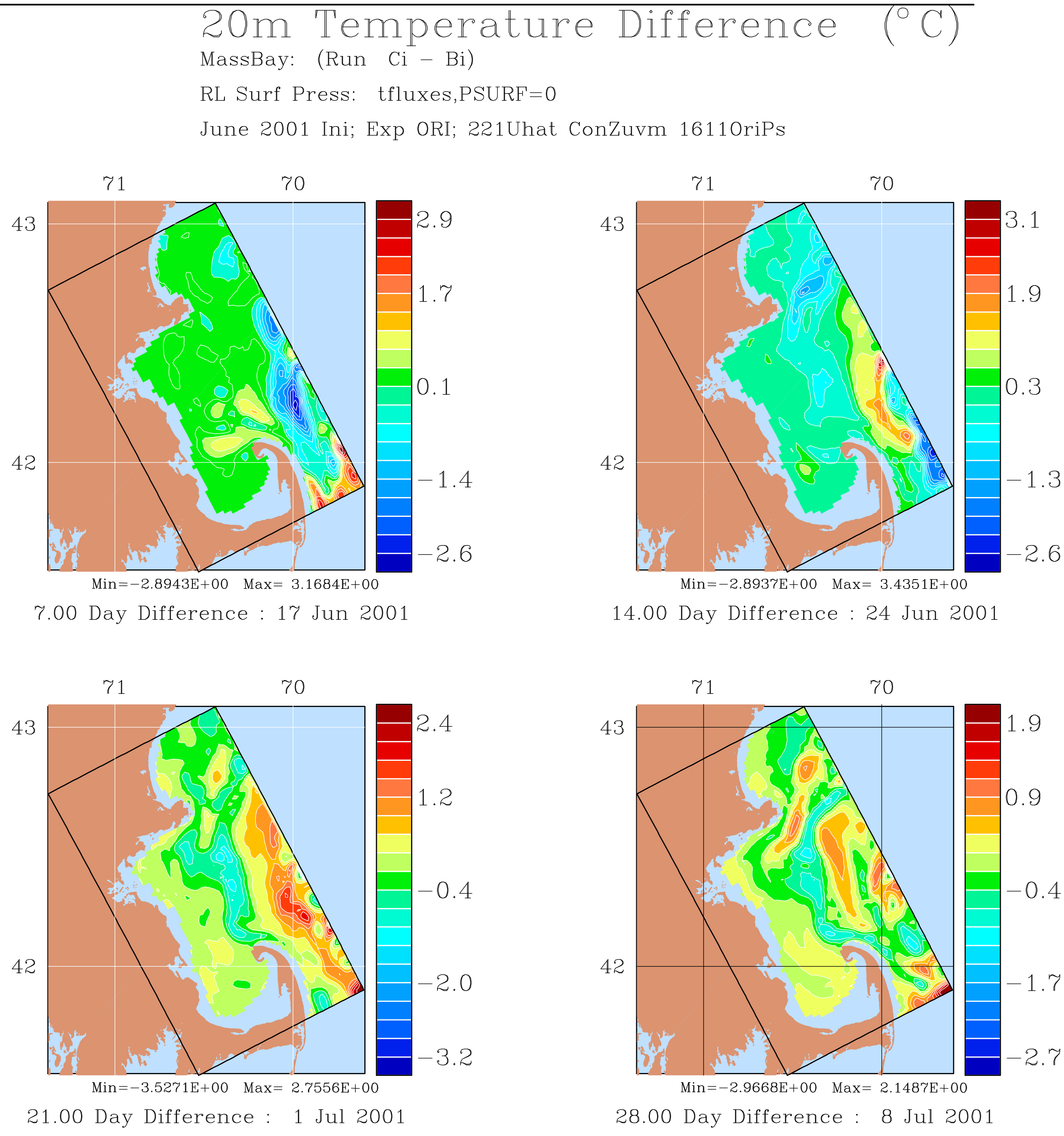


Figure 68 : Mid–level comparison of rigid–lid, surface pressure formulation simulation *(Bi)* to free surface, surface pressure formulation simulation *(Ci)*. Both from "surface streamfunction" initial conditions

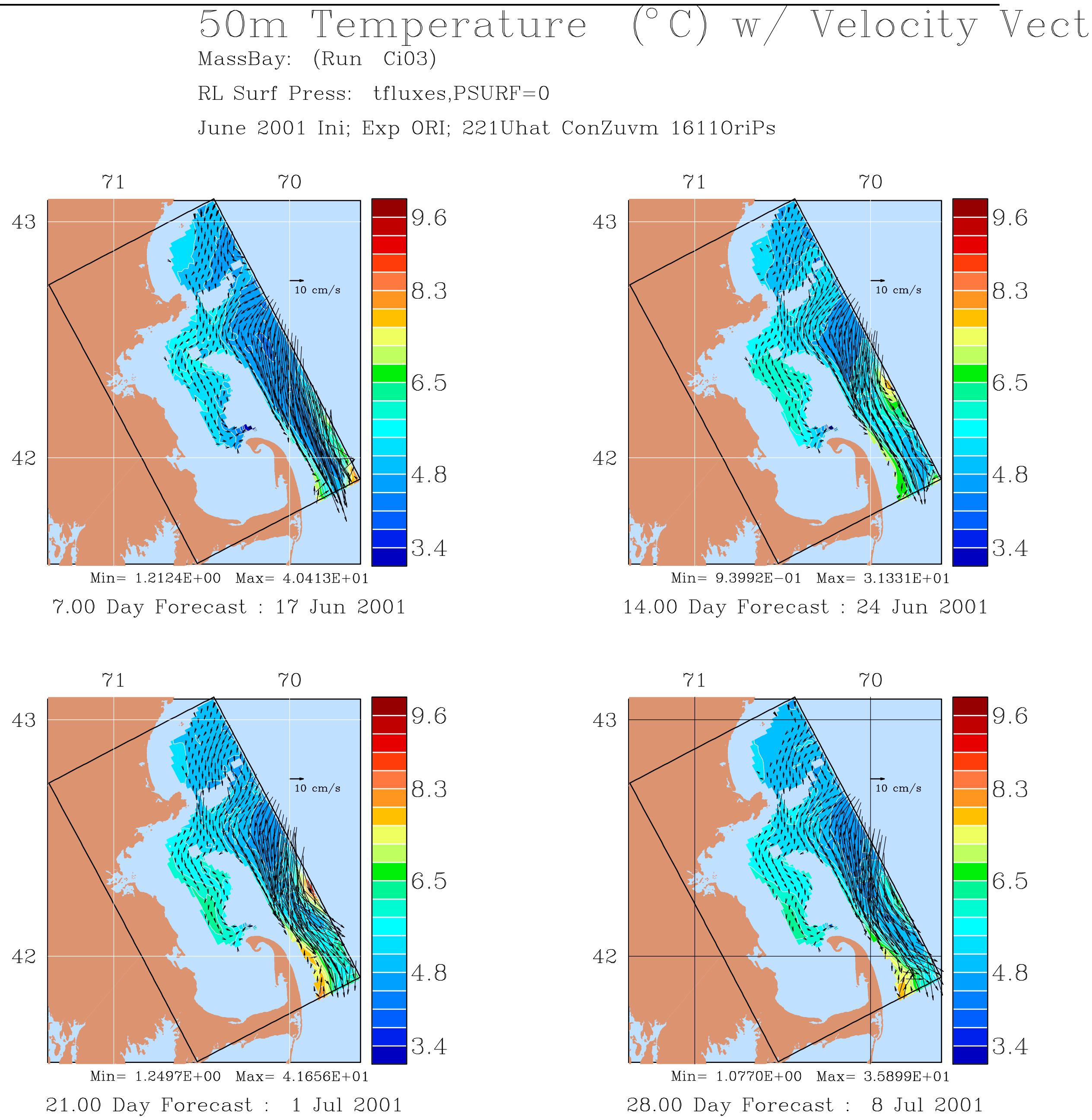


Figure 69 : Free surface, surface pressure formulation simulation from "surface stream-function" initial conditions (psurf = 0). Deep temperature with total velocity vectors.

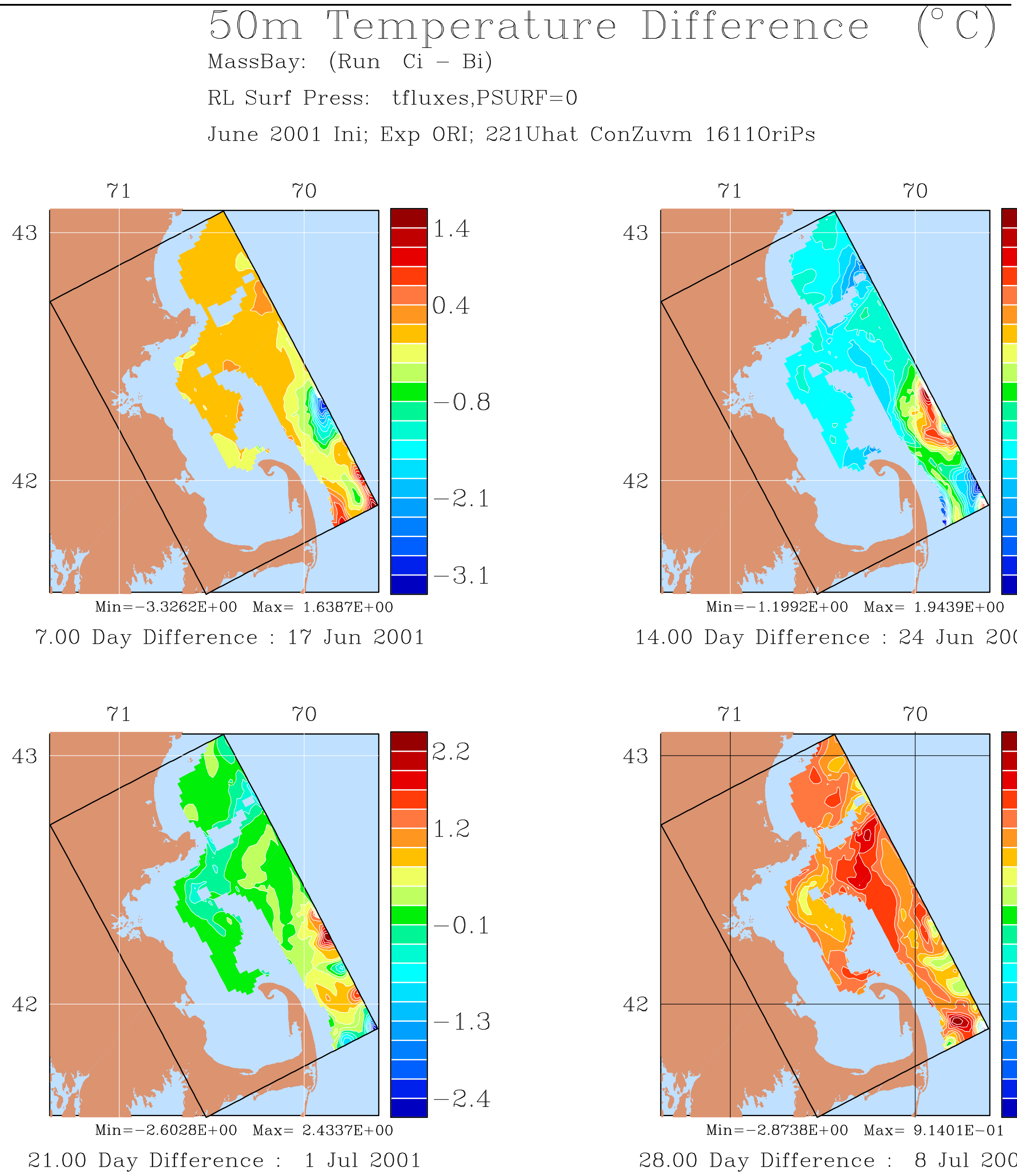


Figure 70 : Deep comparison of rigid–lid, surface pressure formulation simulation *(Bi)* to free surface, surface pressure formulation simulation *(Ci)*. Both from "surface streamfunction" initial conditions

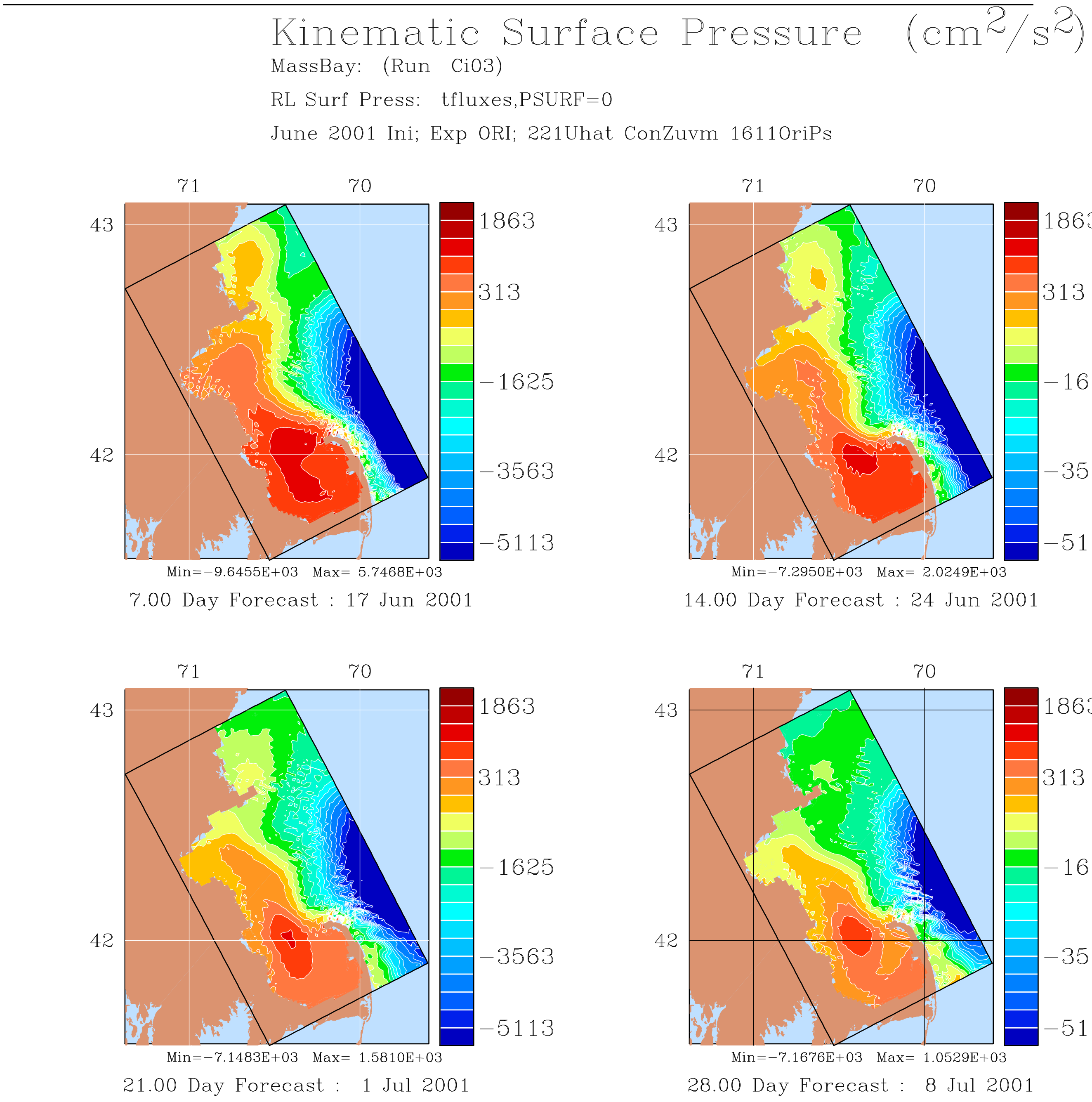


Figure 71 : Free surface, surface pressure formulation simulation from "surface streamfunction" initial conditions (`psurf` $= 0$). Noisy kinematic surface pressure.

*(ii)* Surface Streamfunction & Velocity (`psurf` = 1)

The free surface results and comparisons to rigid–lid surface pressure formulation results are presented in figures 72–80. The kinetic energy experiences more initial growth and then has a sharp decline around day 16, relative to the rigid–lid results. The RMS and PCC skill metrics consistently show better agreement between the 2 pressure formulations than between either and the streamfunction formulation.

The surface flow patterns are similar between the 2 pressure formulations. The free surface case has larger initial velocities, develops a greater advection of the questionable cold water north of Cape Ann and suppresses a gyre north of Cape Ann. The cold plume becomes a dominant feature of the surface temperature difference fields. Similar features occur in the mid–level fields, with the plume being more subtle. The peak mid–level temperature differences occur exterior to the Bay. The deep flows are very similar, with the flows north of Cape Ann being more diffuse. The temperature differences are largest outside of the Bay.

The surface pressure shows similar overall patterns and similar noise to the rigid–lid case, with the exception of a suppressed high, north of Cape Ann, in the free surface case. The free surface case also exhibits an apparent wave, coming off of the exterior of Cape Cod.

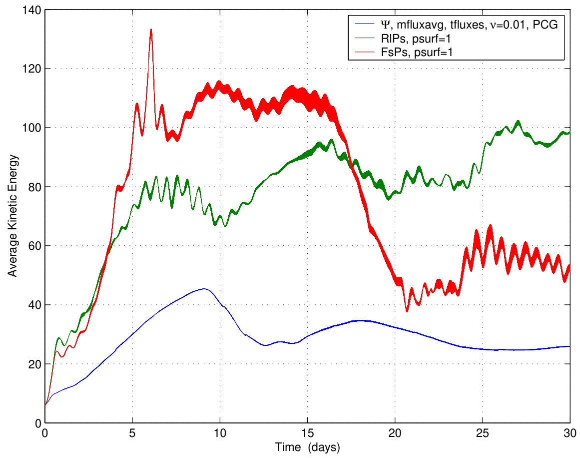


Figure 72 : Kinetic Energy comparison between simulations *(Av)*, *(Bii)* & *(Cii)*.

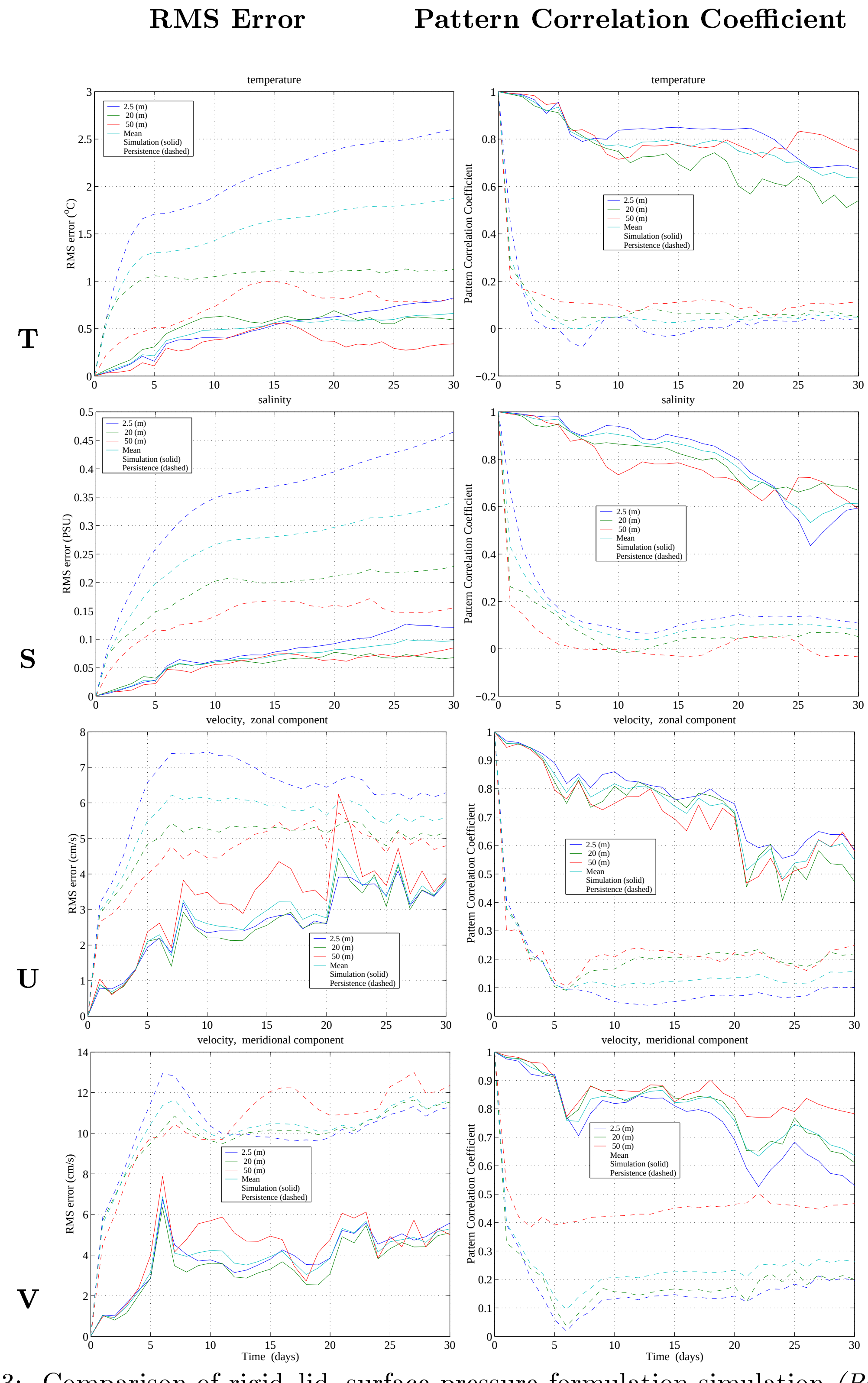


Figure 73: Comparison of rigid–lid, surface pressure formulation simulation *(Bii)* to free surface, surface pressure formulation simulation *(Cii)*. Both from "surface streamfunction & velocity" initial conditions

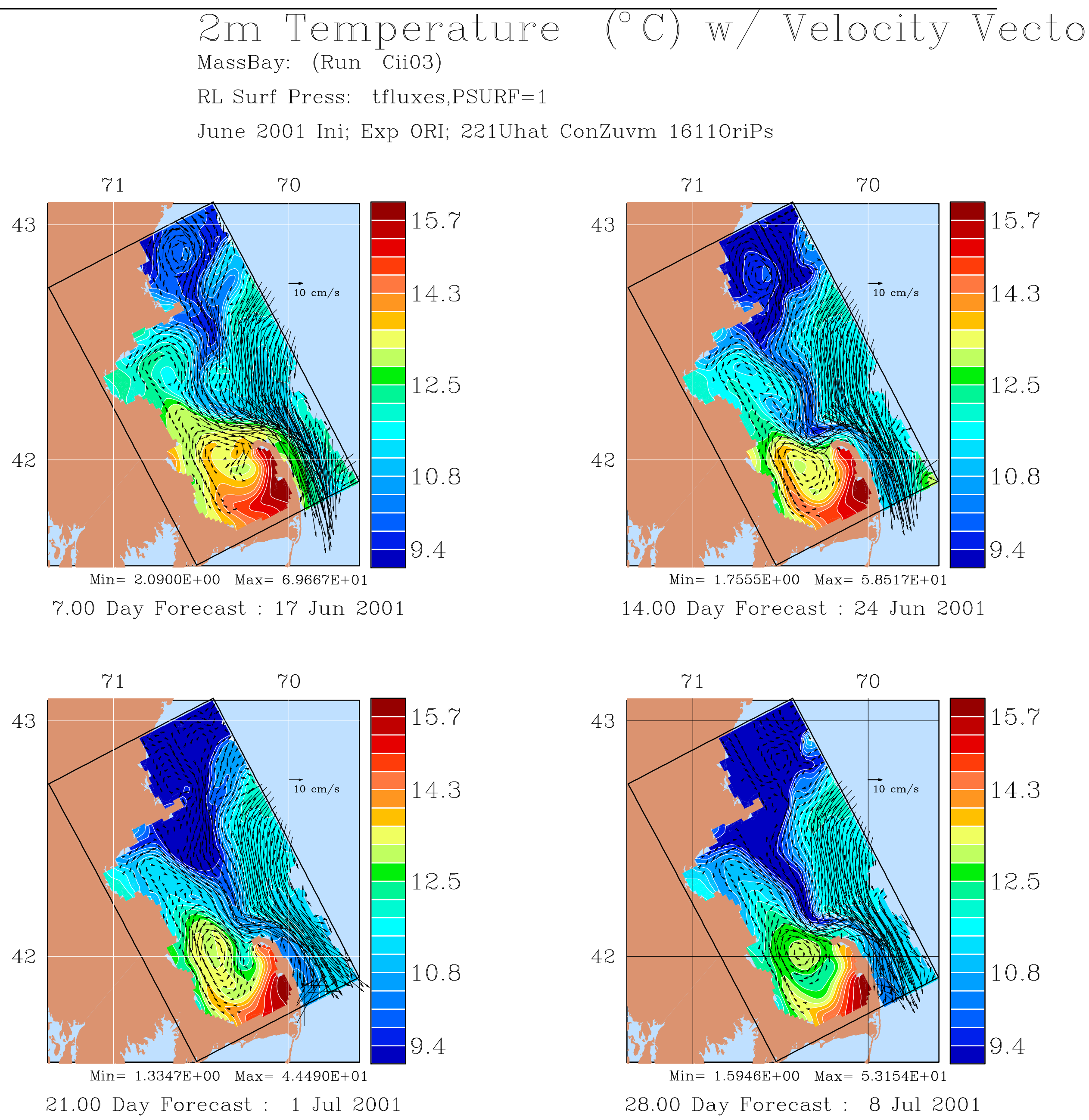


Figure 74 : Free surface, surface pressure formulation simulation from "surface streamfunction & velocity" initial conditions (`psurf` = 1). Near surface temperature with total velocity vectors.

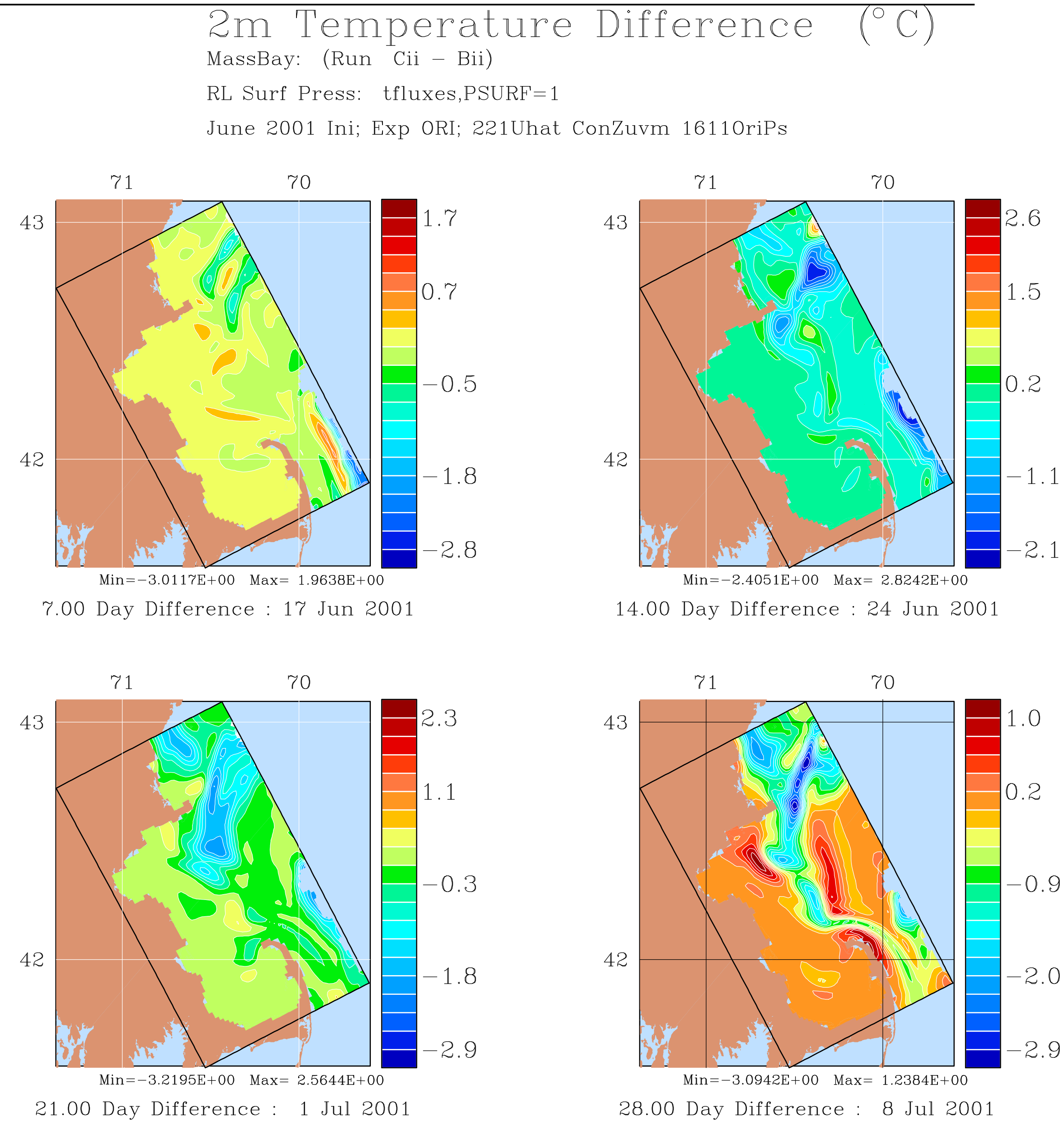


Figure 75 : Near Surface comparison of rigid–lid, surface pressure formulation simulation *(Bii)* to free surface, surface pressure formulation simulation *(Cii)*. Both from "surface streamfunction & velocity" initial conditions

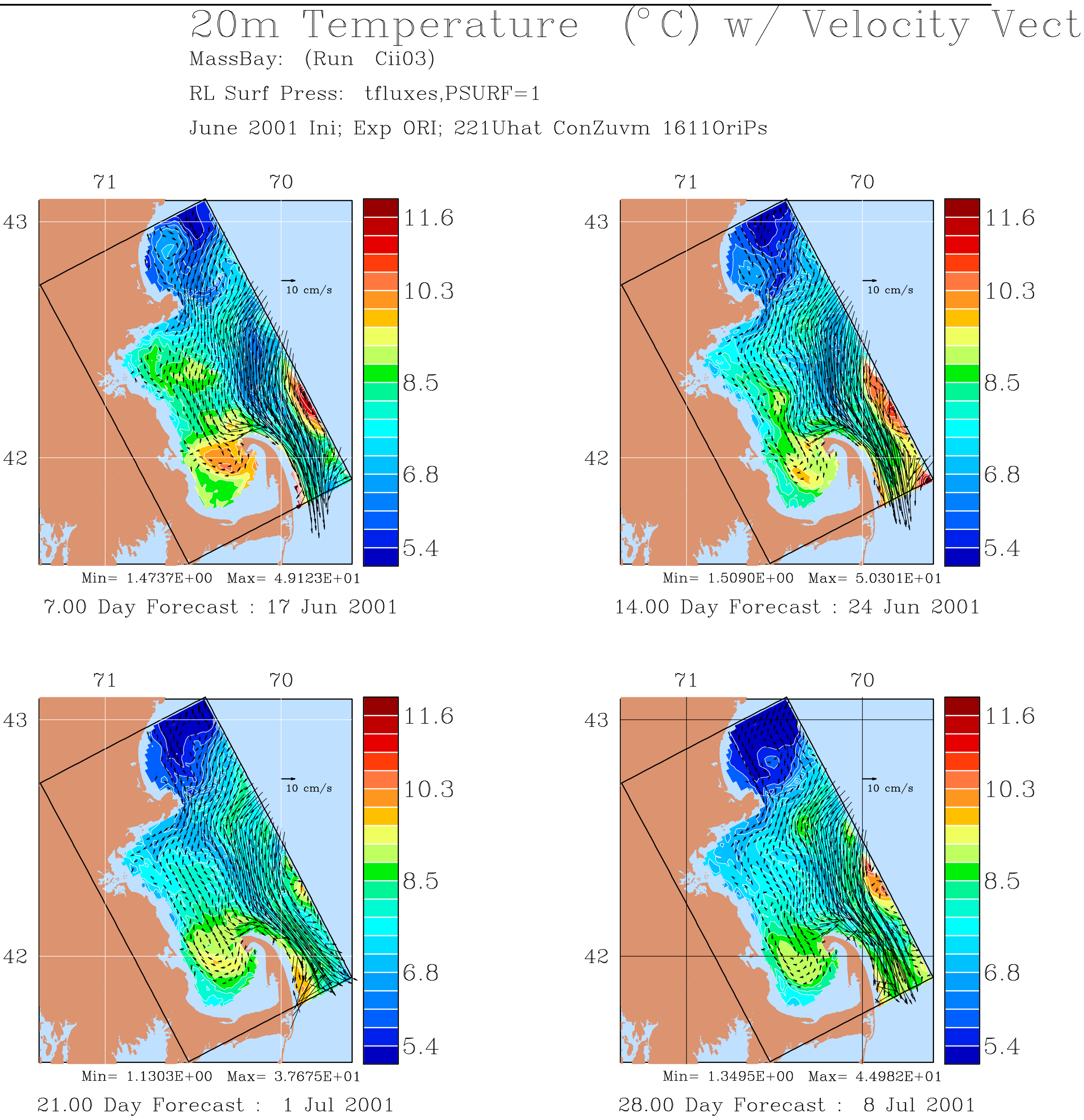


Figure 76 : Free surface, surface pressure formulation simulation from “surface streamfunction & velocity” initial conditions (`psurf` = 1). Mid–level temperature with total velocity vectors.

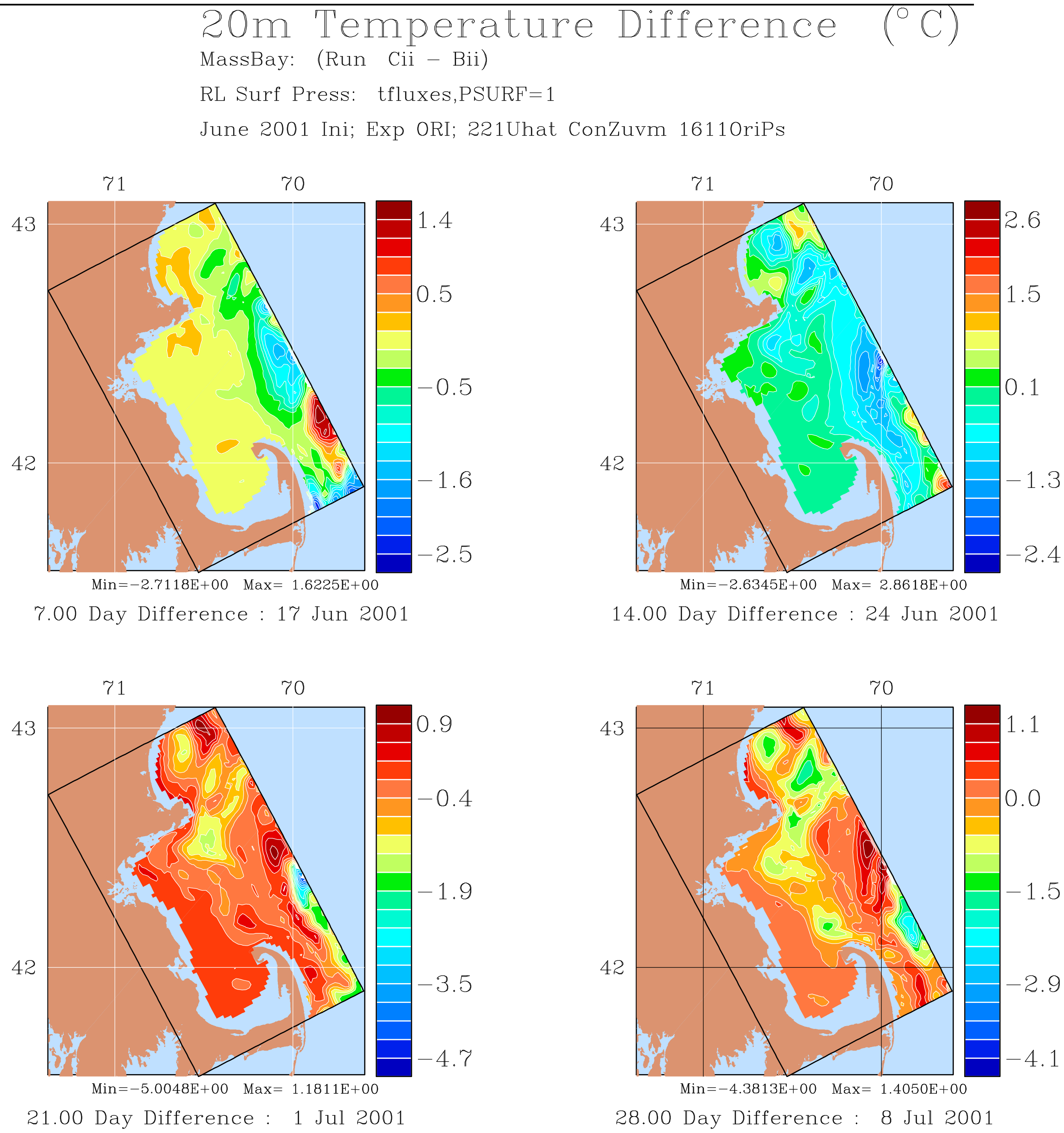


Figure 77 : Mid–level comparison of rigid–lid, surface pressure formulation simulation *(Bii)* to free surface, surface pressure formulation simulation *(Cii)*. Both from “surface streamfunction & velocity” initial conditions

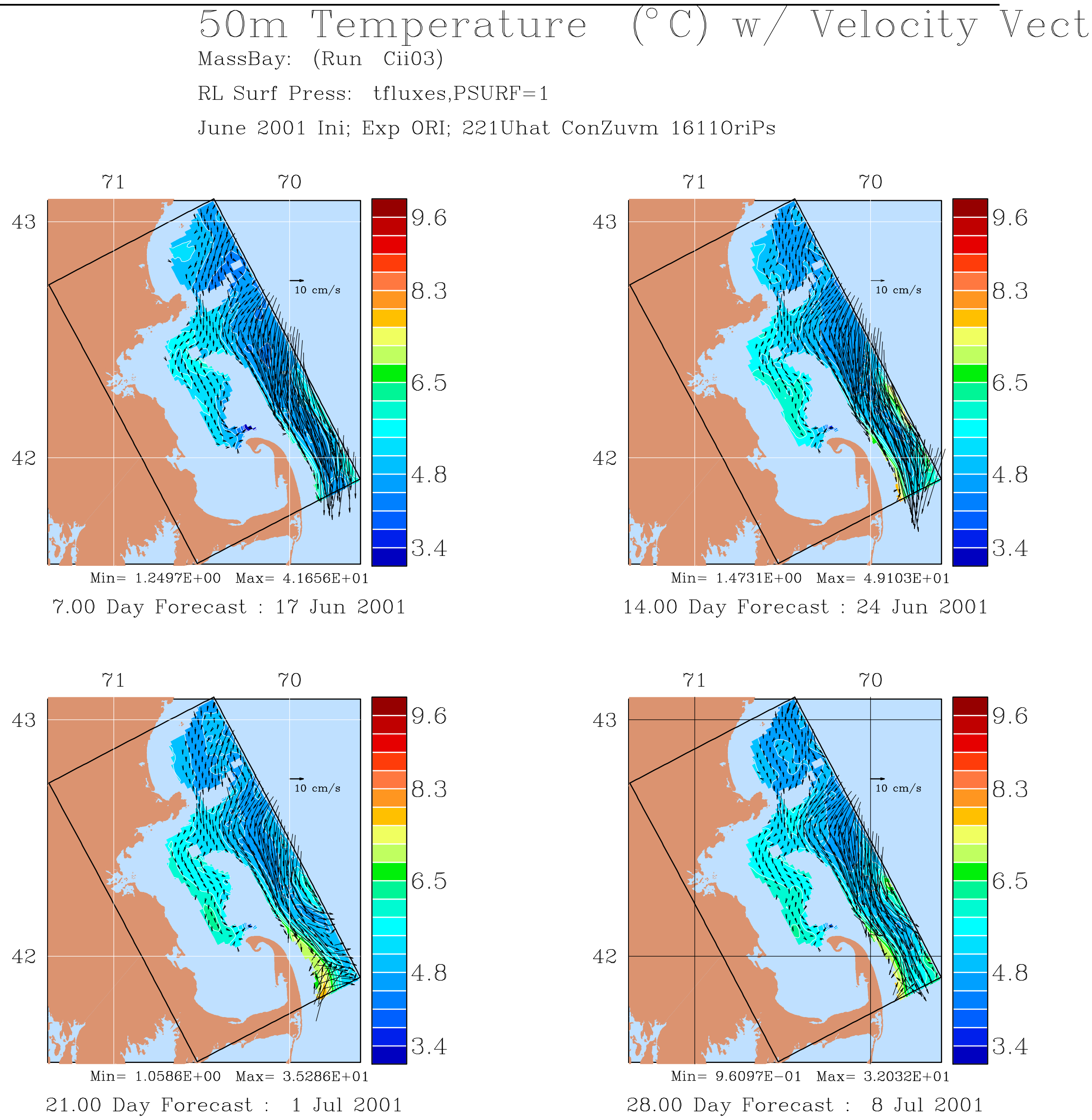


Figure 78 : Free surface, surface pressure formulation simulation from "surface streamfunction & velocity" initial conditions (`psurf` = 1). Deep temperature with total velocity vectors.

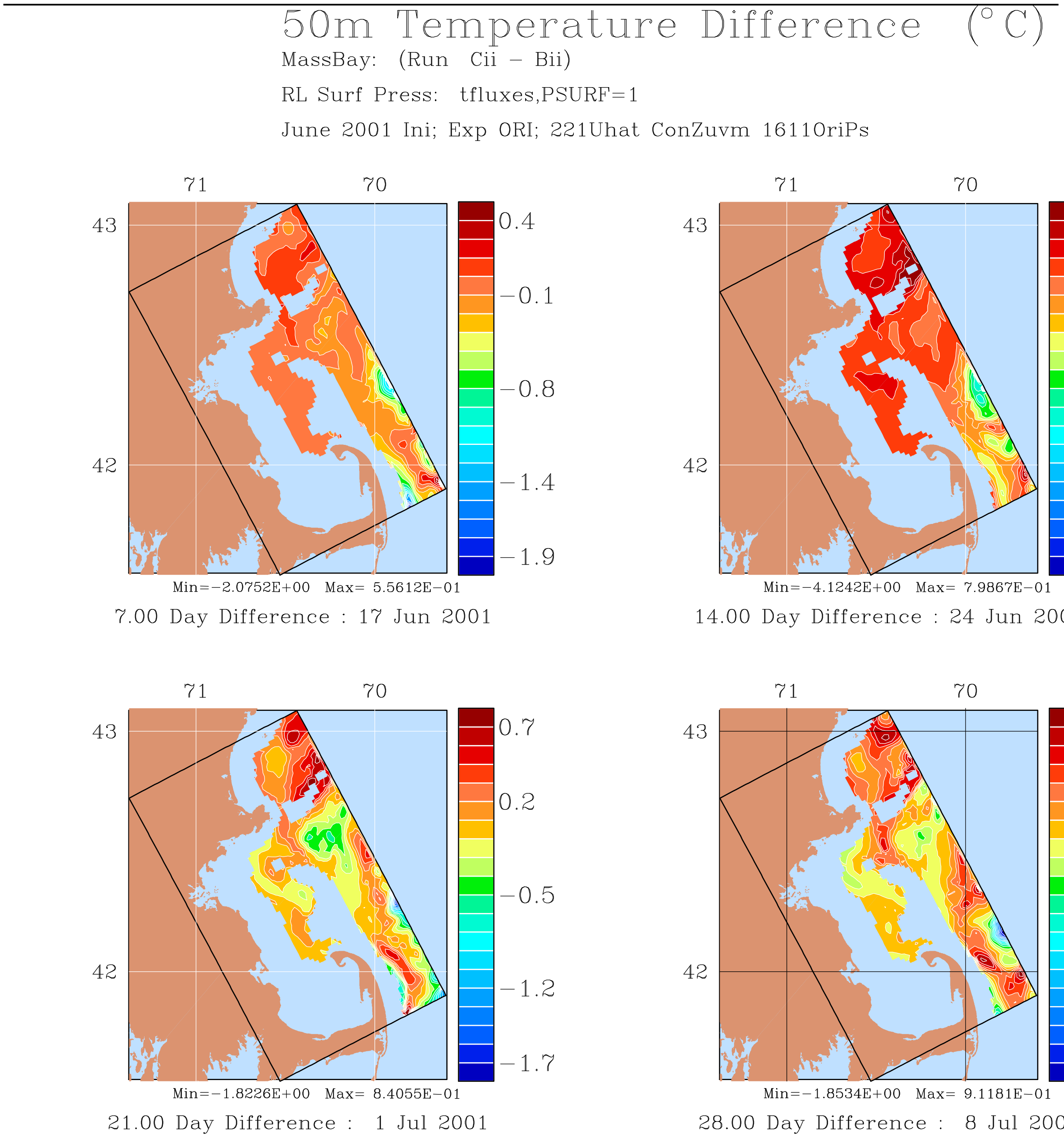


Figure 79 : Deep comparison of rigid–lid, surface pressure formulation simulation *(Bii)* to free surface, surface pressure formulation simulation *(Cii)*. Both from "surface streamfunction & velocity" initial conditions

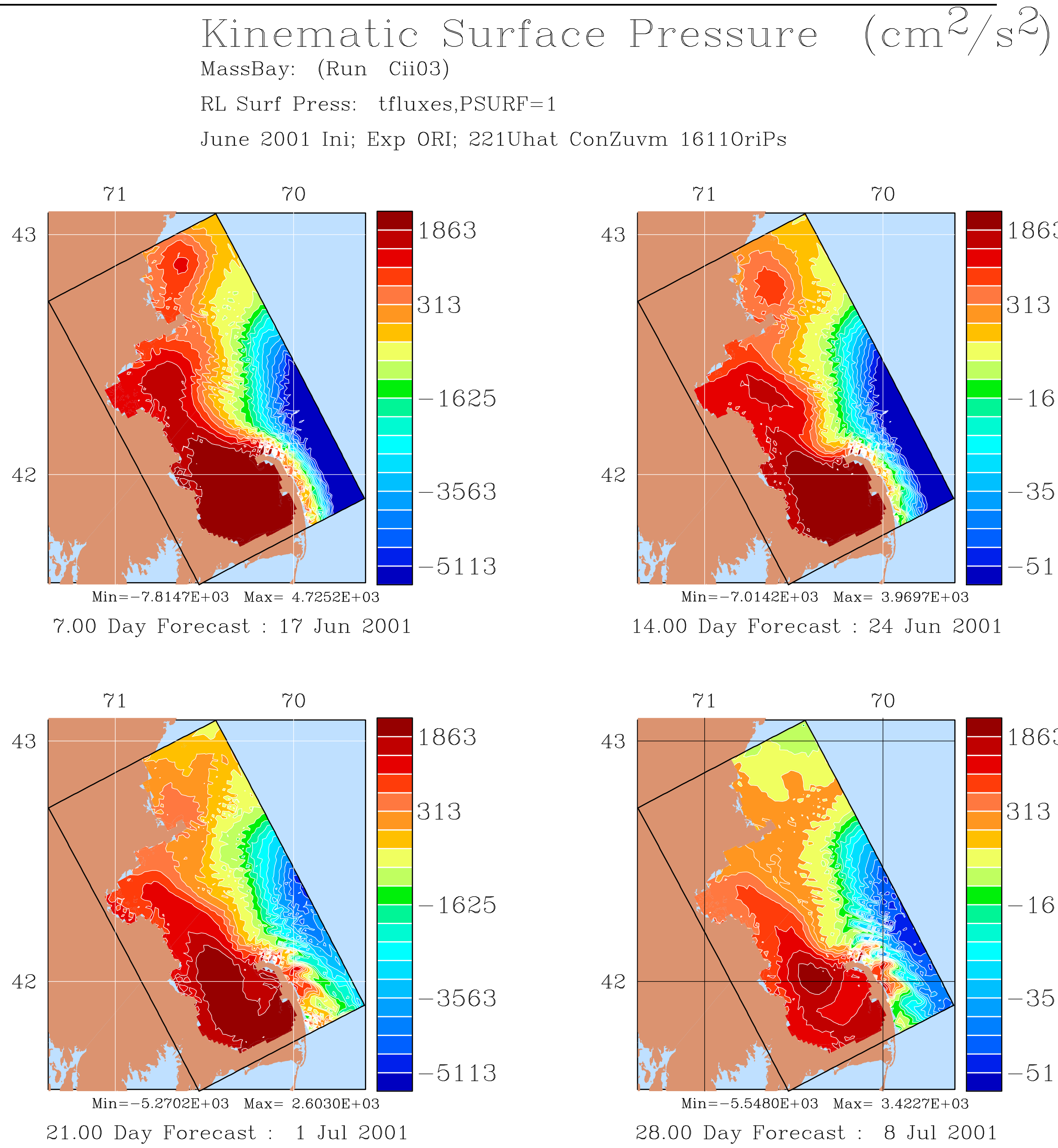


Figure 80 : Free surface, surface pressure formulation simulation from "surface stream-function & velocity" initial conditions (`psurf` $= 1$). Noisy kinematic surface pressure.

*(iii)* Surface Streamfunction & the Barotropic Equation (`psurf` = 1 & CPP option `bctest2`)

The free surface results and comparisons to rigid–lid surface pressure formulation results are presented in figures 81–89. The kinetic energy tracks rigid–lid results fairly well. The RMS and PCC skill metrics consistently show better agreement between the 2 pressure formulations than between either and the streamfunction formulation.

The surface flow patterns are similar between the 2 pressure formulations. The free surface case "breaks" the gyre north of Cape Ann to the east and advects much of the questionable northern cold water to the north. This relative warming becomes a dominant feature of the surface temperature difference fields. Similar features occur in the mid–level fields, with a retention of more warm southern exterior water. The northern relative warming becomes a dominant feature of the mid–level temperature differences. The deep flows are very similar except for a relative flow reversal in the extreme northeast corner. The temperature differences are largest in the southern portion exterior to the Bay.

The surface pressure shows similar overall patterns and similar noise to the rigid–lid case, with the exception that the high north of Cape Ann is elongated to the eastern boundary and intensified in the free surface case. The free surface case also exhibits small apparent waves, coming off of the exteriors of Cape Cod and Cape Ann.

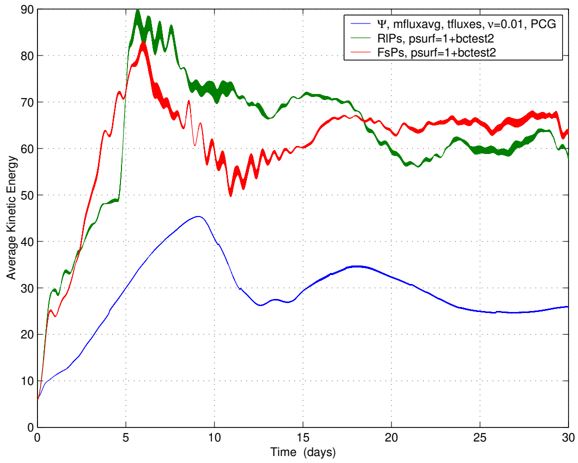


Figure 81 : Kinetic Energy comparison between simulations *(Av)*, *(Biii)* & *(Ciii)*.

**RMS Error** **Pattern Correlation Coefficient**

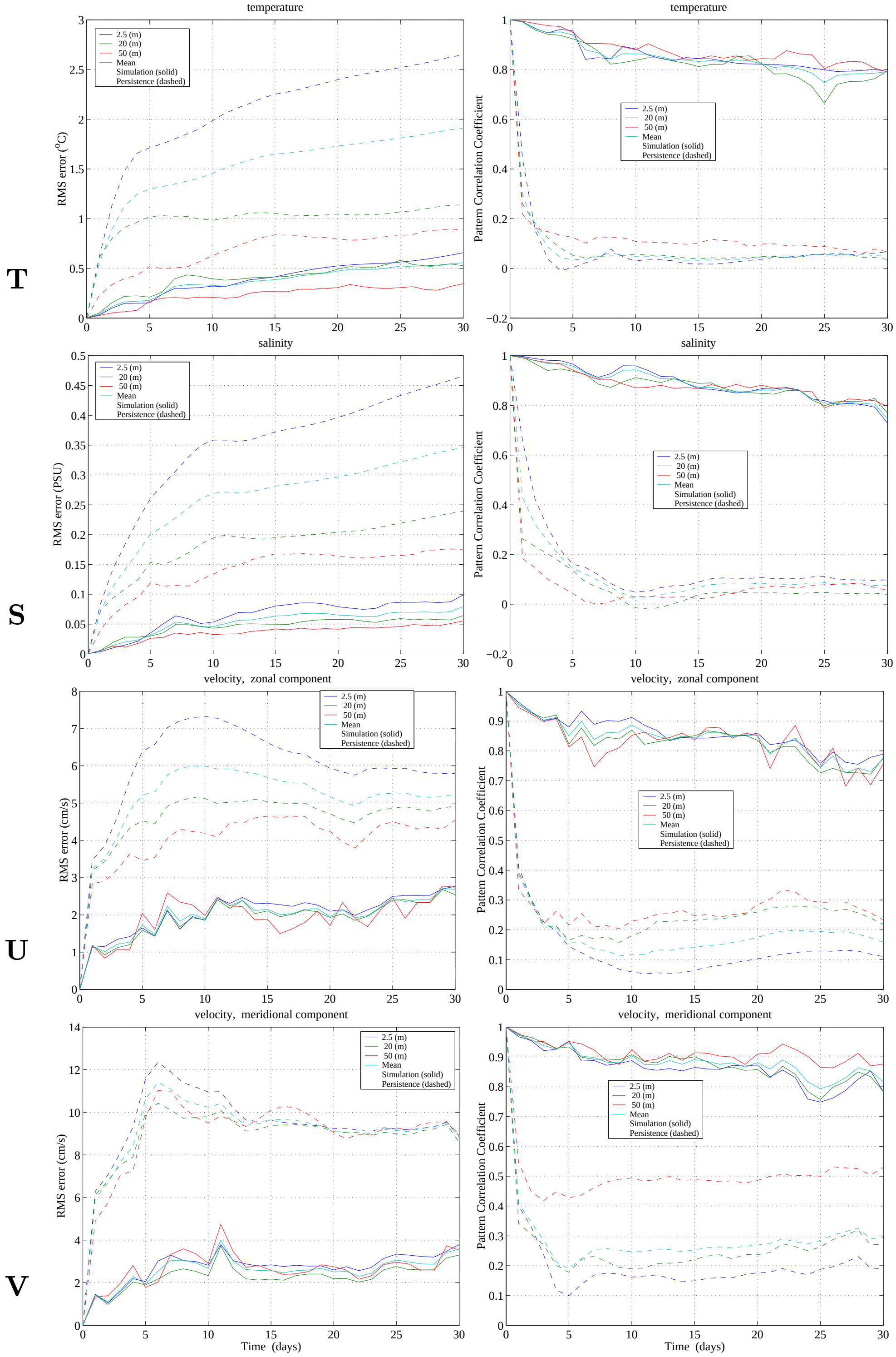


Figure 82: Comparison of rigid–lid, surface pressure formulation simulation *(Biii)* to free surface, surface pressure formulation simulation *(Ciii)*. Both from "surface streamfunction & barotropic equation" initial conditions

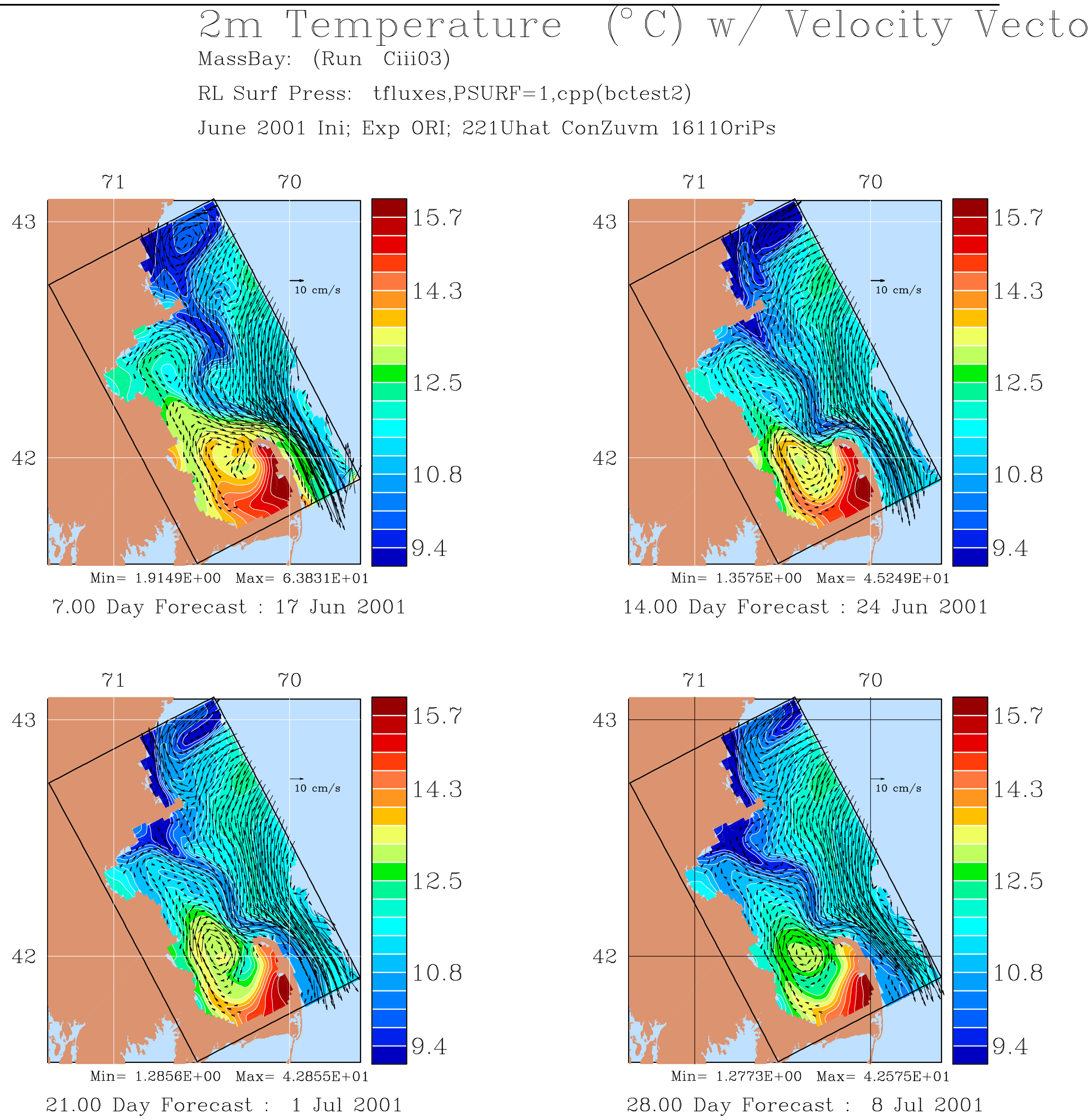


Figure 83 : Free surface, surface pressure formulation simulation from "surface streamfunction & barotropic equation" initial conditions (`psurf` = 1 & CPP option `bctest2`). Near surface temperature with total velocity vectors.

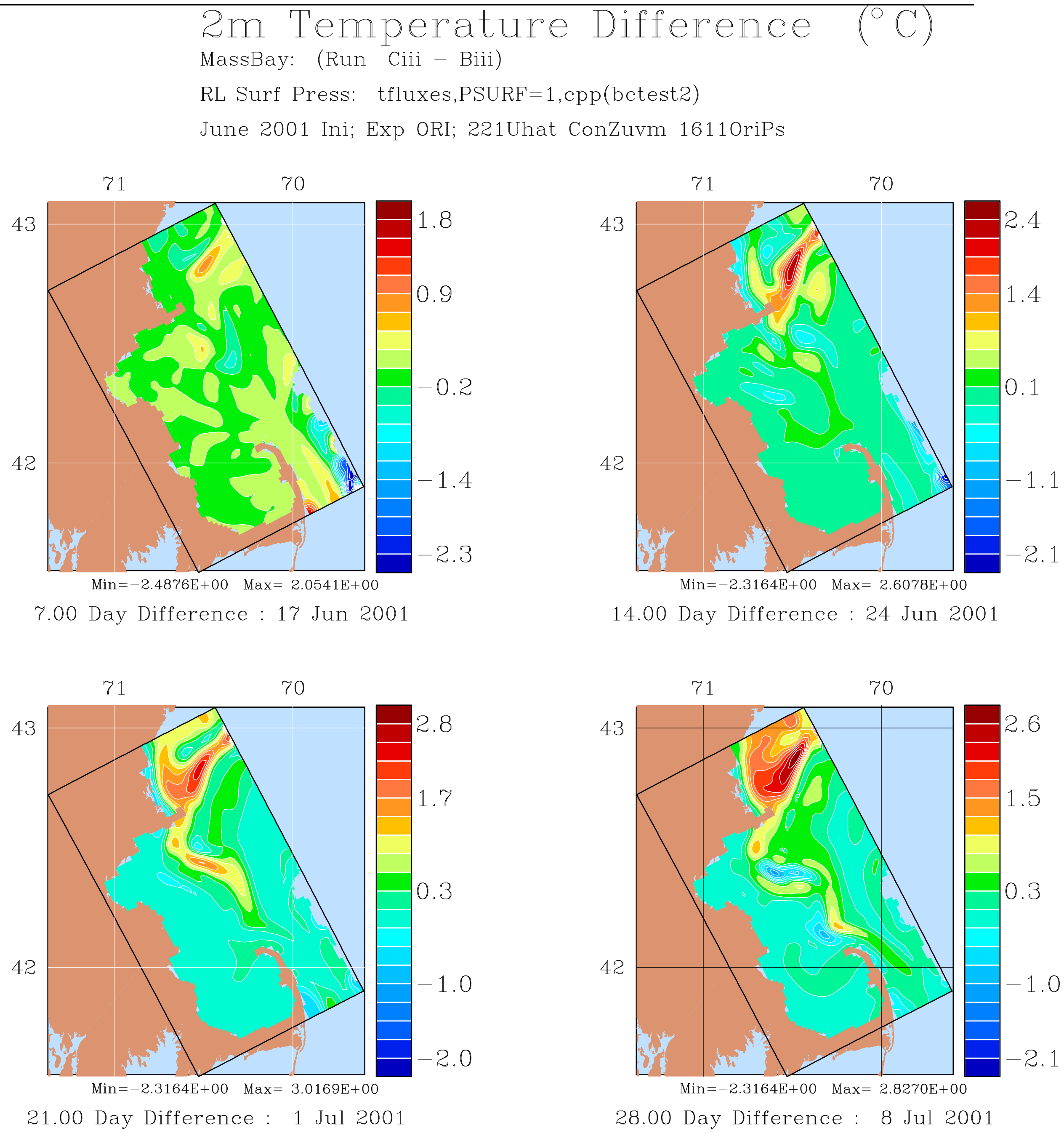


Figure 84 : Near Surface comparison of rigid–lid, surface pressure formulation simulation *(Biii)* to free surface, surface pressure formulation simulation *(Ciii)*. Both from "surface streamfunction & barotropic equation" initial conditions

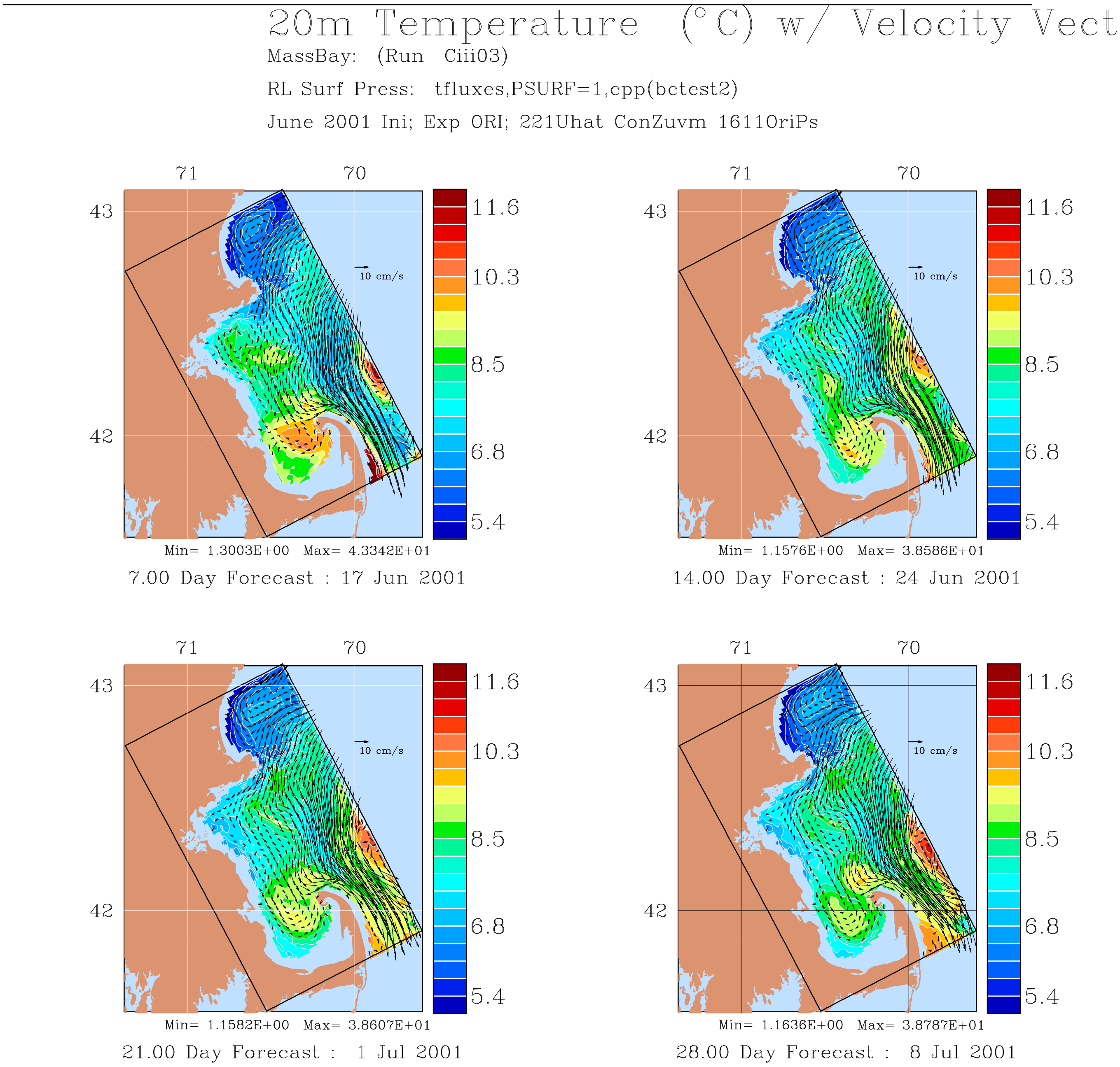


Figure 85 : Free surface, surface pressure formulation simulation from "surface streamfunction & barotropic equation" initial conditions (`psurf` = 1 & CPP option `bctest2`). Mid–level temperature with total velocity vectors.

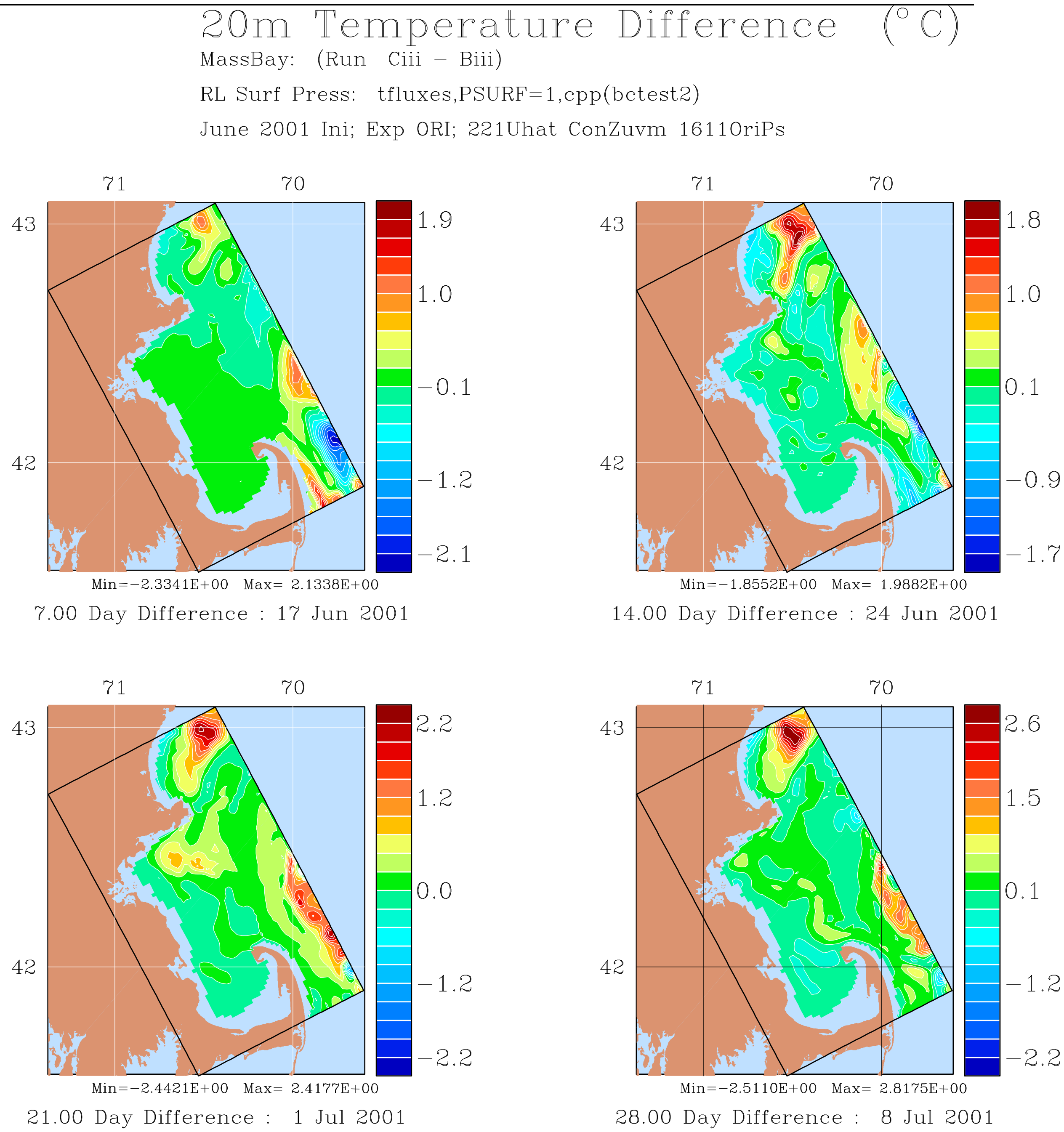


Figure 86 : Mid–level comparison of rigid–lid, surface pressure formulation simulation *(Biii)* to free surface, surface pressure formulation simulation *(Ciii)*. Both from "surface streamfunction & barotropic equation" initial conditions

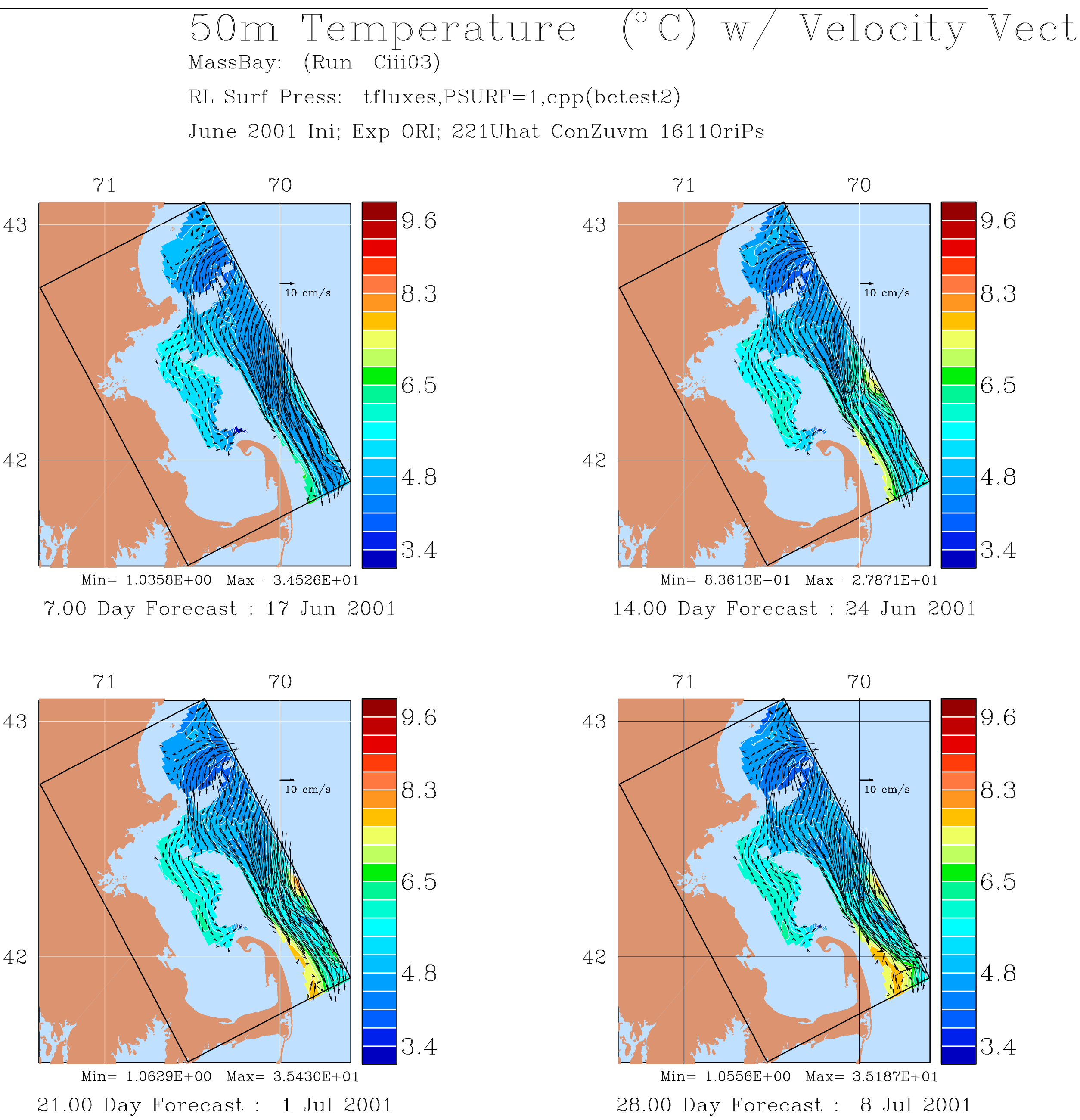


Figure 87 : Free surface, surface pressure formulation simulation from "surface streamfunction & barotropic equation" initial conditions (`psurf` = 1 & CPP option `bctest2`). Deep temperature with total velocity vectors.

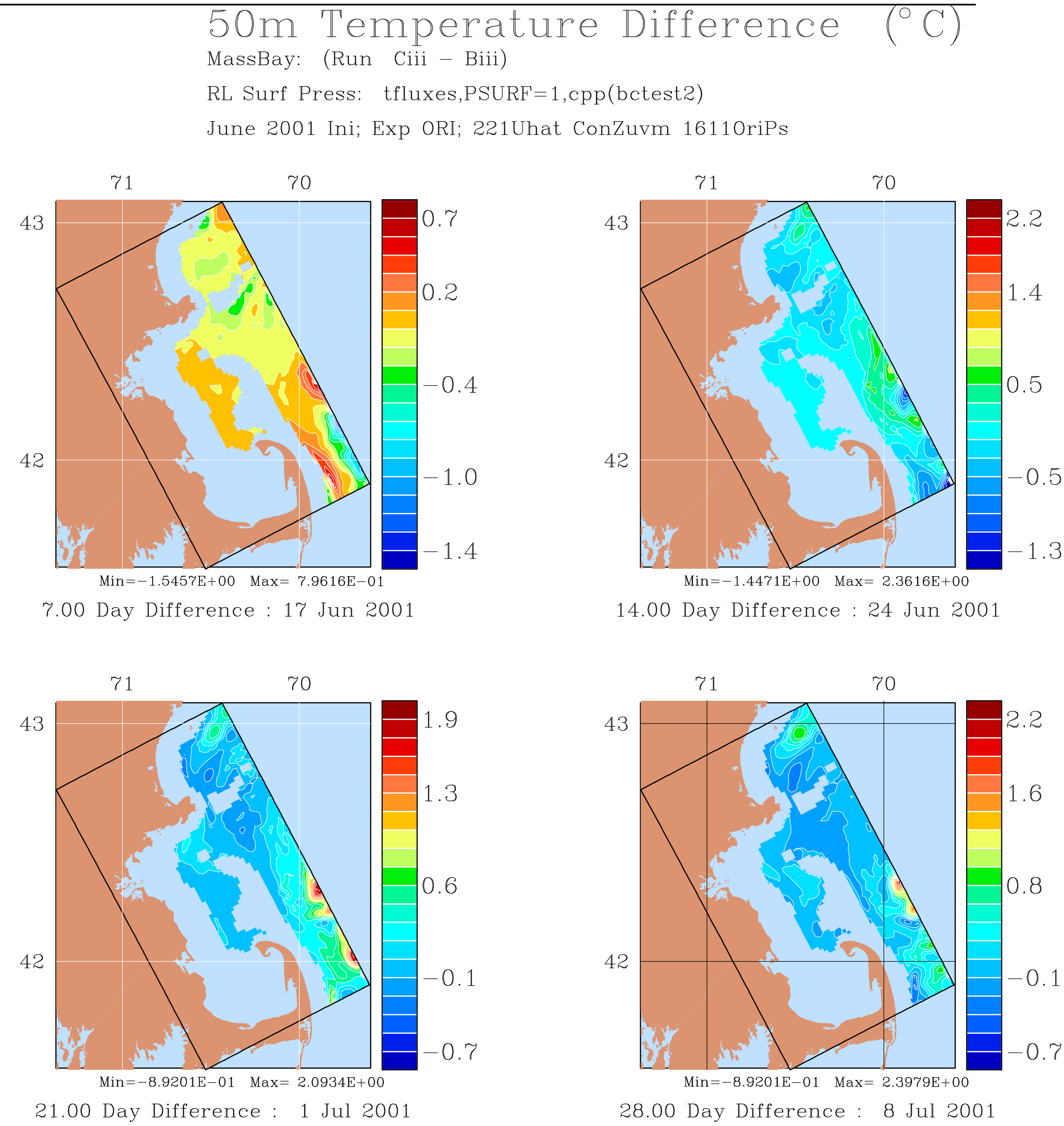


Figure 88 : Deep comparison of rigid–lid, surface pressure formulation simulation *(Biii)* to free surface, surface pressure formulation simulation *(Ciii)*. Both from "surface streamfunction & barotropic equation" initial conditions

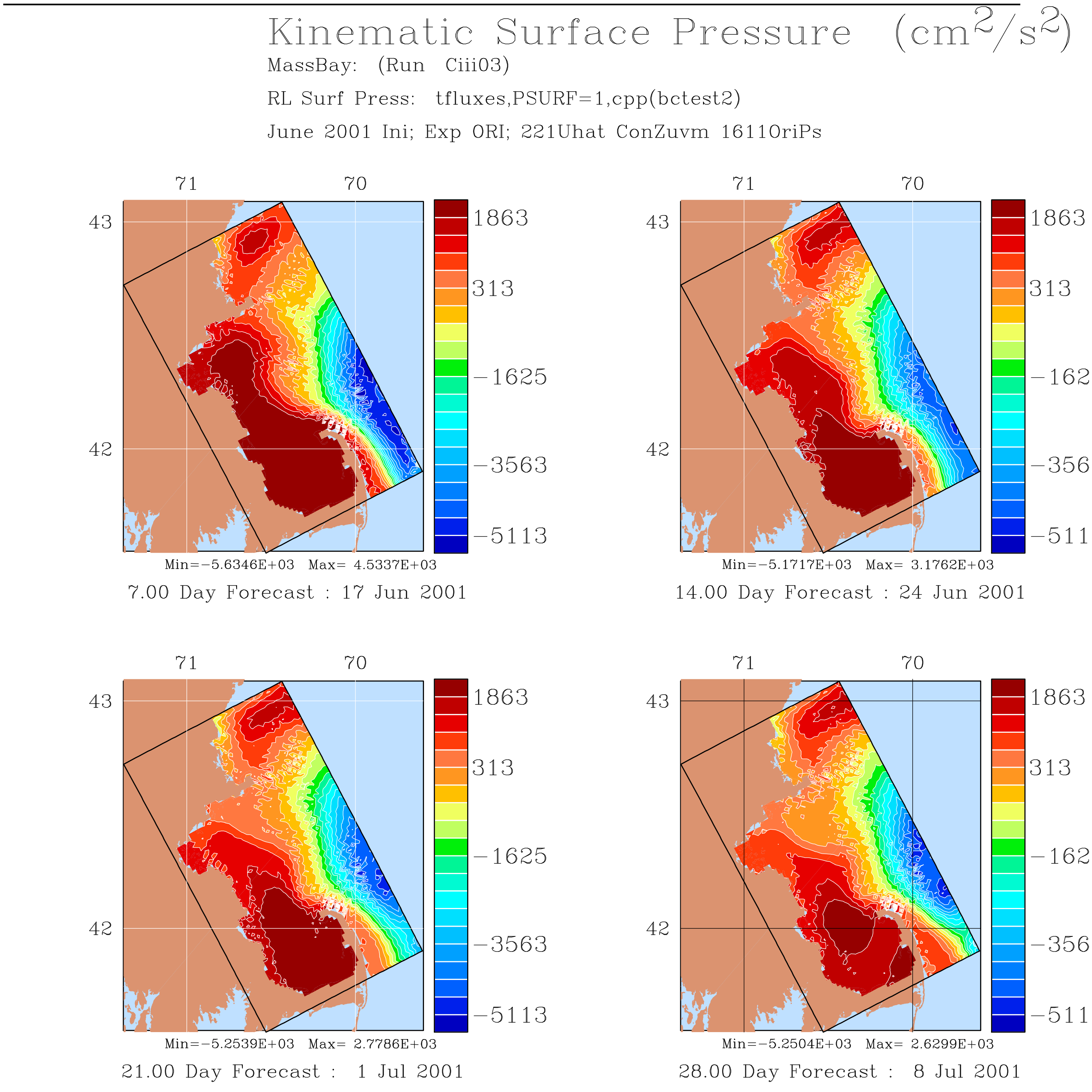


Figure 89 : Free surface, surface pressure formulation simulation from "surface streamfunction & barotropic equation" initial conditions (`psurf` = 1 & CPP option `bctest2`). Noisy kinematic surface pressure.

### Summary

The shallow coastal simulation is a more strenuous test of the free surface algorithm. The surface pressure is showing more noise than was present in the previous cases. This can't be solely due to geometry, or the noise would be present in the initial fields. The noise is small enough that tests with tides can proceed, but it needs to be solved before this code is released.

### Notes

- The closure scheme enforced in PE_initial by the CPP option `bctest1` is needed and should become the only option.
- The "smooth approximation" initialization does not appear to contribute anything and should probably be eliminated. The remaining 3 choices all still appear viable. Further testing is needed to pick between them. A decision is not necessary before the code is released.